

GEOTECHNICAL FRAMEWORK STUDY OF SHELIKOF STRAIT, ALASKA

by

Monty A. Hampton

U.S. Geological Survey

**Final Report
Outer Continental Shelf Environmental Assessment Program
Research Unit 589**

1983

637

TABLE OF CONTENTS

List of Figures 641

List of Tables 642

INTRODUCTION 643

GEOLOGIC SETTING 643

METHODS 651

RESULTS 655

 Sediment Description, Index Properties 655

 Consolidation Properties 574

 Static Strength Properties 680

 Dynamic Strength Properties 682

DISCUSSION 686

REFERENCES 692

APPENDIX : Index Property Charts for Sediment Cores from
 Shelikof Strait 697

LIST OF FIGURES

- Figure 1. Location map of the study area in **Shelikof** Strait.
- Figure 2. A. **Tracklines** of continuous seismic-reflection profiles. Solid lines represent a regional survey contracted by the Conservation Division, and dashed lines represent site surveys on cruises of the R/V **S.P. LEE** (1980) and NOAA ship **DISCOVERER** (1981).
- Figure 3. Bathymetry of **Shelikof** Strait, 20-m contour interval. Depths corrected to mean lower low water.
- Figure 4. Thickness of sedimentary units of probably Pleistocene and younger age. Contour interval: 50 meters except for thickness greater than 500 m where contour interval is 100 m.
- Figure 5. Representative seismic-reflection profiles showing **seismic-stratigraphic** units.
- Figure 6. Thickness of highest seismic-stratigraphic unit that covers most of the seafloor of **Shelikof** Strait. Contour interval: 20 m.
- Figure 7. Pie-diagrams showing relative abundances of textural classes in seafloor sediment samples.
- Figure 8. Mean grain size of seafloor sediment, in phi-units.
- Figure 9. Sediment accumulation rates, in cm/100 yr.
- Figure 10. Water content (percent dry weight) at 1-m depth in sediment cores.
- Figure 11. Bulk sediment density (gm/cm^3) at 1-m depth in sediment cores.
- Figure 12. Average grain-specific gravity in sediment cores.
- Figure 13. Average liquid limit (percent dry weight) in sediment cores.
- Figure 14. Average plastic limit (percent dry weight) in sediment cores.
- Figure 15. Average plasticity index in sediment cores.
- Figure 16.** Liquid limit versus grain size.
- Figure 17. Plastic limit versus grain size.
- Figure 18. Plasticity index versus grain size.

- Figure 19. Plasticity chart.
- Figure 20. Vane shear strength (kPa) at 1m depth in sediment cores.
- Figure 21. Vane shear strength versus water content.
- Figure 22. Average organic carbon content in sediment cores.
- Figure 23. Average calcium carbonate content in sediment cores.
- Figure 24. Graph of compression index versus liquid limit.
- Figure 25. Graph of effective angle of internal friction versus plasticity index. Solid line shows empirical relation derived by **Lambe** and Whitman (1969); dashed line indicates limits of their data.
- Figure 26. Graph of normalized undrained shear strength versus **overconsolidation** ratio.
- Figure 27. Graph of cyclic stress level versus number of cycles to failure.

LIST OF TABLES

- Table 1. Consolidation test results.
- Table 2. Static triaxial strength test results.
- Table 3. Dynamic triaxial strength test results.

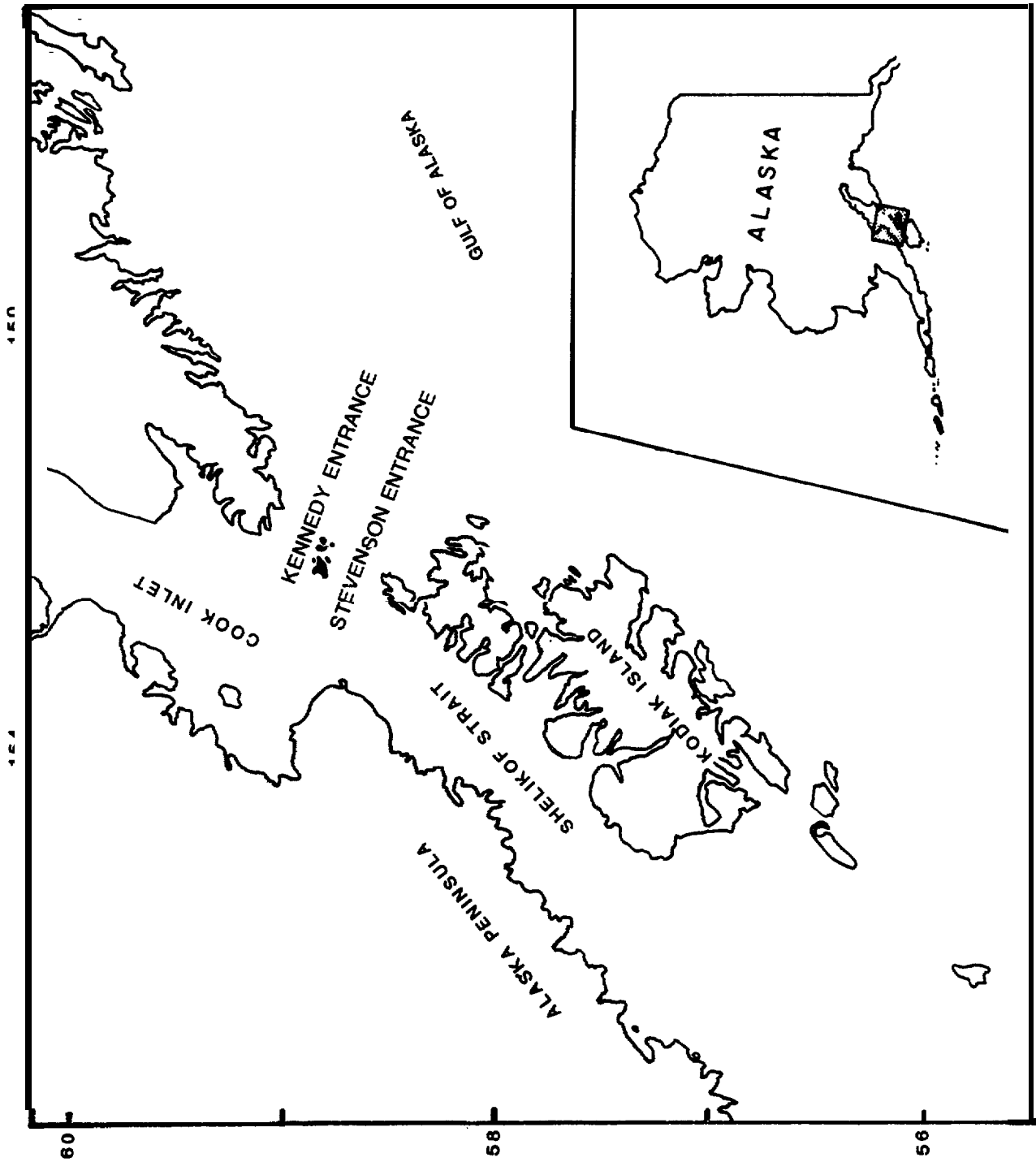
INTRODUCTION

Studies have been conducted by the U.S. Geological Survey to identify geologic conditions that might impose constraints on offshore industrial activities in **Shelikof** Strait, Alaska, an area designated for petroleum leasing (Fig. 1; Hampton and others, 1981; Hampton and Winters, 1981). As part of these studies sediment cores were collected throughout the strait (Fig. 2), and physical properties of sediment samples were measured by laboratory **geotechnical** testing methods. The **geotechnical** data are presented in this report and are evaluated from a regional perspective to infer the reformational response of the sedimentary deposits to static and dynamic loads.

Application of the test data to a regional analysis is restricted by the degree to which core samples are representative of the sedimentary deposits. Interpretive geologic studies indicate that the cores used for geologic testing cover the range of **surficial** sediment types in the Shelikof Strait lease area, but analysis of seismic-reflection profiles reveals the existence of buried stratigraphic units that were not sampled because they lie beneath the maximum core length of 3 m (Hampton and others, 1981; Hampton and Winters, 1981). Therefore, the conclusions reached in this report apply directly to the uppermost deposits in the stratigraphic section, only. Extrapolation beyond the depths of sampling is limited by the vertical uniformity of sediment type.

GEOLOGIC SETTING

Shelikof Strait is a nearly parallel-sided marine channel situated between the Kodiak Island group and the Alaska Peninsula (Fig. 1). The strait marks the location of a northeast-trending inner **forearc** basin that is located



Map of the Gulf of Alaska in Shelikof Strait

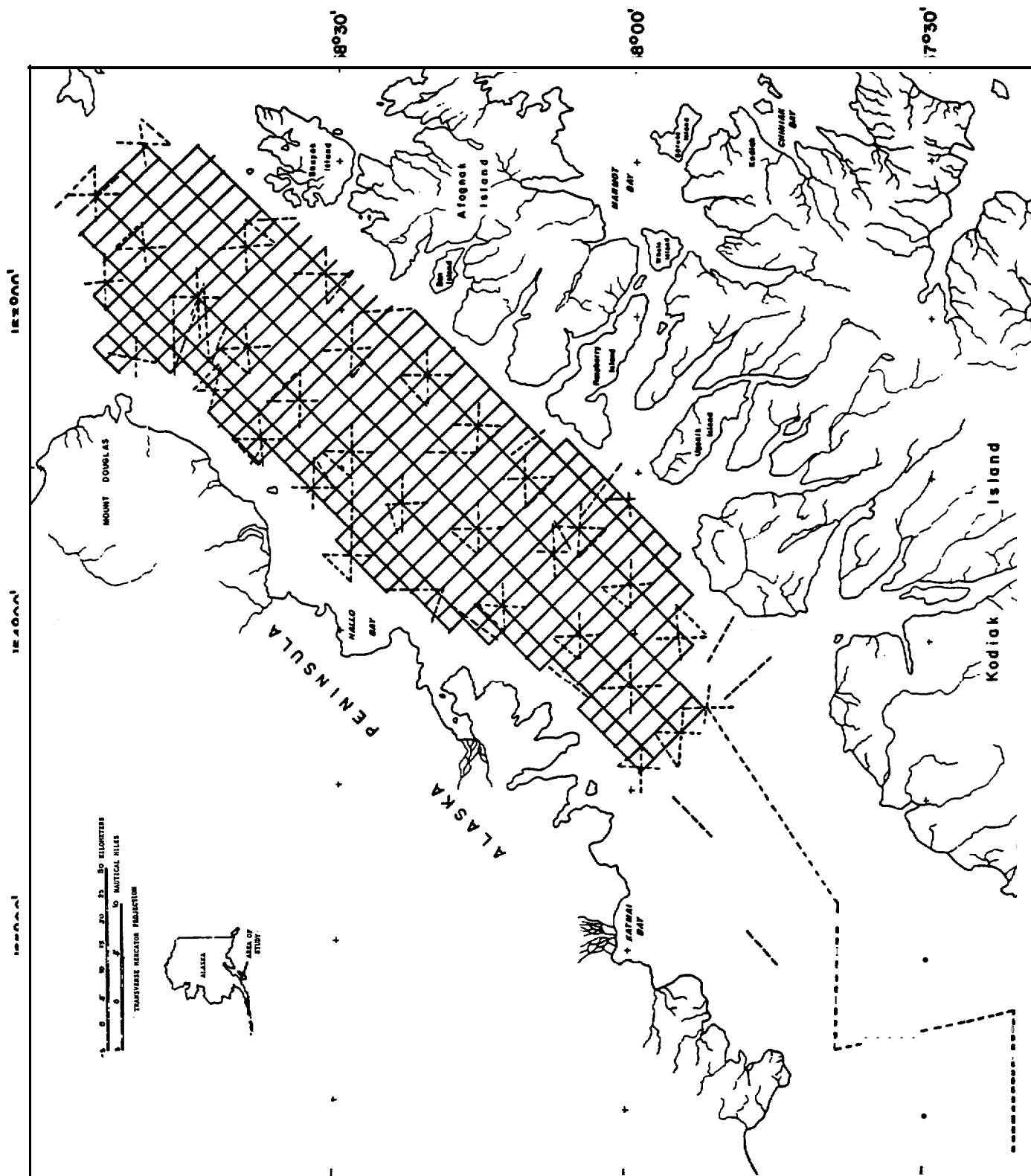


Figure 2-A. Tracklines of continuous seismic-reflection profiles. Solid lines represent a regional survey contracted by the Conservation Division, and dashed lines represent site surveys on cruises of the R/V S.P. LEE (1980) and NOAA ship DISCOVERER (1981).

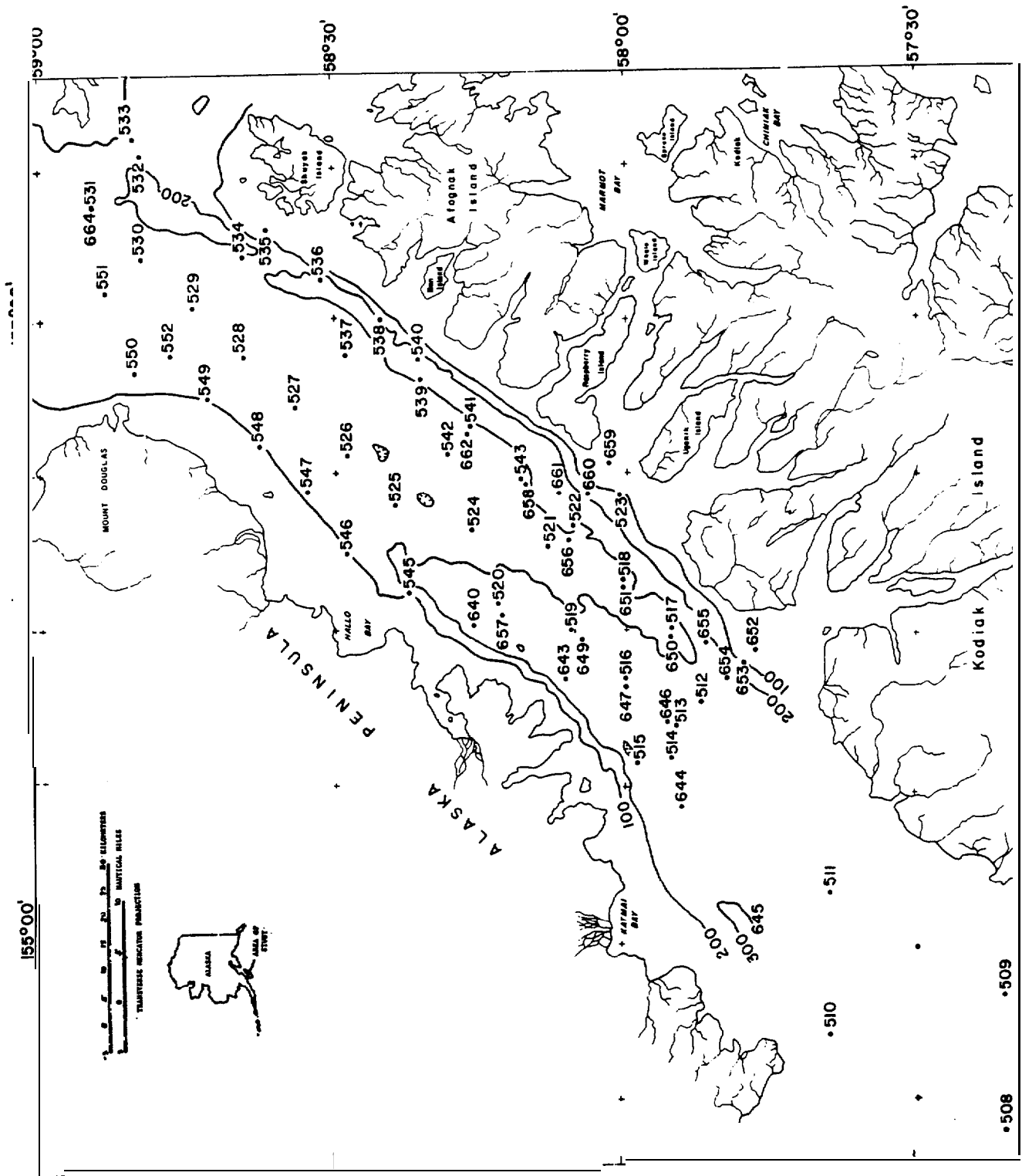


Figure 2-B. Locations of sediment-sampling stations.

near the convergent margin of the North America plate where it is being underthrust by the Pacific plate (von **Huene**, 1979). Large earthquakes are **common** to the region; at least 95 potentially destructive events (magnitude **>6**) have occurred since recording began in 1902. Twelve volcanoes have erupted within the last **10,000** years along the Alaska Peninsula adjacent to the strait.

The seafloor of **Shelikof** Strait consists **of** a gently southwest-sloping central platform bordered by narrow marginal channels parallel to the Kodiak islands and the Alaska Peninsula (Fig. 3). Shallow shelves trend along the adjacent landmasses, and they are connected to the marginal channels by steeply sloping seafloor. Water depth in the northeast part of the strait is generally less than 200 m, whereas in the southwest it generally exceeds 200 m and is as much as 300 m. Superimposed on the platform are some local highs and lows that have **as** much as 100 m relief. Along the axes of the marginal channels are several closed depressions on the order of 30 m relief.

Sedimentary deposits of presumed Pleistocene and Holocene age overlie an irregular unconformity above Tertiary and older bedrock. Thickness of the sediment above bedrock, measured from seismic-reflection profiles, is about 80 to 100 m in the northeast half of the strait and increases abruptly to more **than** 800 m in the southwest (Fig. 4). The thickening reflects a deepening of the unconformity.

Four seismic-stratigraphic units can be distinguished above bedrock (Fig. 5). The lowest unit (unit 1 in Fig. 5) fills the bedrock depression and reaches a thickness of 800 m. This unit is interpreted as being **of** glacial and **glaciomarine** origin (Whitney and others, 1980 a, b). The next highest unit (unit 2 in Fig. 5) is relatively thin (<60 m) and occurs mainly in the

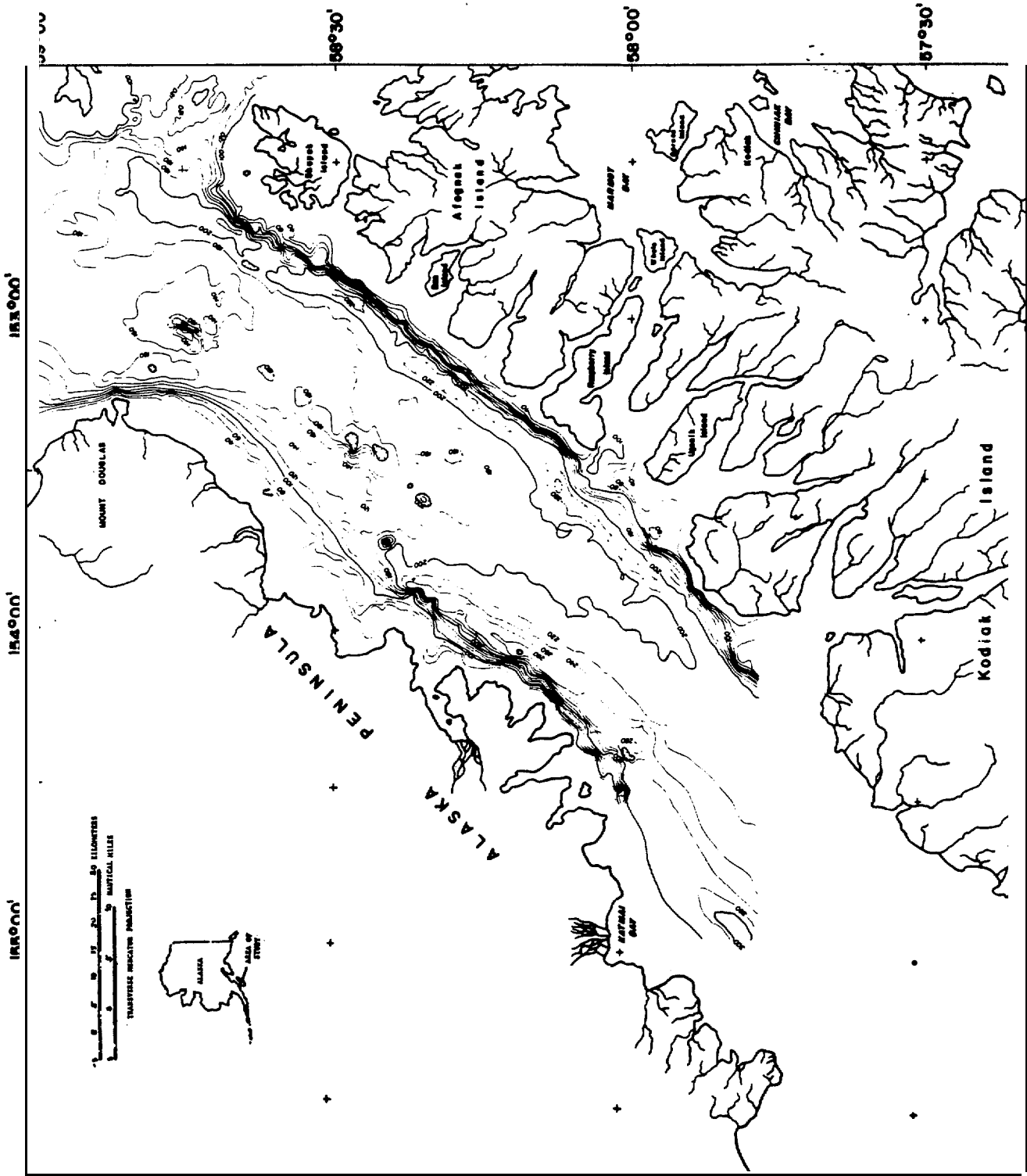


Figure 3. Bathymetry of Shelikof Strait, 20-m contour interval. Depths corrected to mean lower low water.

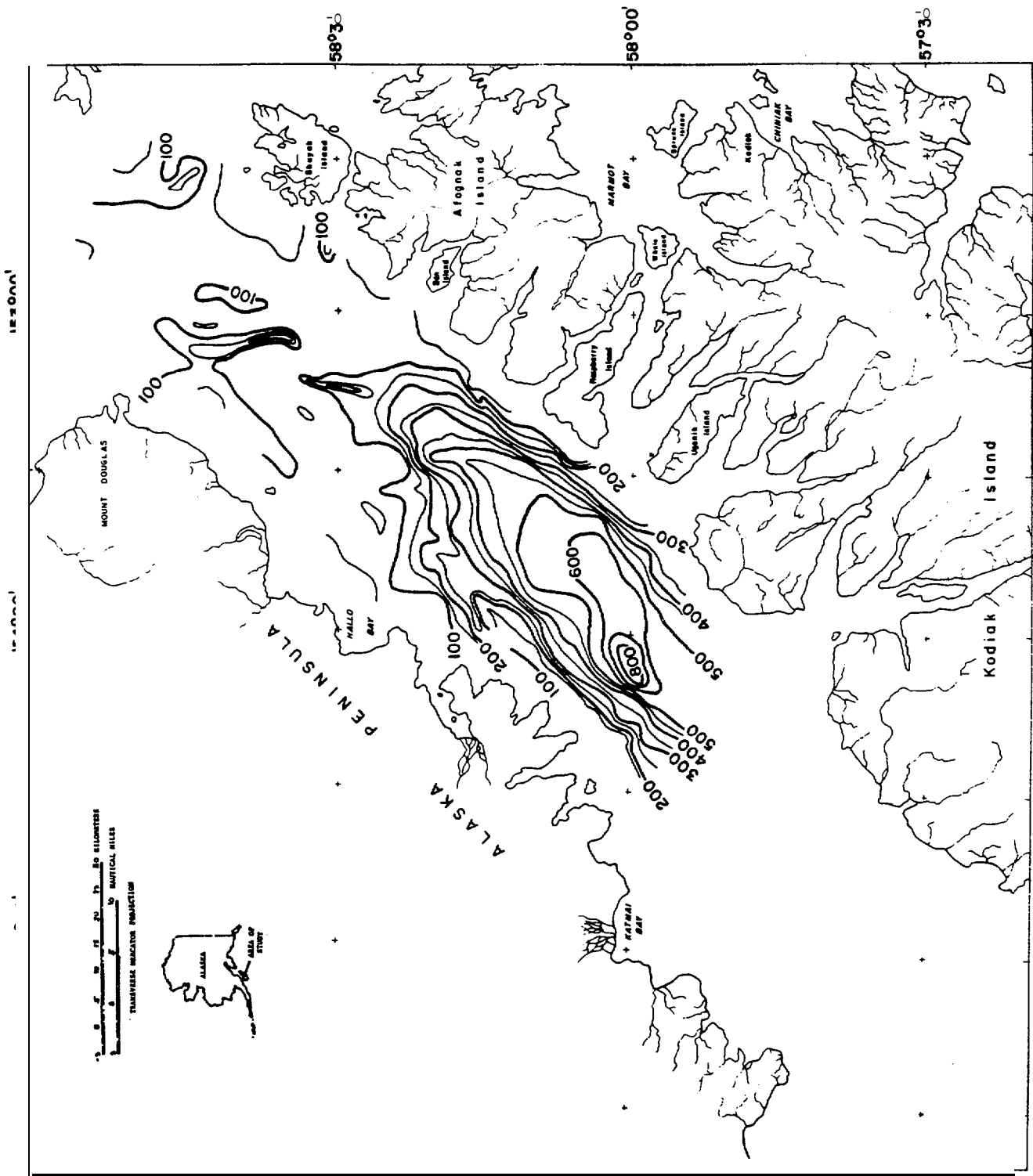


Figure 4. Thickness of sedimentary units of probably Pleistocene and younger age. Contour interval: 50 meters except for thickness greater than 500 m where contour interval is 100 m.

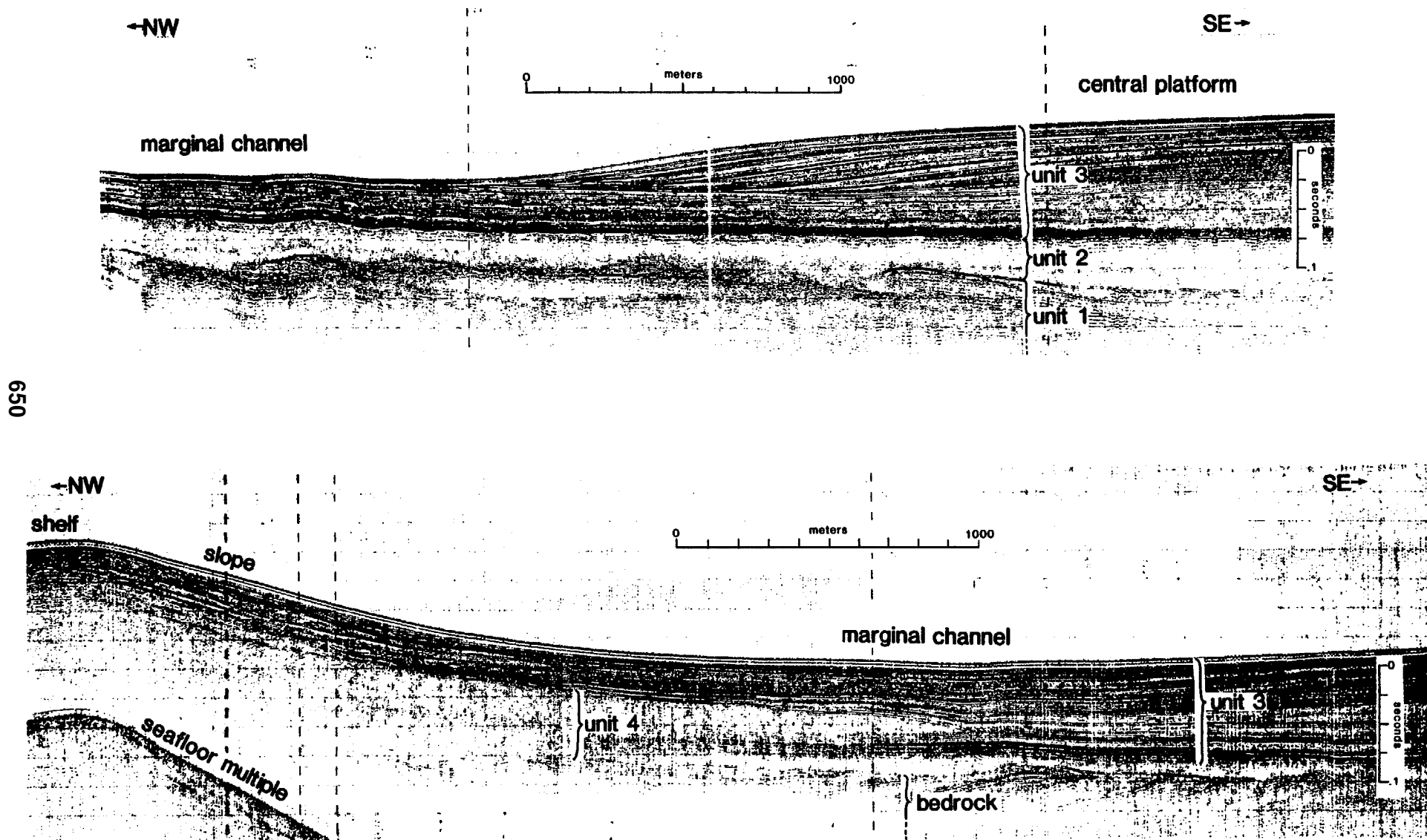


Figure 5. Representative seismic-reflection profiles showing seismic-stratigraphic units.

central part of the strait. Sediment of this unit was deposited within low areas on the upper surface of bedrock and the glacial unit, and it apparently was emplaced by marine processes during the Holocene sea-level rise. The third unit (unit 3 in Fig. 5), which covers essentially all of the seafloor in the central part of the strait (platform and marginal channels), is up to 180 m thick (Fig. 6) and was deposited by the modern-day oceanic current regime of southwesterly **baroclinic** flow from Cook Inlet and the eastern Gulf of Alaska (**Muench** and Schumacher, 1980). Unit 4 in Figure 5 underlies the shallow shelves and interfingers seaward with unit 3. It is composed of sediment eroded from the adjacent landmasses. The cores subjected to **geotechnical** testing and discussed in this paper were taken from unit 3.

METHODS

Sediment cores were collected at 65 stations on two cruises in **Shelikof** Strait, in June 1980 aboard the USGS **R/V S.P. LEE** and in July and August 1981 aboard the NOAA ship **DISCOVERER** (Fig. 2). A gravity coring system with 8.5-cm diameter plastic liners in steel core barrels was used on the 1980 cruise, whereas a **vibracoring** system with a 10-cm square cross-section plastic liner in thin-wall stainless steel barrel was employed on the 1981 cruise. Some grab samples were taken at locations **of** coarse sediment where the coring devices were ineffective.

Two cores were taken at most stations. One was designated mainly for geological analysis. It was cut into 1-m or 1.5-m-long sections, then split lengthwise for geological description and vane-shear strength testing. **Subsamples** were taken for index property determinations.

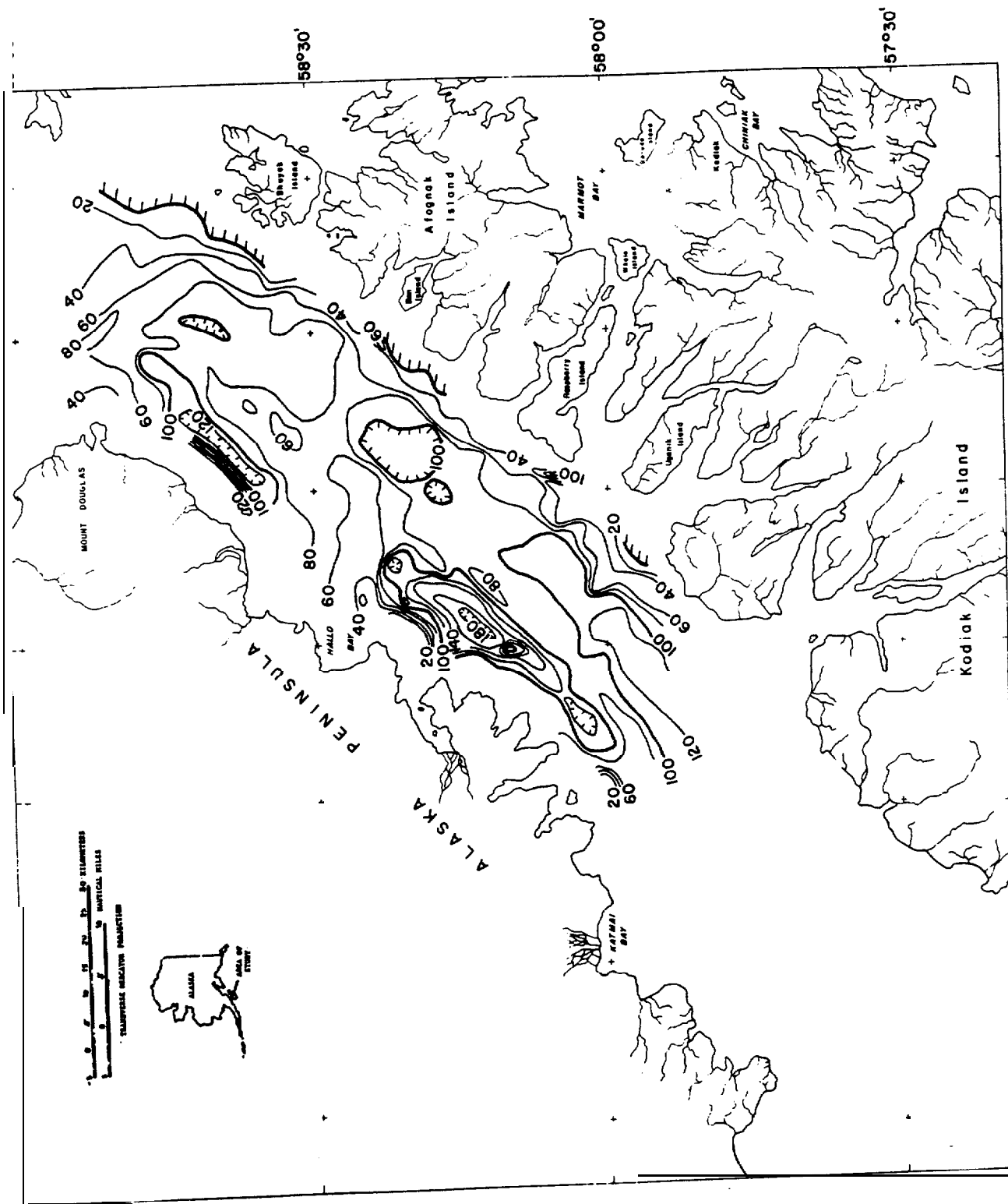


Figure 6. Thickness of highest seismic-stratigraphic unit that covers most of the seafloor of Shelikof Strait. contour interval: 20 m.

The second core was taken expressly for **geotechnical** testing. It was cut into 1-m-long sections, wrapped in cheesecloth, covered with microcrystalline wax, and stored upright in a refrigerator. These cores were later subjected to a suite of **geotechnical** tests in laboratories at the USGS and at a commercial testing company.

Several index properties were determined for **subsamples** of the sediment cores. Grain size was measured by sieving and pipetting into four size classes: gravel (>2 mm), sand (2-0.062 mm), silt (0.062-0.004 mm), and clay (<0.004 mm). Water content, as a percentage of dry sediment weight, was determined from the weight of sediment samples before and after even drying at **105°C**. A correction for salt content of sea water (3.5%) was made to the weighings. Atterberg limits were determined according to standard procedures (American Society for Testing and Materials, 1976), except that samples were not sieved prior to testing. Carbon content was measured with a LECO carbon determinator with induction furnace and acid digestion. Vane shear determinations of undrained shear strength were made on split core halves with a motorized device at a vane rotation rate of **90°/min**. The vane is 1/2 inch diameter by 1/2 inch high and was inserted into the sediment to a depth twice the height of the vane.

Consolidation tests were run on **subsamples** from **geotechnical** cores to determine sub-failure reformational properties. Most tests were run on an oedometer in a stress-controlled mode (**Lambe**, 1951). Others were run in a **triaxial** loading cell under constant rate of strain conditions (**Wissa** and others, 1971). The consolidation tests measure change in volume with change in applied load. The results are normally plotted as void ratio ($e = \text{volume of voids} / \text{volume of solids}$) versus the logarithm of effective (buoyant)

vertical stress (p'). Two useful parameters are derived from these curves: the compression index and the maximum past pressure. The compression index (**Cc**) is the slope of the straight-line portion of the e -log p' curve and indicates the amount of compression produced by a particular load increment. The maximum past pressure (σ'_{vm}) is the greatest effective overburden stress to which the sediment has ever been exposed and is determined from the e -log p' curve by a simple graphical construction (Casagrande, 1936). The ratio of σ'_{vm} to the effective overburden stress at the time of sampling (σ'_{vo}) is the overconsolidation ratio (OCR), which is a measure of unloading that the sediment may have experienced, by erosion for example. A third parameter, the coefficient of consolidation (c_v), is determined for each load increment of the one-dimensional consolidation test and is related to the rate of consolidation.

Static **triaxial** tests were run on cylindrical samples 3.6-cm diameter and 7.6-cm long in order to determine strength properties of the sediment. Tests were run under undrained conditions with pore pressure measurements (Bishop and Henkel, 1964). Most samples were consolidated **isotropically** prior to testing, but some were consolidated **anisotropically**.

Dynamically loaded triaxial tests were also run, with the axial stress on samples varied **sinusoidally** at 0.1 Hz. Both compression and tension were applied at a predetermined percentage of the static strength. These tests can be used to evaluate the failure conditions of sediment under repeated loading, such as by earthquakes.

A first set of **triaxial** tests was run on sediment samples that were consolidated to somewhat arbitrary stress levels. However, the later testing program followed the normalized stress parameter (**NSP**) approach (Ladd and

Foott, 1974), whereby consolidation stresses are chosen on the basis of maximum past pressure (σ'_{vm}), as determined from consolidation tests. Typically, the **triaxial** test specimen was consolidated to four times σ'_{vm} , which eliminates some of the disturbance effects associated with coring. **Overconsolidation** was artificially induced in some tests by rebounding the specimen to lower stress levels before applying the **triaxial** load. Measured values of undrained shear strength (S_u) are normalized with respect to effective overburden stress (σ'_v). A premise of the NSP method is that the ratio S_u/σ'_v is constant for a particular value of **OCR**. Moreover, a relation exists between S_u/σ'_v and **OCR** that allows prediction of sediment strength at depths below the level of sampling (Mayne, 1980).

RESULTS

Sediment description, index properties: Sediment samples could only be collected to shallow depths (<3 m) beneath the seafloor. Therefore, most are from the highest **stratigraphic** unit (unit 3, Fig. 5). However, judging from seismic-reflection profiles over sampling stations, a few outcrops of other units were also sampled. Seismic-reflection profiles also show that unit 3 has a typical thickness of about 80 to 100 m (Fig. 6). The appearance of acoustic reflectors within this unit indicates some **lithologic** variability with depth, but there is no reason to suspect radical changes in sediment type, except for possible thin beds of volcanic ash. The physical properties for the cores should therefore be representative of the terrigenous component of the unit as a **whole**, but drill-hole samples would be necessary to confirm this.

The texture of **surficial** sediment on the central platform and in the adjacent marginal channels grades from gravelly and sandy material in the northeast part of the strait to mud in the southwest (Figs. 7 and 8; Appendix). A general fining trend from northwest to southeast across the platform also exists.

The two grab samples of coarse sediment recovered from Stevenson Entrance appear to have been taken from outcrops of unit 1. Most of the coarse **clasts**, which range to boulder size, are angular to subangular, and some are faceted. This supports the hypothesis that unit 1 was deposited by glacial processes.

A few grab samples of coarse material were also recovered from the shallow shelves and from the adjacent slopes. They probably are from unit 4. Coarse **clasts** have similar morphology to those from unit 1, perhaps reflecting glacial transport at some point in their history.

Sediment cores from the platform and marginal channels in the central portion of the strait have a fairly uniform stratigraphy with depth. Sandy sediment in the northeast end of the strait is predominantly greenish-gray, with variations from black to yellowish brown. Sand-filled burrows, pebble **clasts**, and whole or broken shells are common. In progressively finer-grained cores to the southwest, color remains greenish-gray but is less varied, and shells and **clasts** are rare.

A layer of volcanic ash occurs in many cores. Maximum thickness of the layer is nearly 20 cm. It is size-graded, with the coarsest basal fragments a few millimeters diameter. The color is from tan to white with a pink cast. The refractive index of the ash is 1.485 ± 0.002 , which in this region is unique to the outfall from the 1912 **Katmai** eruption (**Nayudu**, 1964; Pratt and others, 1973). Depth of the ash beneath the seafloor was used to calculate

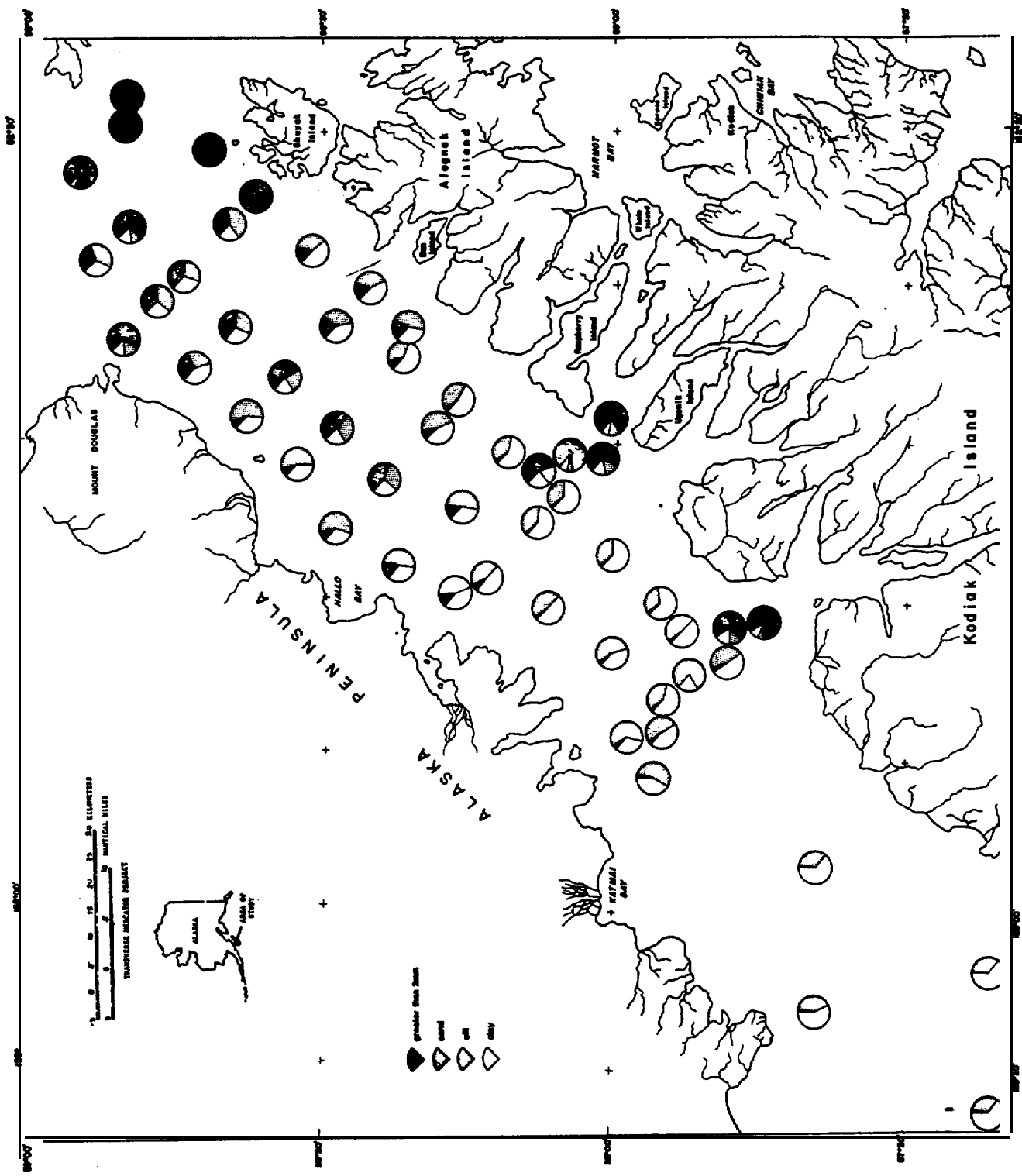


Figure 7. Pie-diagrams showing relative abundances of textural classes in seafloor sediment samples.

values of post-1912 **sediment accumulation rate (Fig. 9)**. **Accumulation rate varies significantly throughout the** strait. It is greatest near the Alaska Peninsula at the southwest end of the strait, whereas it is near zero at places in the marginal channel along the Kodiak island group.

Water content of sediment is shown in Figure 10 as interpolated values at 1-m depth in cores. It is calculated as a percentage **of** dry sediment weight, and therefore, values in excess of 100% are possible if the weight of water exceeds the weight of sediment grains. **Water content generally decreases to the northeast, inversely correlating with grain size. Moreover, water content increases across the strait, from the Alaska peninsula to Kodiak Island.** Bulk sediment density at 1-m depth, which is calculated from water content and grain specific gravity, correspondingly decreases down and across the strait (Fig. 11). Average grain specific gravity itself shows no discernible trend (Fig. 12).

Atterberg limits describe the plasticity of sediment, in terms of the liquid limit (water content that separates plastic and liquid behavior) and the plastic limit (water content that separates semi-solid and plastic behavior). Useful derivatives are the plasticity index (difference between the liquid and plastic limits), and the liquidity index (position of the natural water content relative to the liquid and plastic limits). Certain trends in plasticity are evident in **Shelikof Strait**. Average liquid limit, plastic limit, and plasticity index increase down the strait toward the southwest, and also generally across the strait, toward the southeast (Figs. 13, 14, and 15; Appendix). These properties also generally increase with decrease **in** mean grain size (Figs. 16, 17, and 18), although **the** data for plastic limit are quite scattered. Plastic limit is **less** variable than liquid limit, which is typically the case (Mitchell, 1976; Richards, 1962).

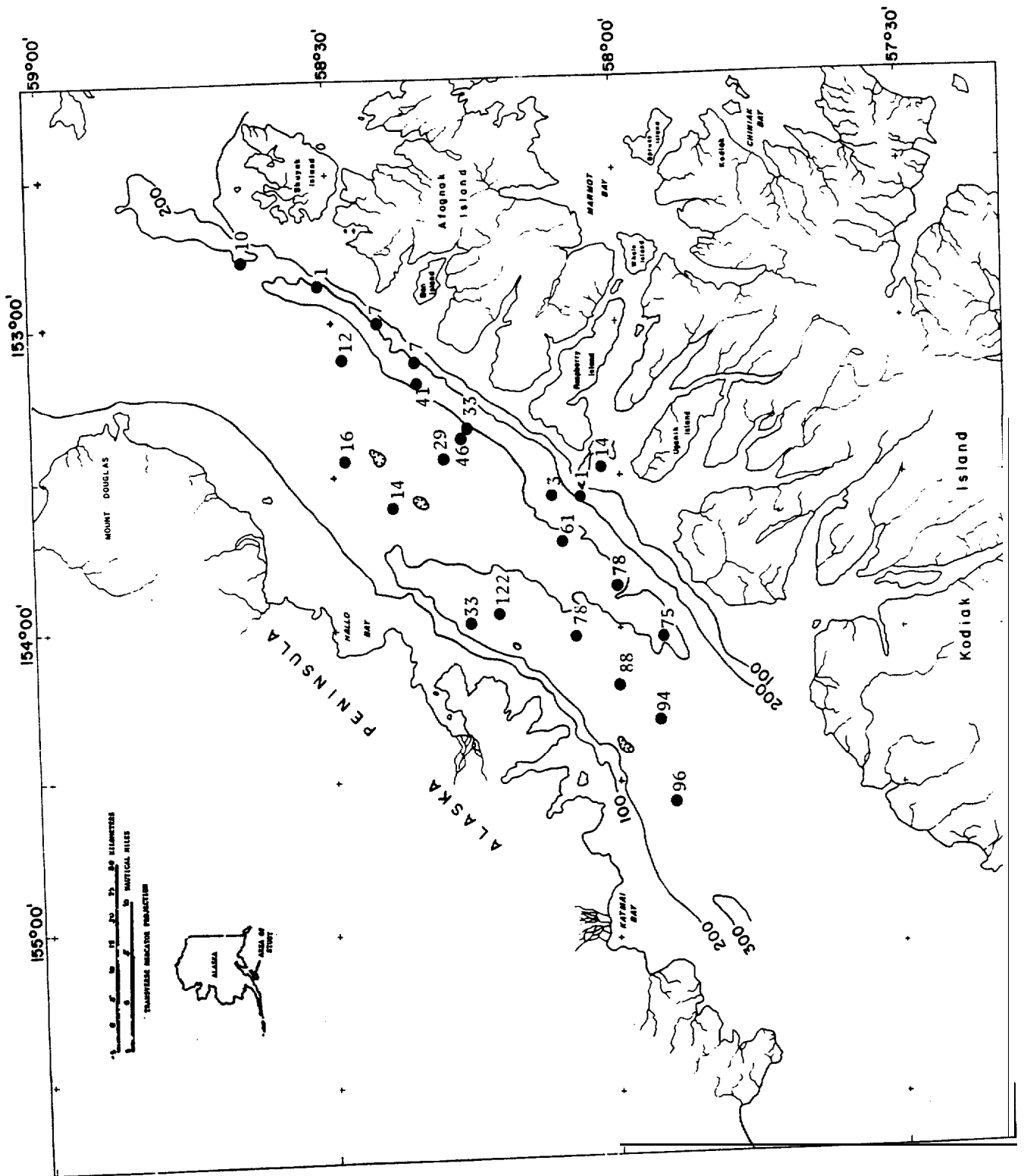


Figure 9. Sediment accumulation rates, in cm/100 yr.

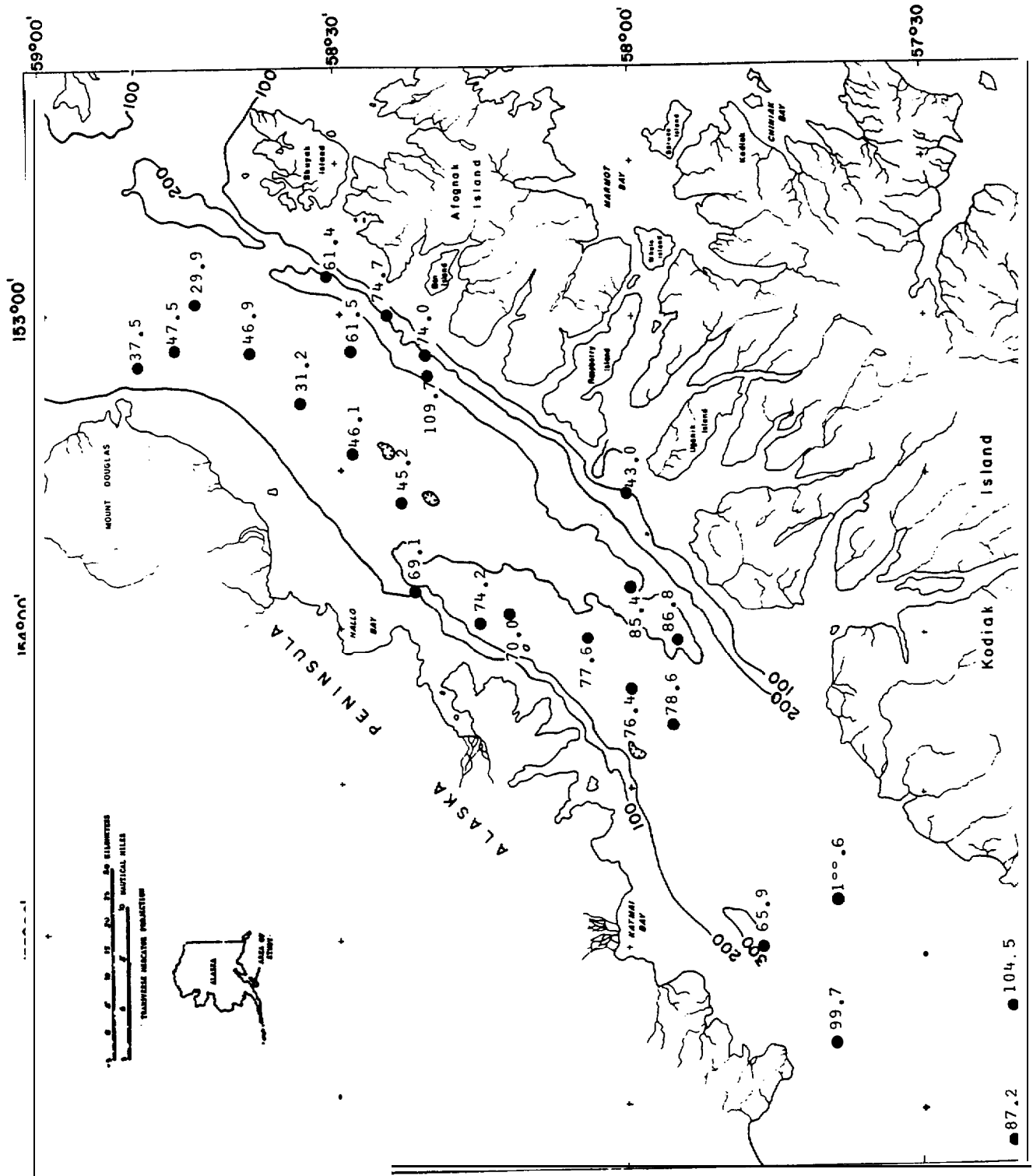


Figure 10. Water content (percent dry weight) at 1-m depth in sediment cores.

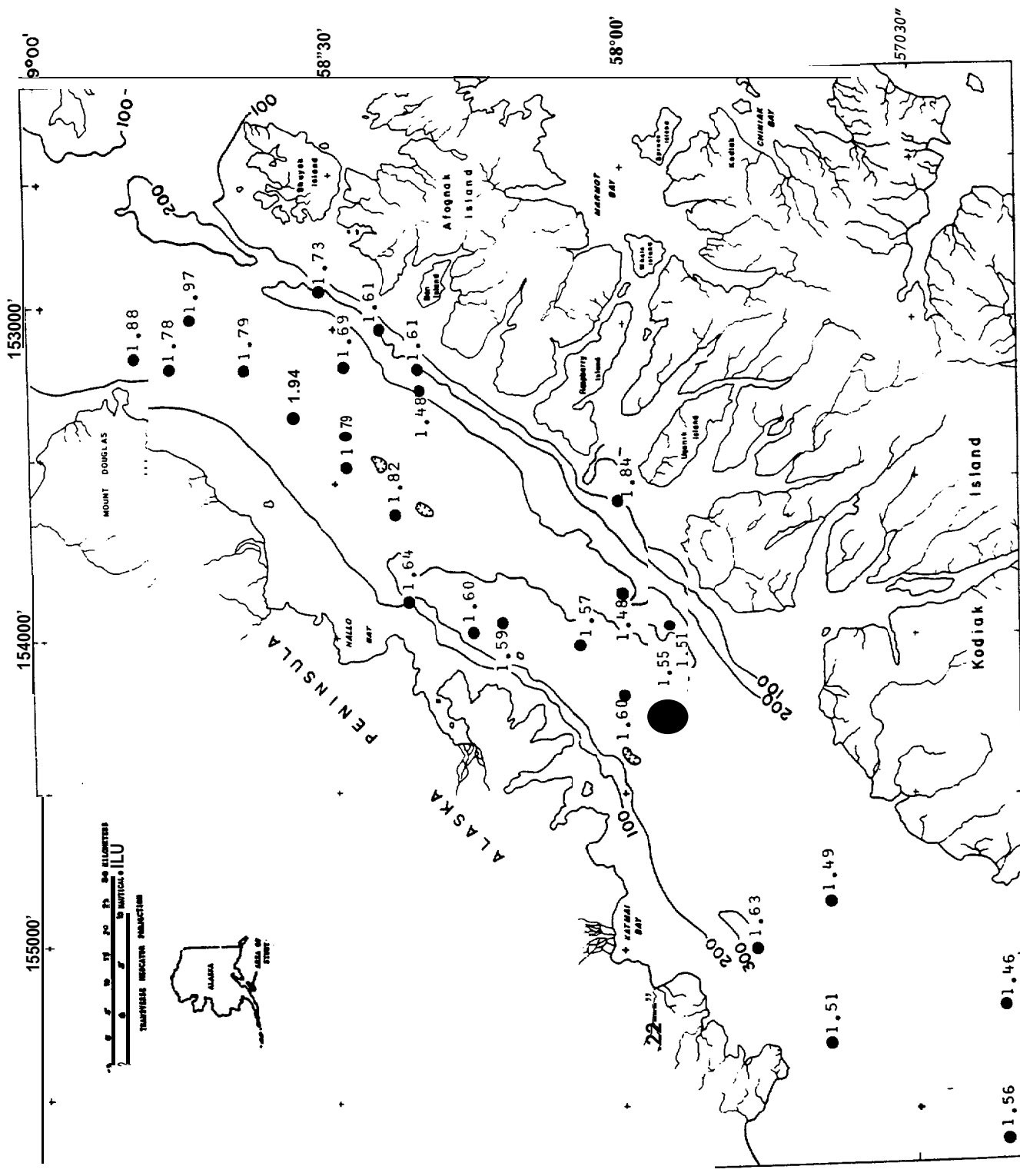


Figure 1. Bulk sediment density (gm/cm^3) at 1-m depth in sediment cores

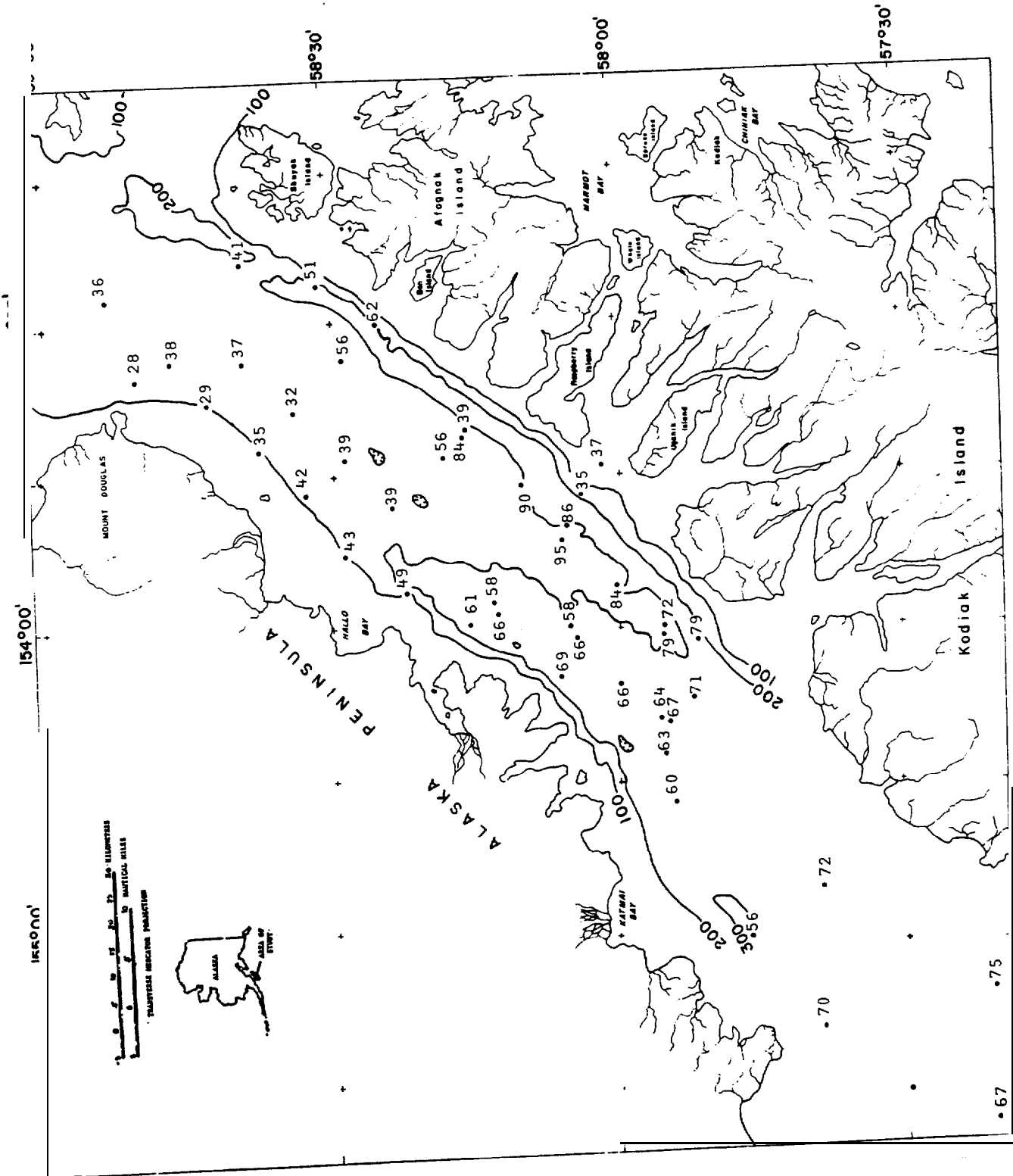


Figure 13. Average liquid limit (percent dry weight) in sediment cores.

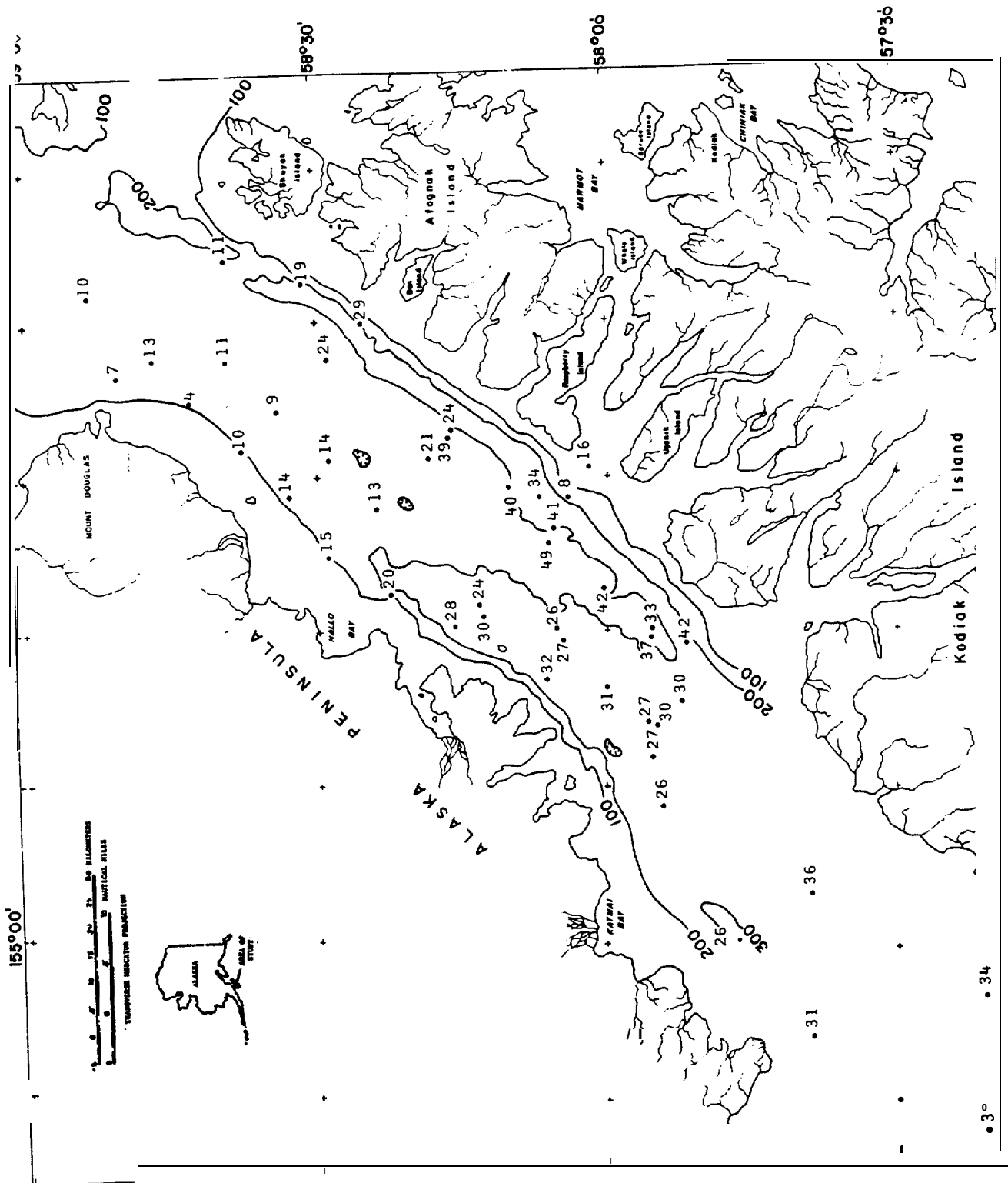


Figure 15. Average plasticity index in sediment cores.

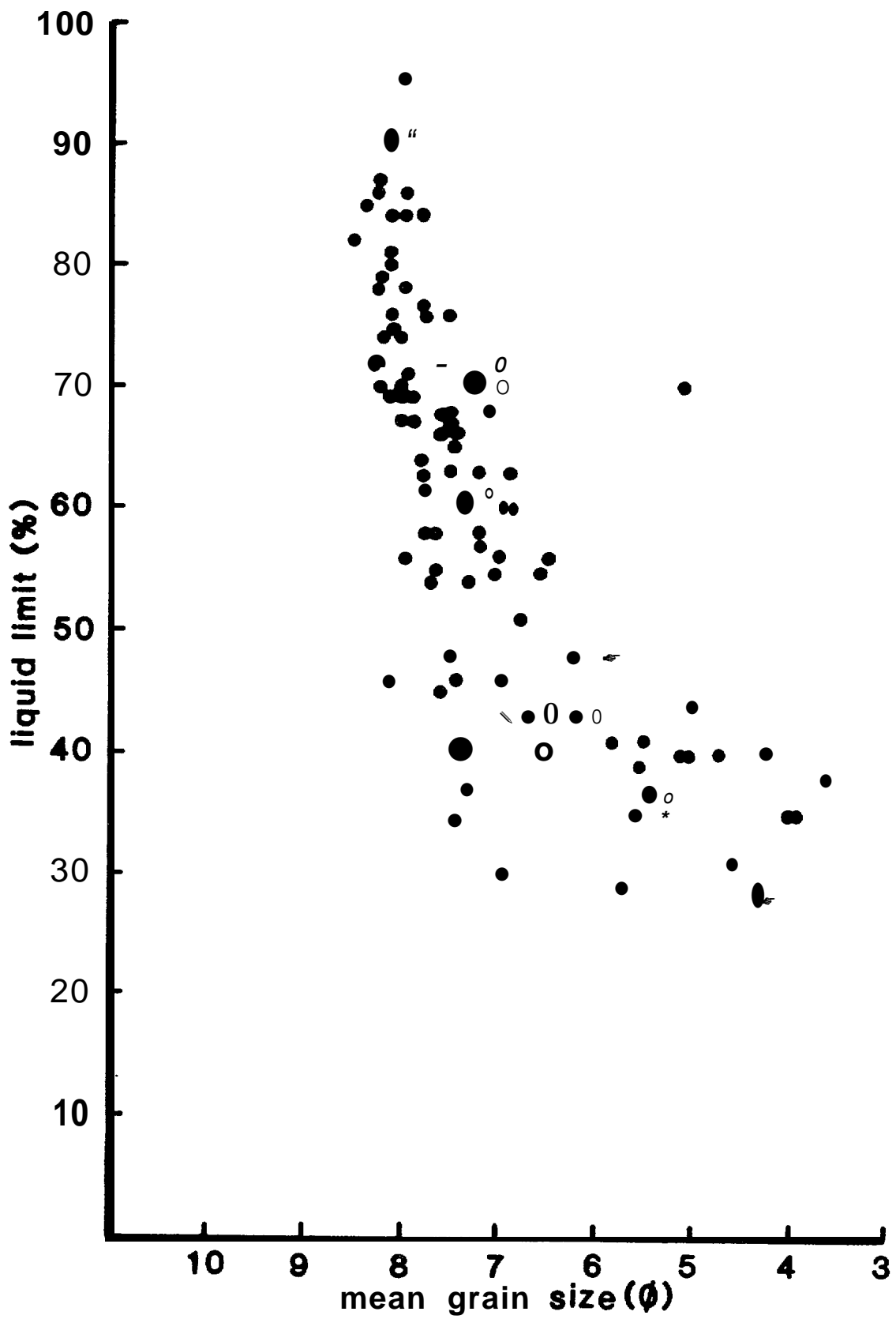


Figure 16. Liquid limit versus grain size.

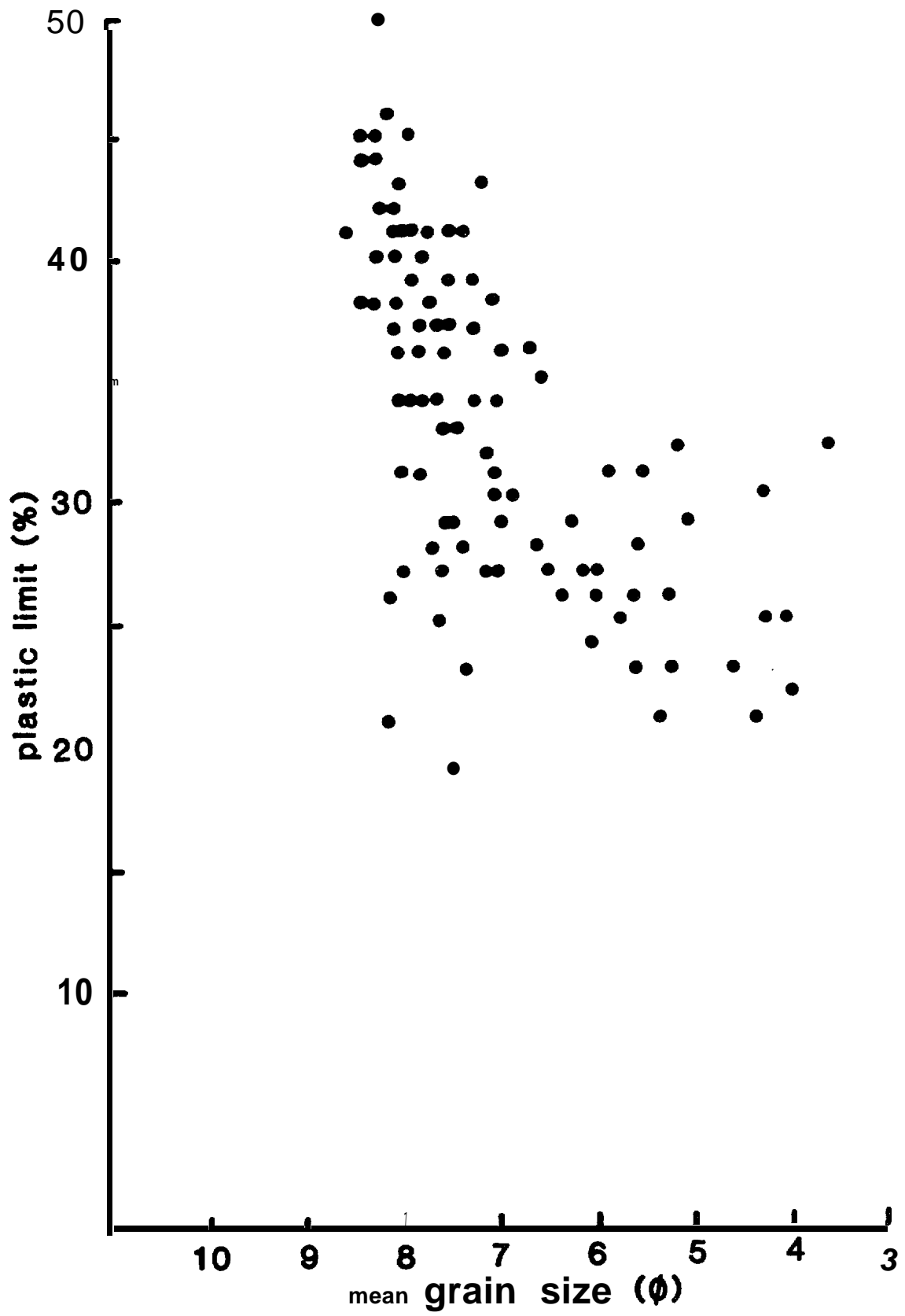


Figure 17. Plastic limit versus grain size.

Correlations have been made between liquid limit and compressibility (Herrmann and others, 1972; Skempton, 1944). The majority of Shelikof Strait samples fall within the medium ($30 < \text{liquid limit} < 50$) and high (liquid limit >50) compressibility ranges.

Nearly all measured liquidity indices in Shelikof Strait are greater than 1 (Appendix), which is usual for near-seafloor marine sediment. Sediment with a liquidity index greater than one behaves as a liquid when remolded.

A plot of liquidity index versus plasticity index - termed a plasticity chart (Casagrande, 1948) shows a trend parallel to the A-line that divides basic soil types (Fig. 19). Most sediment samples from Shelikof Strait plot below the A-line, which is typical of inorganic silt and silty clay of high compressibility. The linear trend of data points is expected for samples taken throughout the same sedimentary deposit (Terzaghi, 1955; Richards, 1962).

Undrained shear strength of sediment samples (S_u), as measured with a laboratory miniature vane shear device, generally decreases toward the southwest end of the strait, and thus correlates with the water content trend, although there is much scatter (Figs. 20 and 21; Appendix). The consistency of most of the near-seafloor sediment can be classified as very soft ($S_u < 12$ kilopascals), but some is soft ($12 \text{ kPa} < S_u < 24 \text{ kPa}$) to medium ($24 \text{ kPa} < S_u < 48 \text{ kPa}$) (Terzaghi and Peck, 1948). Hampton and others (1981) showed that shear strength is anisotropic in Shelikof Strait sediment cores. Values of shear strength measured with the axis of vane rotation perpendicular to the axis of core samples exceed the values of strength measured with the axis of vane rotation parallel to the core axis. The magnitude of sediment strength thereby depends on the orientation of the applied stress.

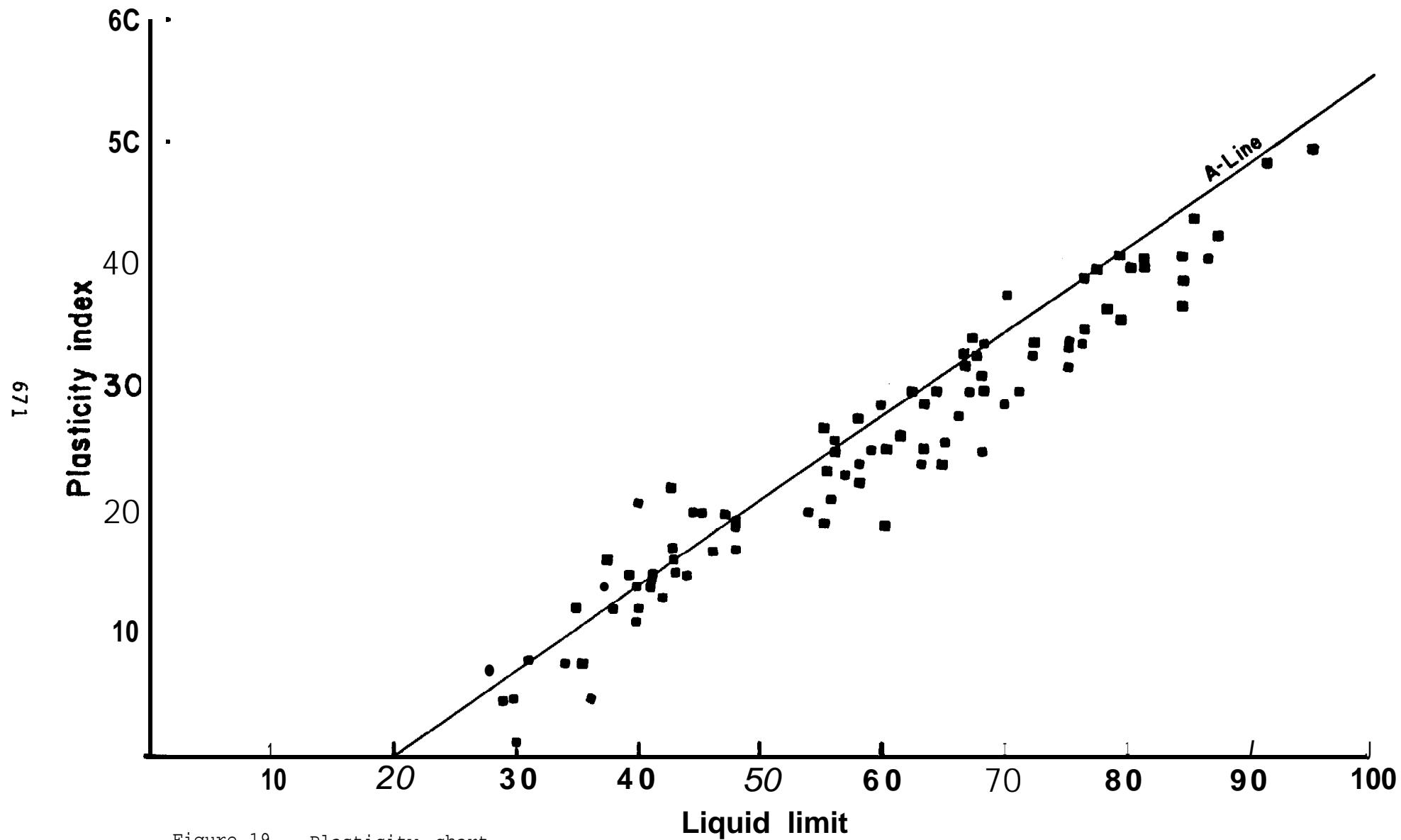


Figure 19. Plasticity chart.

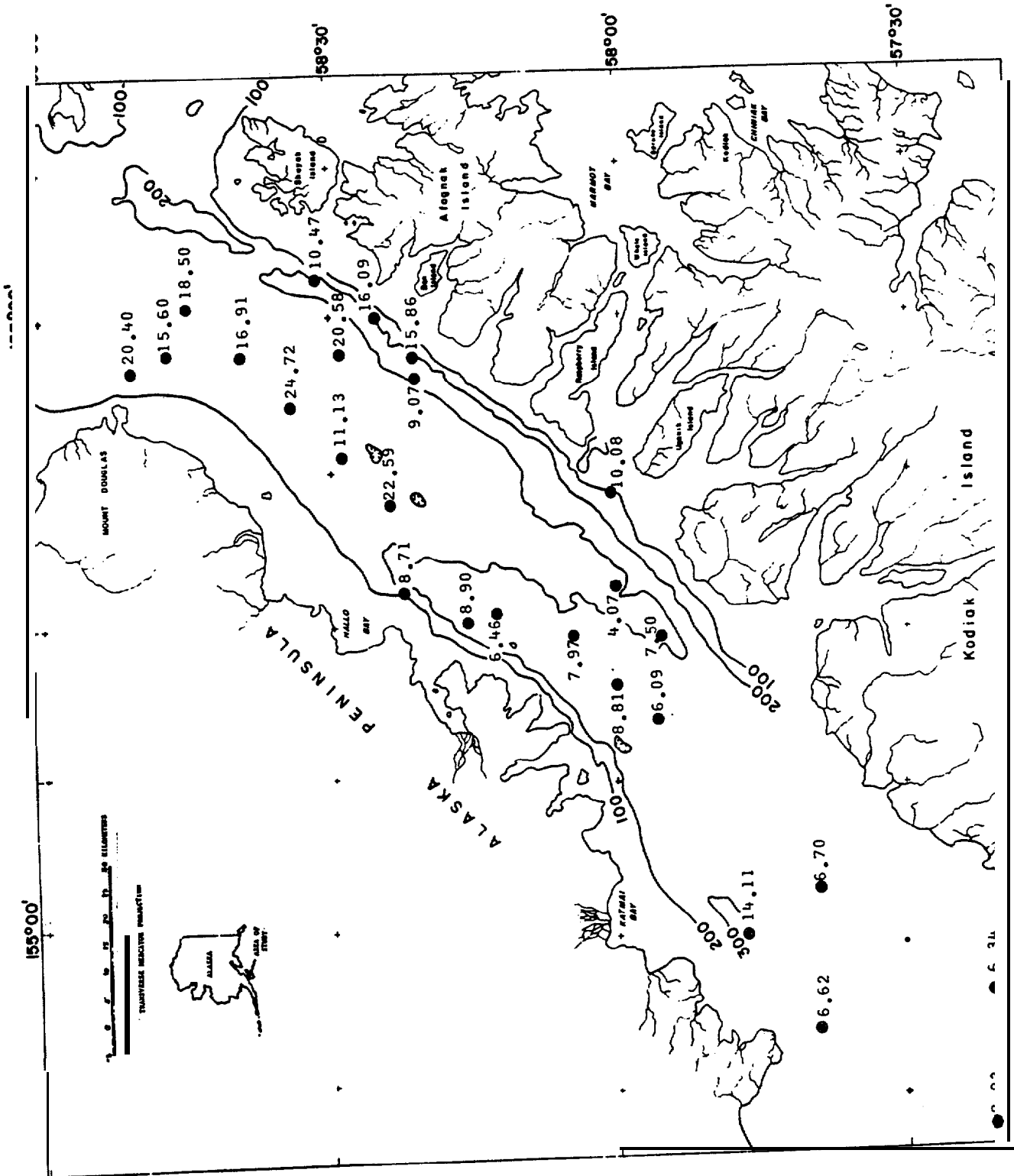


Figure 20. Vane shear strength (kPa) at 1m depth in sediment cores.

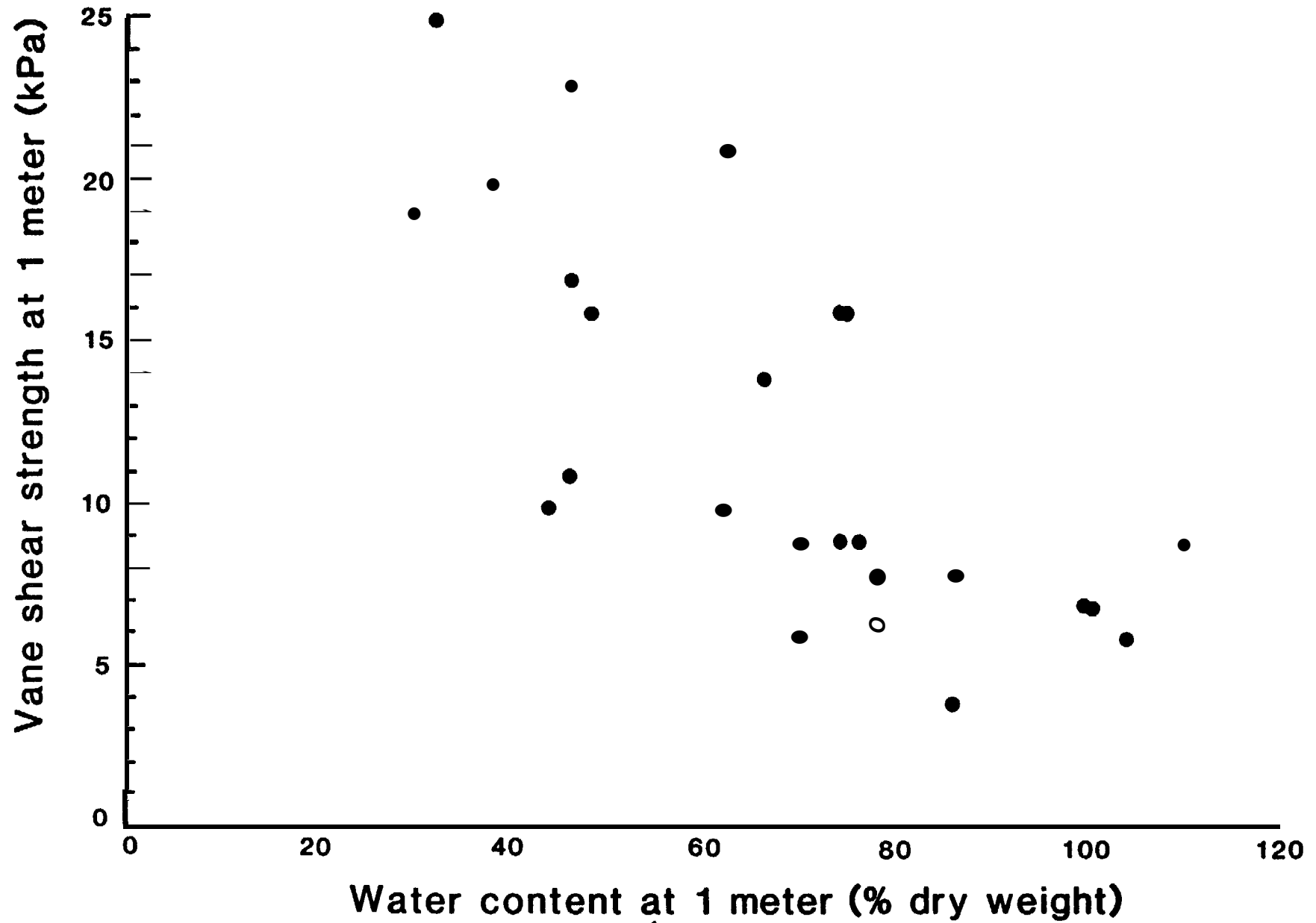


Figure 21. Vane shear strength versus water content.

Sediment samples from Shelikof Strait are characterized by low to intermediate content of organic carbon, compared to other marine areas (Bordovskiy, 1965, 1969; Gardner and others, 1980; Lisitzin, 1972; Rashid and Brown, 1975). Most values are between 0.40% and 1.50%. Organic carbon generally increases down the strait toward the southwest, as well as across the strait toward the southeast (Fig. 22; Appendix A). Correlations with other physical properties were shown by Hampton and others (1981). Organic carbon content correlates positively with water content and plasticity index, whereas an inverse correlation is found with grain size and vane shear strength. Correlations similar to those described above have been reported by others for low organic-carbon content sediment (Bordovskiy, 1965, 1969; Bush and Keller, 1981; Keller and others, 1979; Lisitzin, 1972; Mitchell, 1976; Odell and others, 1960).

Percent calcium carbonate is typically low in Shelikof Strait sediment (Fig. 23; Appendix). Most values are less than 3.50%. Two locations with anomalously high values, off Shuyak Island and in Stevenson Entrance, are near the boundary of the strait.

Consolidation properties: Consolidation properties as determined from laboratory tests are listed in Table 1. All tests indicate a maximum past pressure (σ'_{vm}) greater than the present overburden pressure (σ'_{vo}). The ratio $\sigma'_{vm}/\sigma'_{vo}$ is the overconsolidation ratio (OCR) and is greater than 1.0 for all tests. The usual implication is that the sediment has experienced unloading as a consequence of erosion. However, there is no geological evidence for erosion; in fact, sediment is accumulating at high rates throughout most of the strait (Fig. 9). The high values of OCR probably

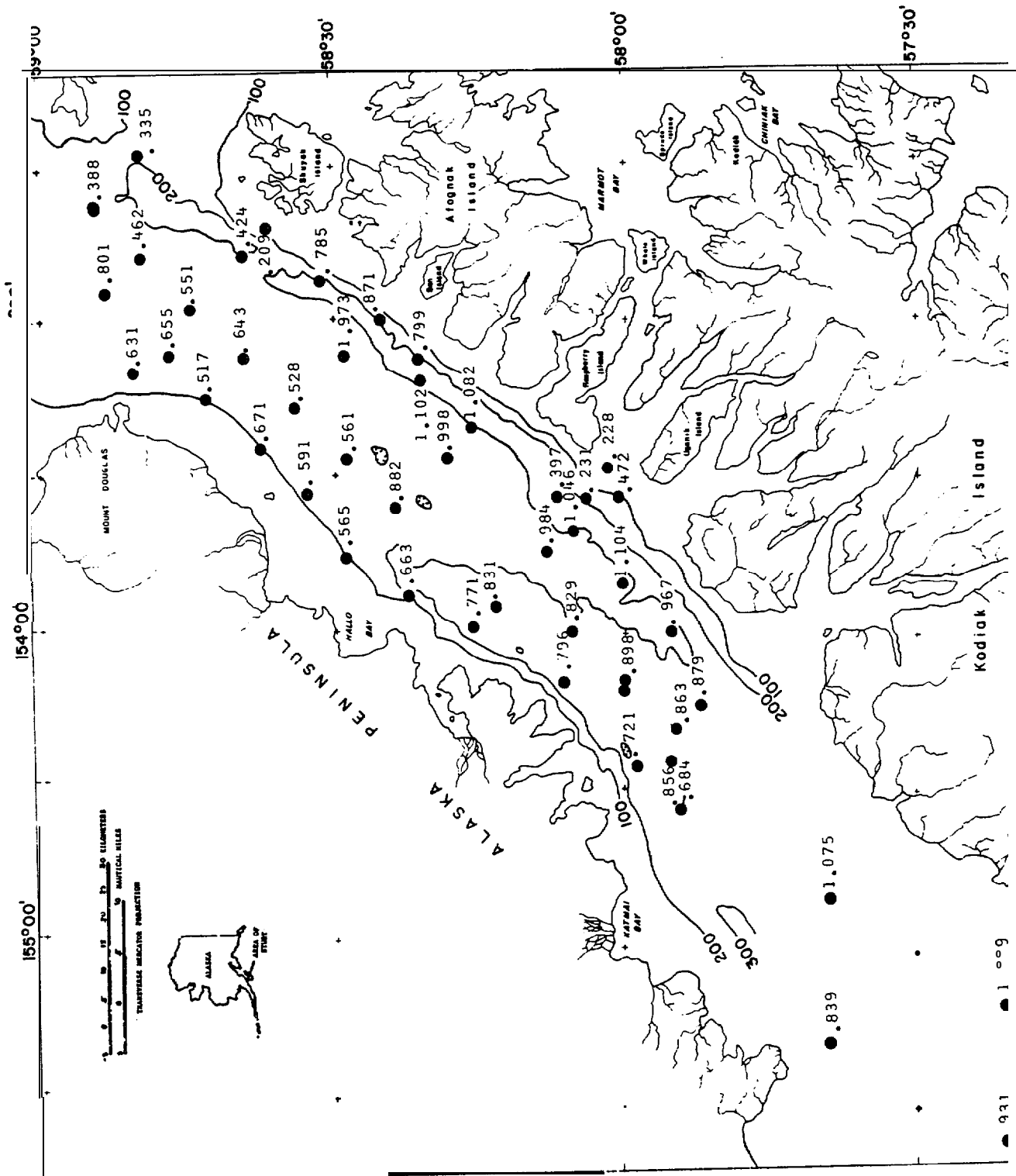


Figure 22. Average organic carbon content in sediment cores.

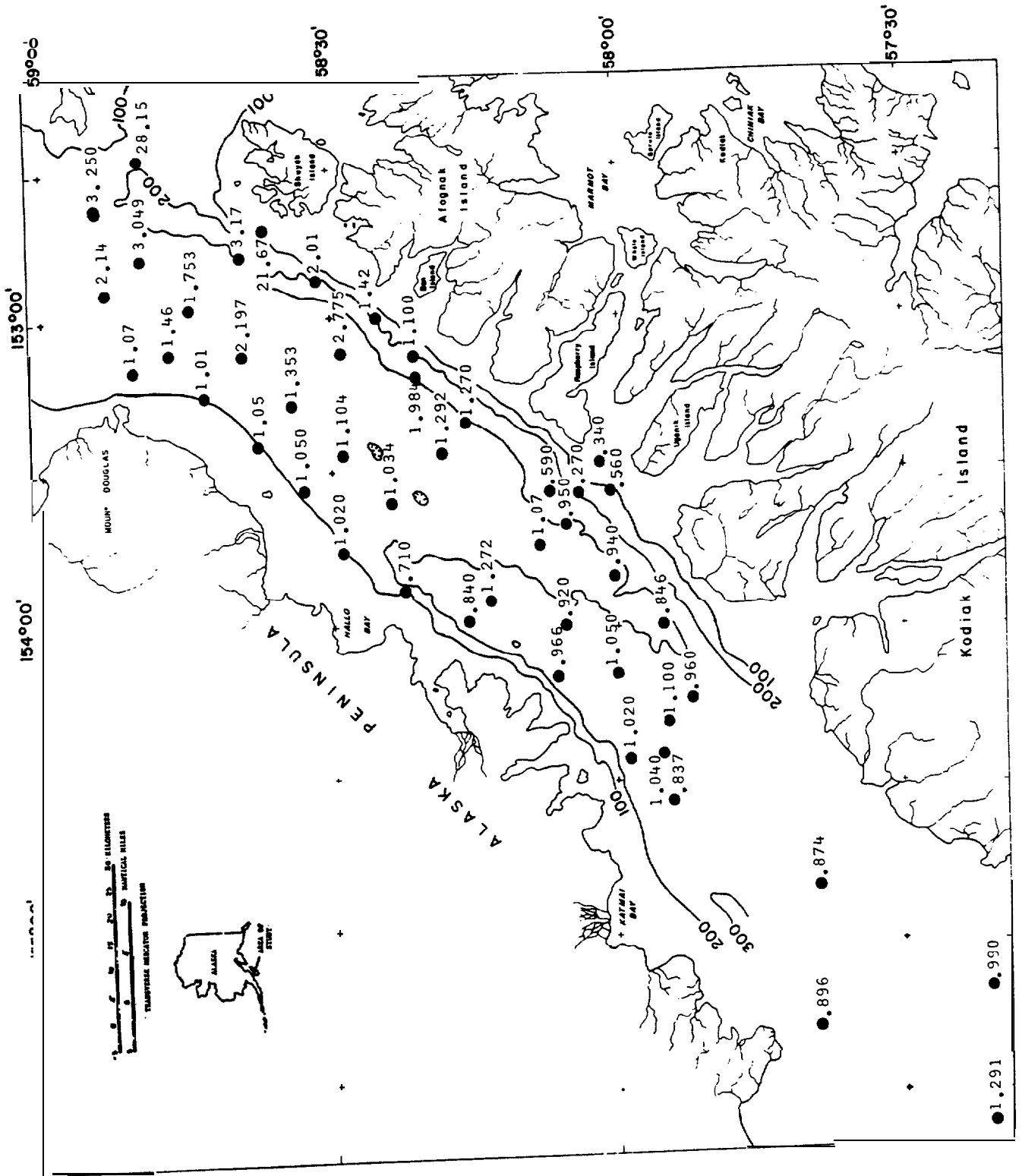


Figure 23. Average calcium carbonate content in sediment cores.

Table 1. Consolidation test results.

Station number	Depth in core (cm)	σ_{vo} (kPa)	σ'_{vm} (kPa)	CC	$c_v \times 10^{-2}$ (cm^2/sec)		OCR
					from	to	
507	39	1.1	6.0	0.94	0.17	1*10	5
	171	5.0	32.0	0.76	0.22	1.13	6
509	89	3.7	20.0	0.86	0.27	2.67	5
	94	3.7	23.0	0.88	0.12	0.81	6
511	64	2.8	15.0	0.52	0.05	2.17	5
	111	4.6	9.0	0.66	0.09	1.10	2
	191	9.8	12.0	0.45	0.18	1.38	1
649	41	2.0	56.0	0.33	0.04	1.30	28
	116	6.1	30.0	0.54	0.12	0.97	5
	167	8.9	29.0	0.60	0.08	1.40	3
525	45	3*3	26.0	0.30	0.30	1.52	8
	96	6.9	28.0	0.26	0.35	1.68	4
	165	13.8	64.0	0.26	0.54	2.23	5
528	64	4.7	43.0	0.28	0.18	1.57	9
	144	10.4	45.0	0.29	0.31	3.59	4
540	47	2.8	20.0	0.50	0.11	0.50	7
	131	6.1	48.0	0.54	0.20	0.67	8
	201	11.6	65.0	0.37	0.16	0.98	6

represent initial cementation of sediment particles or grain interlocking and are not indicative of **overconsolidation** in the strict sense of the term.

Compression index (C_c) is a measure of the amount of consolidation that occurs for a given increment in load. The coarse sediment at the northeast end of the strait is less compressible than the progressively finer sediment to the southwest, as indicated by a southwest trend of increasing C_c (Table 1). Richards (1962) reported a range of 0.20 to 0.87 for C_c measured on samples of marine sediment from many areas, and most values from Shelikof Strait fall within this range.

Compression index commonly shows a linear relation to liquid limit (LL). The data from Shelikof Strait, when plotted in this manner, exhibit a general trend, but with much scatter (Fig. 24). Skempton (1944) found that the relation can be expressed as

$$C_c = 0.009 (LL - 10),$$

and the regression equation for Shelikof Strait sediment is similar:

$$C_c = 0.006 (LL + 5.7).$$

The rate at which consolidation occurs in response to loading determines the coefficient of consolidation (c_v). It is directly related to permeability of a sediment and inversely related to the compressibility. The coefficient is calculated for each load increment during a laboratory consolidation test from plots of deformation versus time. As shown in Table 1, C_v commonly varies through one to two orders of magnitude for a single test. No general trend in the data is evident, although the high expected permeability and low compressibility of **coarse-grained** sediment would suggest a decrease of C_v to the southwest. Measurements of C_v for clay sediment from various marine locations by Richards and Hamilton (1967) are in the range $3.2 - 6.0 \times 10^{-4} \text{ cm}^2/\text{sec}$, which are lower than typical values in Shelikof Strait.

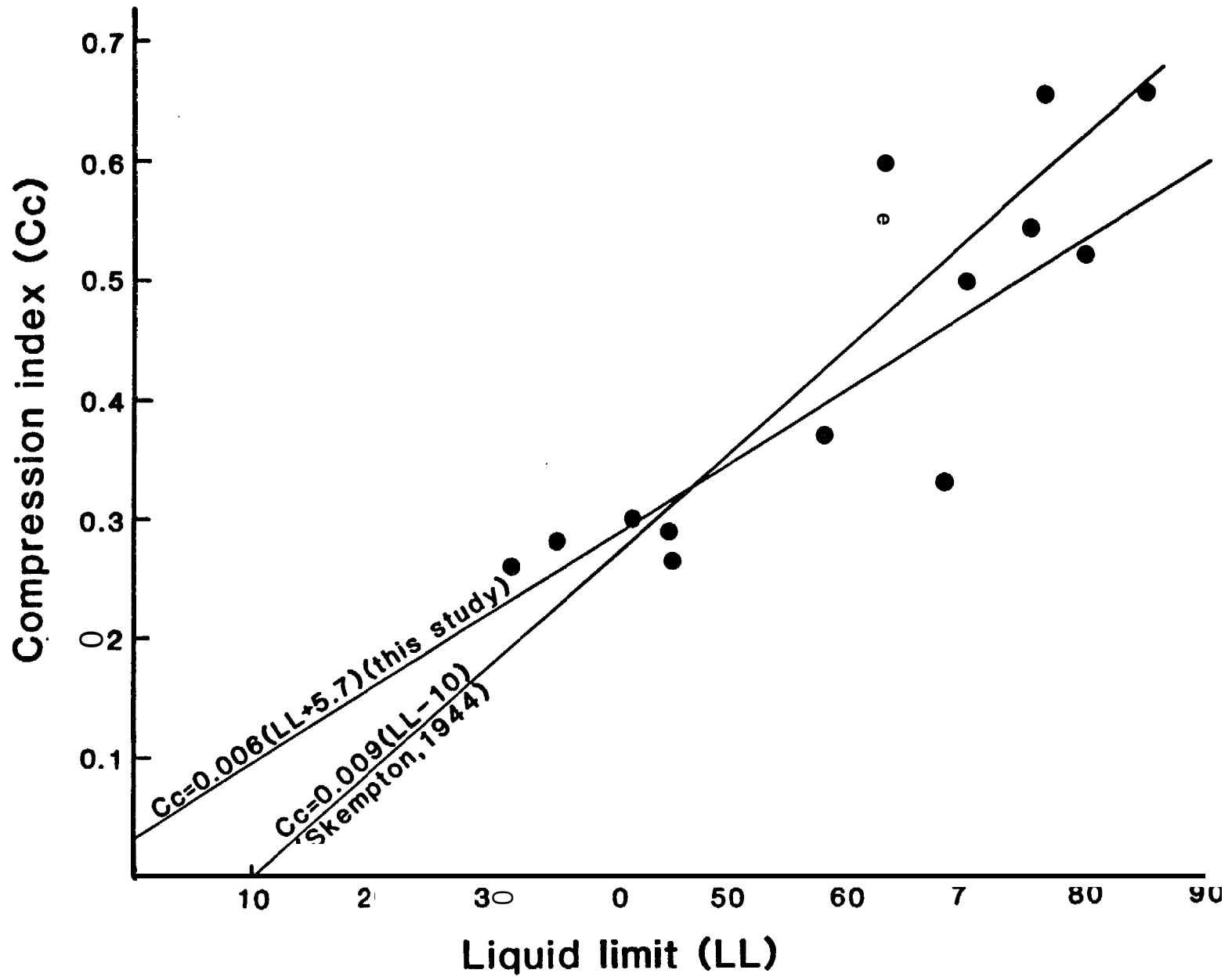


Figure 24. Graph of

index versus liquid limit.

Static strength properties: Sediment properties derived from static triaxial strength tests are listed in **Table 2**. The primary measured property is the undrained shear strength (S_u). It is the maximum sustainable shear stress within a sample subjected to a particular consolidation stress (σ'_c). S_u acts along a plane inclined at 45° to the axial load. The arisen of S_u divided by the effective normal stress across this plane is the effective **angle of internal friction (ϕ')**, whose magnitude is an indication of the strength behavior of the sediment under slow (drained) loading conditions. In comparison, the ratio S_u/σ'_c gives an indication of the strength behavior during rapid (undrained) loading conditions. **The difference in drained and undrained strength behavior depends on the pore water pressure generated in response to the tendency for volume change when the sediment is axially loaded.** If a sediment has a high tendency for volume change, the difference in strength between rapid and slow loading can be substantial.

The effective angle of internal friction for the normally consolidated sediment samples ($OCR = 1$) in this study is relatively high ($35^\circ - 46^\circ$). Compare with values given by **Lambe and Whitman (1969, p. 149 and 306)**. The higher values ($> 40^\circ$) are in the finer sediment cores from the southwest **half** of the strait (**Table 2**). Therefore, sediment from **Shelikof Strait** appears to be atypically strong under conditions of drained loading, with the finer **sediment** exhibiting higher strength. Samples tested at $OCR > 1$ tend to have ϕ' comparable to that of **normally** consolidated samples, except for station 649 where some overconsolidated samples have significantly higher values. The data indicate similar drained behavior of normally consolidated and **overconsolidated** sediment in the **strait**.

Table 2. Static triaxial strength test results.

Station number	Depth in core (cm)	σ'_c (kPa)	Induced OCR	S_u (kPa)	S_u / σ'_c	ϕ (degrees)
507	30	53.9	1	18.8	0.3	39
	130	140.0	1	73.5	0.5	46
509	120	172.4	1	73.4	0.4	40
	170	47.0	4.1	68.9	1.5	<42
511	17	20.7	3	25.4	1.2	39
	28	2.8		8.8	3.1	64
	44	1.4		9.6	6.3	64
	180	48.2	1	27.0	0.6	43
121	8.3	5.8	18.6	3.2	41	
649	86	24.0	5.9	57.6	2.4	<40
	86	46.7	3	52.3	1.1	<54
	109	0.3		13.0	43.3	<57
	109	142.3/70.7	1	58.3	0.4	39
	127	4.4	8	12.3	2.8	<69
	132	160.5	1	76.5	0.5	41
525	8	1.4		18.5	13.2	48
	73	19.3	6	47.5	2.5	34
	85	6.9		25.2	3.6	45
	152	282.5	1	121.6	0.4	37
528	37	1.4		18.6	12.8	50
	80	179.2	1	79.8	0.4	35
	94	6.9		19.0	2.8	43
	122	30.3	3.6	77.4	2.5	38
	139	178.8/89.6	1	66.7	0.3	41
540	29	15.2	6	24.2	106	40
	69	1.4		15.4	11.0	60
	120	10.3		16.7	1.6	47
	140	199.8	1	79.9	0.4	35
	159	114.0	1.8	82.8	0.7	40

Lambe and Whitman (1969, p. 307, Figs. 21-24) detected a relation between ϕ' and plasticity index for normally consolidated soil. Triaxial data for which there are plasticity index values in Shelikof Strait plot within the range of Lambe and Whitman's data, except for the core at station 511, which is abnormally strong for sediment with such high plasticity (Fig. 25).

Evaluation of undrained strength, in terms of S_u/σ_c' , requires some judgment in order to detect trends. In particular, the tests run at low consolidation stress (σ_c') seem to give erratic values of S_u/σ_c' . This was also shown to be the case for triaxial data from nearby Kodiak Shelf (Hampton, in press). Tests run at high values of consolidation stress (which corrects some of the effects of disturbance) and OCR = 1 have values of S_u/σ_c' between 0.3 and 0.6, with no areal trend (Table 2). The value of S_u/σ_c' increases with OCR for each core tested.

The static triaxial test data are plotted according to the NSP approach in Figure 26. The slope (A) of the line for each core is a measure of the change in undrained strength with OCR. Most cores have A values between 0.79 and 0.97. Mayne (1980) compiled the results of many triaxial tests and found a mean value of A = 0.64 with a standard deviation of 0.18. The sediment in Shelikof Strait, with its relatively high values of A, would tend to retain more of its strength after unloading compared to most sediment examined by Mayne (1980). The A = 1.43 calculated for the sediment of station 528 is greater than the theoretical limit of A = 1.0, and further testing is required to resolve this conflict.

Dynamic strength properties: The data from triaxial strength tests are given in Table 3. The quantity τ_{cyc}/S_u is the cyclic stress level, the average

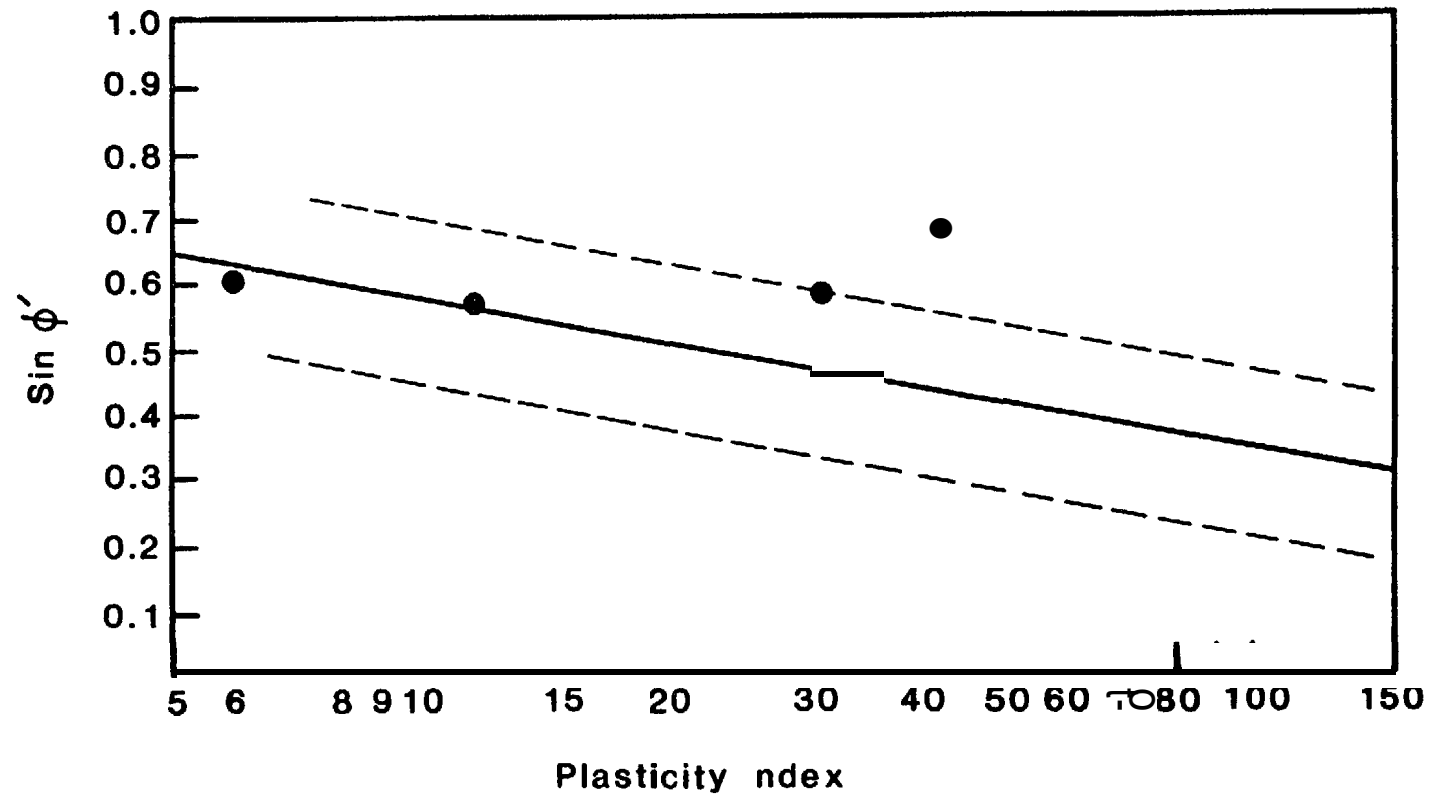


Figure 25. Graph of effective angle of internal friction versus plasticity index. Solid line shows empirical relation derived by Lambe and Whitman (1969); dashed line indicates limits of their data.

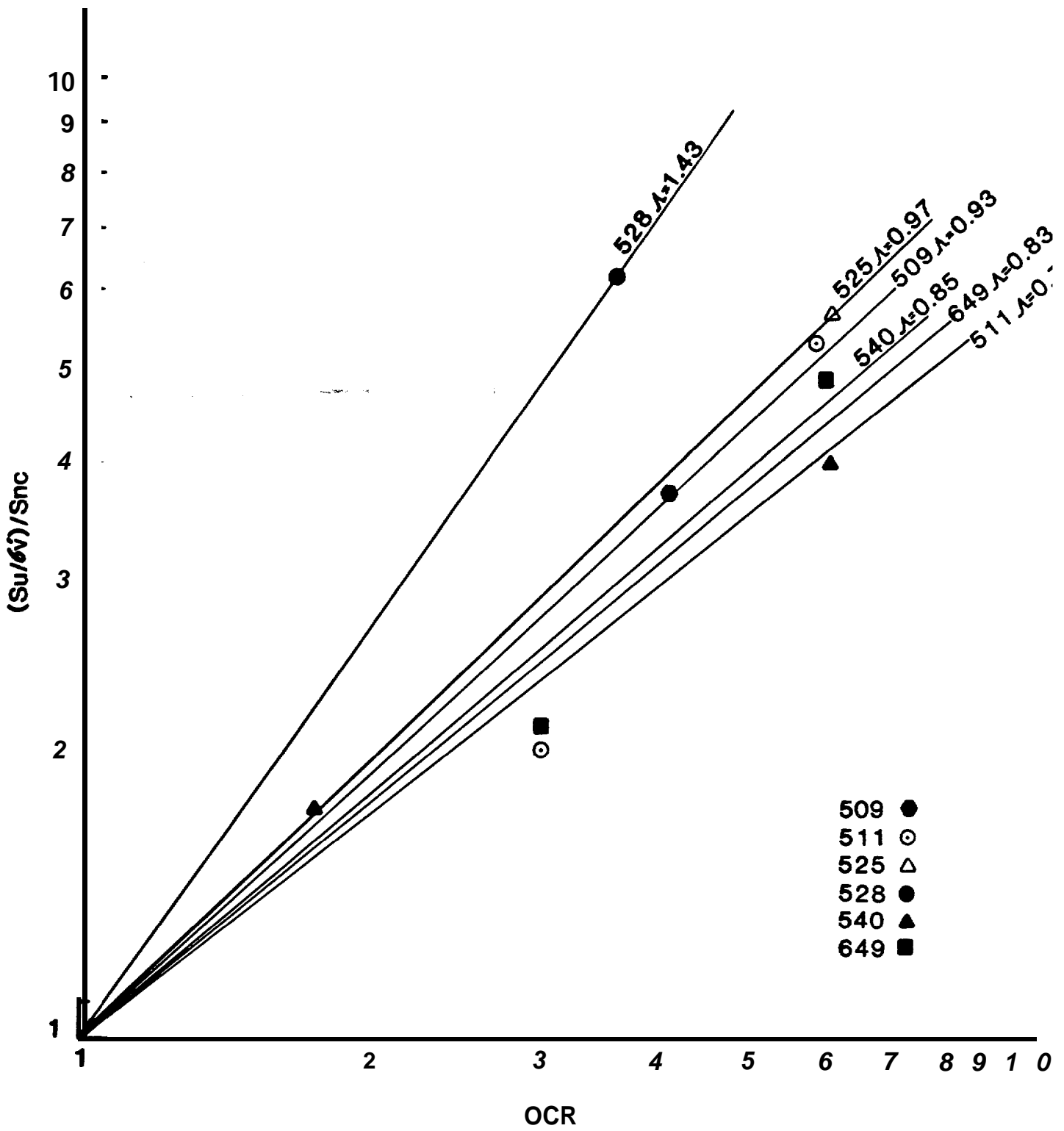


Figure 26. Graph of normalized undrained shear strength versus overconsolidation ratio.

Table 3. Dynamic triaxial strength test results.

Station number	Depth in core (cm)	u_c (kPa)	Induced OCR	τ_{cyc}/s_u (%)	Cycles to failure
509	137	173.6	1	49	145
	137	175.0	1	66	64
511	152	46.9	1	70	10
	167	46.9	1	47	48
649	96	153.1	1	70	22
	96	146.0	1	56	450
	140	30.2	4.4	79	17
	140	139.8	1	72	39
525	135	282.4	1	47	30
	117	282.4	1	70	7
528	23	27.5	4	32	51
	178	179.1	1	70	13
	193	179.1	1	46	110
540	152	199.8	1	71	12
	227	199.8	1	43	900+
	238	299.8	1	56	28

value of shear stress (τ_{cyc}) applied sinusoidally with full stress reversal at 0.1 Hz, expressed as a percentage of the static undrained shear strength (S_u). Pore water pressure and strain accumulate with repeated application of τ_{cyc} . At some point, the pore water pressure approaches the confining stress, strain increases abruptly, and the sediment fails. In our tests, failure was chosen when 20% strain was reached.

Samples typically fail in fewer cycles at progressively higher stress levels. Figure 27 shows the number of cycles to failure versus stress level for Shelikof Strait samples. Although there is some scatter, the data fall within the range of test results on terrigenous sediment from other areas (Lee and others, 1981; Anderson and others, 1980; Hampton, in press). Moderate cyclic strength degradation is indicated; that is, after 10 cycles of loading (as might be imparted by an earthquake, for example), the samples fail at stress levels between 60% and 80% of their static strength.

DISCUSSION

The primary geotechnical concerns in Shelikof Strait include settlement of structures, bearing capacity under static and cyclic loading lateral load capacity, and anchor breakout resistance. Natural slope failures are not a serious problem because only one small sediment slide has been documented (Hampton and others, 1981). There is some evidence for gas-charged sediment, but the problem of low strength that might exist in sediment of this type was not addressed in the present study.

Quaternary sediment in Shelikof Strait covers bedrock to a thickness of from 20 m to more than 800 m (Fig. 4). The sequence consists of Pleistocene glacial and glaciomarine sediment at the base, overlain by Holocene marine

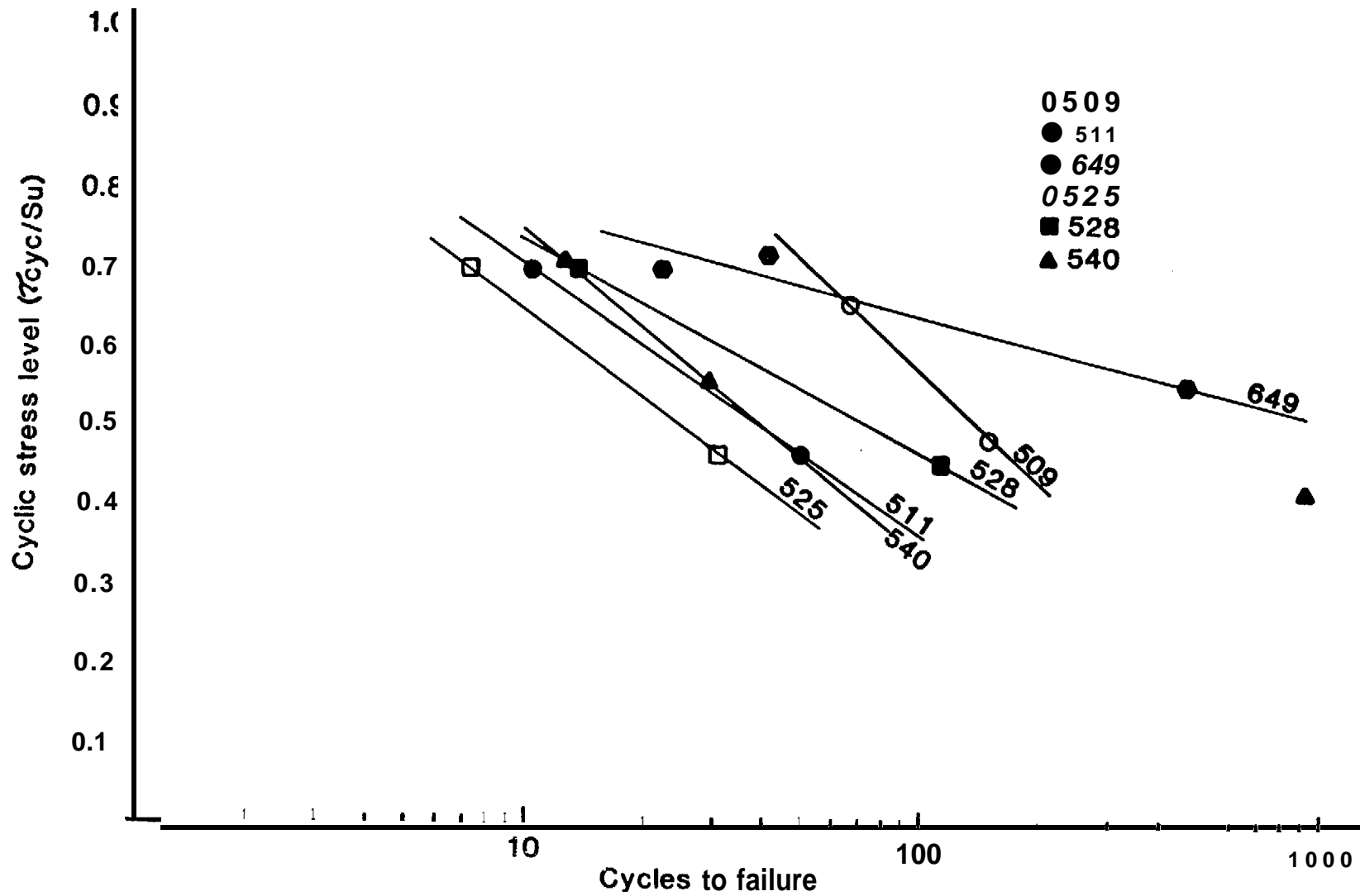


Figure 27. Graph of cyclic stress level versus number of cycles to failure.

deposits. The highest stratigraphic unit, deposited by oceanic currents as exist today, has accumulated to a thickness of 80-100 m over most of the strait; the total range is about 20 m to 180 m. Geotechnical testing was performed only on samples from this uppermost unit. A geotechnical analysis based on these data probably addresses most situations of engineering concern. Deeper stratigraphic units appear from interpretive geologic studies to be relatively coarse-grained (Hampton and Winters, 1981; Whitney, Holden, and Lybeck, 1980; Whitney, Hoose, Smith, and Lybeck, 1980), and they probably are stable, but deep drill-core samples would have to be obtained in order to confirm this by geotechnical testing.

The pattern of grain-size variation (Figs. 7 and 8) evidently reflects progressive sorting by the southwesterly flowing barotropic current that dominates circulation in the strait. The present study and the previous report by Hampton and others (1981) show that some index properties vary in relation to grain size. Properties that show a direct correlation and therefore increase to the southwest down the strait and to the southeast across the strait include water content, liquid limit, plastic limit, plasticity index, and organic carbon content (Figs. 10, 13, 14, 15, and 22). Properties that correlate inversely with grain size include bulk sediment density and undrained (vane) shear strength (Figs. 11 and 20).

Consolidation tests indicate that sediment samples are overconsolidated, but this probably is a near-seafloor diagenetic or fabric phenomenon rather than a result of erosion, because net sediment accumulation is presently occurring throughout the strait (Table 1, Fig. 9). The fine-grained sediment to the southwest has high values of compression index (C_c), which indicates that it is more compressible than the coarser material to the northeast. The rate of consolidation, as shown by the coefficient of consolidation (C_v), is

highly variable for each consolidation test and does not show an areal trend (Table 1). Intuitively, a higher value of c_v would be expected for the coarser-grained sediment because of its normally higher permeability and lower compressibility, but apparently this is not the case.

Another unexpected result is that the static drained strength, in terms of the effective angle of internal friction (ϕ), is higher for the fine-grained sediment than it is for the coarser-grained samples (Table 2). Drained strength does not vary appreciably with OCR. Undrained static strength behavior does not exhibit significant areal variation. Values of s_u/σ_c' for tests run at OCR = 1 are between 0.3 and 0.6. This parameter increases with OCR for each core that was tested. The NSF pore-pressure parameter (A) varies from 0.79 to 0.97, which indicates significant static strength increase with OCR (Fig. 26). Again, no areal trend is apparent. But, because few data points were used to plot the lines in Figure 26 and because large scatter of data exists for some individual cores, additional strength testing at more levels of OCR would add precision to the plots and perhaps reveal some systematic variation.

Test data for most cores define similar response to cyclic loading over a broad range of number of cycles required to cause failure (e.g., cores 511, 525, 528, and 540 in Fig. 27). Dynamic strength degradation varies over a limited range at low number of cycles; for instance, it is between about 60% and 80% for 10 cycles.

Geotechnical properties of Shelikof Strait sediment can be compared with data from other studies to determine if the sediment has normal reformational behavior. However, few data exist for some properties, which makes the evaluations tentative.

Most values of compression index fall within the range of 0.20 to 0.87 reported by Richards and Hamilton (1967) for silty clay to highly colloidal clay; one test on the core from station 507 has a high value of 0.94 (Table 1). Skempton's (1944) classification of compressibility based on liquid limit indicates that Shelikof Strait samples are moderately to highly compressible (Appendix). Substitution of the class-boundary values of liquid limit (moderate compressibility: $30 < LL < 50$; high compressibility: $LL > 50$) into the regression equation for Shelikof Strait data (Fig. 24),

$$C_c = 0.006 (LL + 5.7),$$

indicates that the range of moderate compressibility is $0.21 < C_c < 0.33$ and the high range is $C_c < 0.33$, which is consistent with classifying the sediment as moderately to highly compressible (Table 1).

Effective friction angle (ϕ') for sediment in Shelikof Strait is high ($35^\circ - 46^\circ$) compared to the range ($20^\circ - 40^\circ$) reported by Lambe and Whitman (1969, p. 149 and 306) for normally consolidated sediment. Apparently, no compilations of ϕ' exclusively for terrigenous marine sediment have been made. Hampton (in press) reports ϕ' mostly in the $30^\circ - 40^\circ$ range for terrigenous samples from the Kodiak Shelf. Shelikof Strait terrigenous sediment is relatively strong under drained loading conditions.

Lambe and Whitman (1969, p. 452, Fig. 29.19) present data on the undrained strength of normally consolidated marine clay, and values of s_u/σ_c' are between about 0.2 and 0.4. The range for normally consolidated Shelikof Strait samples is 0.3 to 0.6, so they are relatively strong under conditions of undrained loading. s_u/σ_c' for normally consolidated terrigenous

sediment from the Kodiak Shelf are also high, from 0.4 to 1.0 (Hampton, in press) .

Values of the NSP factor A are high (0.79 - 0.97) compared to the average value of 0.64 (standard deviation = 0.18) in the extensive compilation by **Mayne** (1980). The implication is that the increase of strength with **overconsolidation** is higher than normal.

The low to moderate **cyclic** strength degradation of Shelikof Strait samples is similar to the behavior of clay sediment reported in other studies (Lee and others, **1981**; Anderson and others, 1980; Hampton, in press). Sediment failure in response to large earthquakes certainly is a possibility, but the potential is not as great as has been predicted for some deposits of silt in the northeast Gulf of Alaska (cyclic strength at 10 cycles as low as 40% of the static strength; Lee and Schwab, in press) and volcanic ash on the Kodiak Shelf (cyclic strength at 10 cycles is 12% of the static strength; Hampton, in press). The deposit of **Katmai** ash in **Shelikof** Strait was not subjected to **geotechnical** testing. However, its in situ density is so great that normal gravity coring devices could not penetrate the **layer**. The relative density appears to be high and therefore the liquefaction potential is low. The possibility that more deeply buried ash layers are present and might be highly susceptible to liquefaction cannot be evaluated with the information presently available.

REFERENCES

- American Society for Testing and Materials, 1976, Annual Book of ASTM Standards. Philadelphia, ASTM, 485 p.
- Anderson, K.H., Pool, J.H., Brown, S.F., and Rosenbrand, W.F., 1980, Cyclic and static laboratory tests on Drammen clay. Journal of the Geotechnical Engineering Division, ASCE, v. 106, p. 499-529.
- Bishop, A.W., and Henkel, D.J., 1964, The Measurement of Soil Properties in the Triaxial Test. London, Edward Arnold Ltd., 228 p.
- Bordovskiy, O.K., 1965, Accumulation of organic matter in bottom sediments. Marine Geology, v. 3, p. 33-82.
- Bordovskiy, O.K., 1969, Organic matter of recent sediments of the Caspian Sea. Oceanology, v. 9, p. 799-807.
- Busch, W.H., and Keller, G.H., 1981, The physical properties of Peru-Chile continental margin sediments - the influence of coastal upwelling on sediment physical properties. Jour. Sedimentary Petrology, v. 51, p. 705-719.
- Cassagrande, A., 1948, Classification and identification of soils. Transactions, American Soc. Civil Engineers, v. 113, p. 901-991.

Gardner, J.V., Dean, W.E., and **Vallier**, T.L., 1980, **Sedimentology** and geochemistry of surface sediments, outer continental shelf, southern Bering Sea. *Marine Geology*, v. 35, p. 299-329.

Hampton, M.A., in press, **Geotechnical** framework study of the Kodiak Shelf, Alaska. U.S. Geological Survey Open-File Report.

Hampton, M.A., and Winters, **W.J.**, 1981, Environmental geology of **Shelikof** Strait, OCS sale area 60, Alaska. Proceedings 13th Offshore Technology Conference, p. 19-34.

Hampton, M.A., Johnson, K.H., **Torresan**, M.E., and Winters, W.J., 1981, Description of seafloor sediment and preliminary geo-environmental report, **Shelikof** Strait, Alaska. U.S. Geological Survey Open-File Report 81-1133, 86 p.

Herrmann, H. G., Rucker, **K.**, and **Babineau**, P.H., 1972, LOBSTER and FMS: Devices for monitoring long-term seafloor foundation behavior. **Naval** Civil Engineering Laboratory, Technical Report R-775, 63 p.

Keller, G.I-I., Lambert, D.N., and Bennett, R.H., 1979, **Geotechnical** properties of continental slope deposits - Cape Hatteras to Hydrographer Canyon. **Sot. Economic Paleontologists and Mineralogists Special Publication 27**, p. 131-151.

Ladd, C. C., and Foott, R., 1974, New design procedure for stability of soft clays. Journal of the **Geotechnical** Engineering Division, **ASCE**, v. 100, p. 763-786.

Lambe, T.W., 1951, Soil Testing for Engineers. New York, John Wiley and sons, 165 p.

Lambe, T.W., and Whitman, R.V., 1969, Soil Mechanics. New York, John Wiley and sons, 553 p.

Lee, H.J., Edwards, B.D., and Field, M.E., 1981, **Geotechnical** analysis of a submarine slump, Eureka, California. Proceedings 13th Offshore Technology Conference, p. 53-65.

Lee, H.J., and Schwab, W.C., in press, **Geotechnical** framework, northeast Gulf of Alaska. U.S. Geological Survey Open-File Report.

Lisitzin, A.P., 1972, **Sedimentation in the World Ocean.** Soc. **Economic Paleontologists and Mineralogists Special Publication 17, 218 p.**

Mayne, P.W., 1980, Cam-clay predictions of undrained strength. Journal of the Geotechnical Engineering Division, ASCE, v. 106, p. 1219-1242.

Mitchell, J.K., 1976, Fundamentals of Soil Behavior. New York, John Wiley and Sons, Inc., 422 p.

Muench, R. D., and Schumacher, J.D., 1980, Physical oceanographic and meteorological conditions in the northwest Gulf of Alaska. NOAA Technical Memorandum ERL PMEL-22, 147 p.

Nayudu, Y.R., 1964, Volcanic ash deposits in the Gulf of Alaska and problems of correlation of deep-sea ash deposits. *Marine Geology*, v.1, p. 194-212.

Odell, R.T., Thornburn, T.H., and McKenzie, L.T., 1960, Relationships of Atterberg limits to some other properties of Illinois soils. Proceedings of the Soils Society of America, v. 24, p. 297-300.

Pratt, R.M., **Scheidegger, K.F., and Kulm, L.D., 1973,** Volcanic ash from DSDP site 178, Gulf of Alaska. Initial Reports of Deep sea Drilling Project, V. XVIII, p. 833-834.

Rashid, M.A., and Brown, J.P., 1975, Influence of marine organic compounds on engineering properties of remolded sediment. *Engineering Geology*, v. 9, p. 141-154.

Richards, A.F., **1962,** Investigation of deep-sea sediment cores, II. Mass physical properties. U.S. Navy Hydrographic Office Tech. Rept. 106, 146 p.

Richards, A.F., and Hamilton, E.L., 1967, Investigations of deep-sea sediment cores, III. Consolidation. In: Richards, **A.F.** (ed.), *Marine Geotechnique*, Urbana, University of Illinois Press, p. 93-117.

- Skempton, A.W., 1944, Notes on the compressibility of clays. Geological Society of London, Quarterly Journal, v. 100, p. 119- 35.
- Terzaghi, K., 1955, Influence of geological factors on the engineering properties of sediments. Economic Geology, 50th Anniversary Volume 1905-1955, p. 557-618.
- Terzaghi, K., and Peck, R.B., 1948, Soil Mechanics in Engineering Practice. New York, John Wiley and Sons.
- von Huene, R., 1979, Structure of the outer convergent margin off Kodiak Island, Alaska, from multichannel seismic records. In: Watkins, J.S., Montadert, L., and Dickerson, P.W., (eds.), Geological and Geophysical Investigations of Continental Margins, AAPG Memoir 29, Tulsa, American Association of Petroleum Geologists, p. 261-272.
- Whitney, J., Holden, K.D., and Lybeck, L., 1980, Isopach map of Quaternary glacial-marine sediments, outer continental shelf, Shelikof Strait, Alaska. U.S. Geological Survey Open-File Report 80-2036, 1 p.
- Whitney, J., Hoose, P.J., Smith, L.M., and Lybeck, L., 1980, Geologic cross sections of the outer continental shelf, Shelikof Strait, Alaska. U.S. Geological Survey Open-File Report 80-2036, 1 p.
- Wissa, A.E., Christian, J.T., Davis, E.H., and Heiberg, S., 1971, Consolidation at constant rate of strain. Journal of the Soil Mechanics and Foundation Division, ASCE, v. 97, p. 1393-1410.

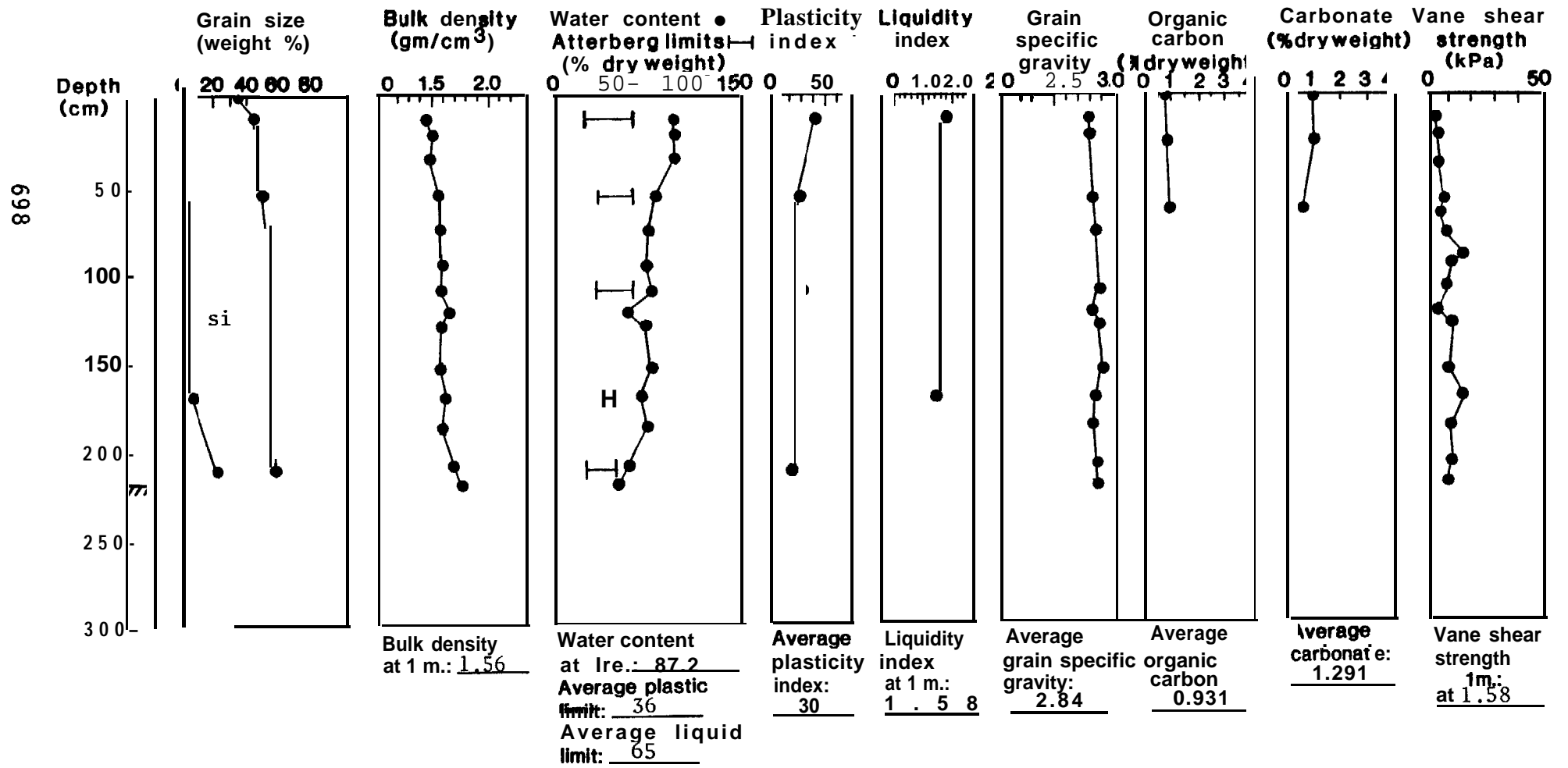
APPENDIX:

INDEX PROPERTY CHARTS FOR SEDIMENT CORES

FROM **SHELIKOF** STRAIT

•

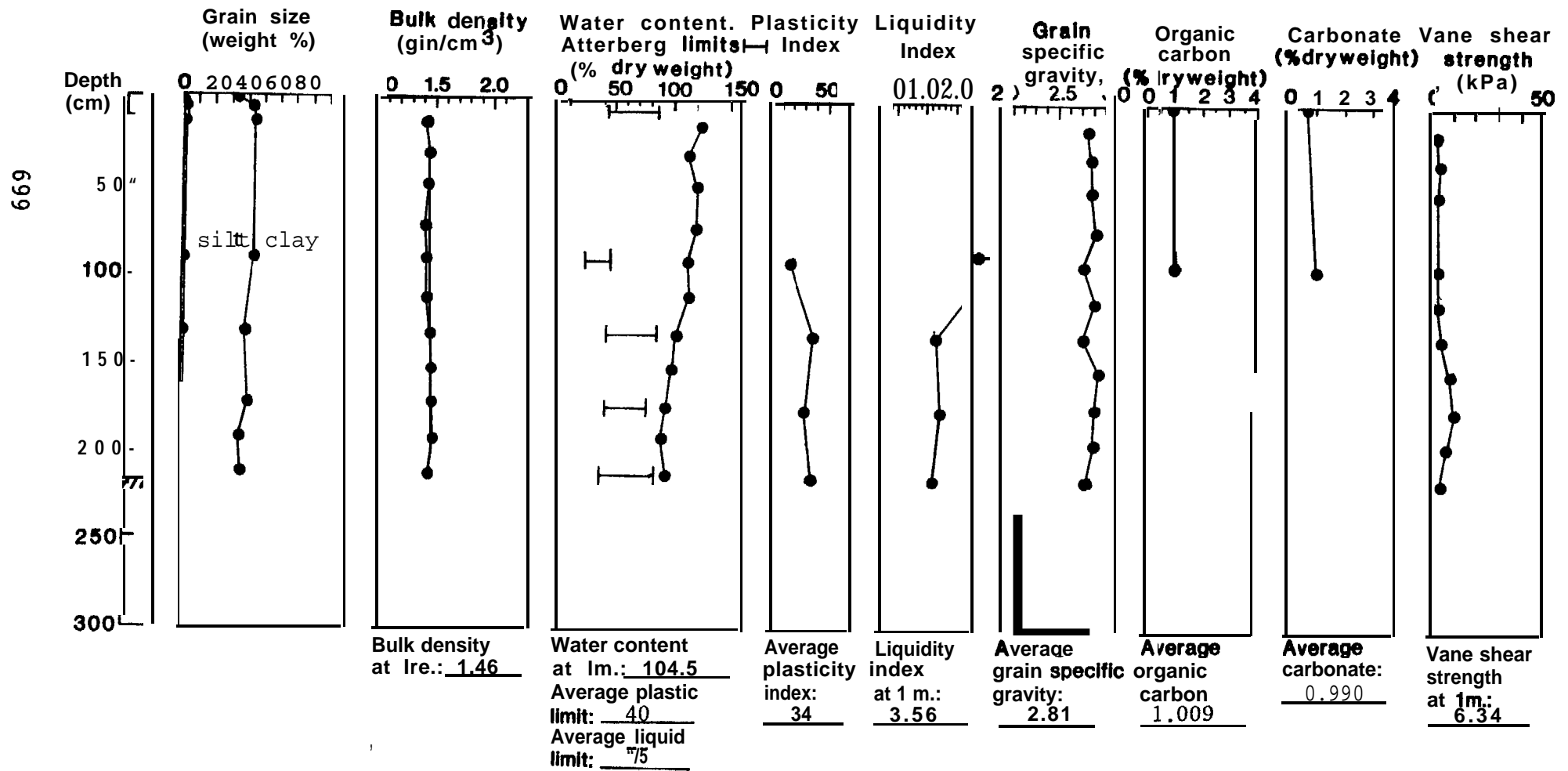
Station 508 Location 57°21.01'N_155°36.41'W Water depth 270m



Station 509

Location 57°21.29'N 155°08.66'W

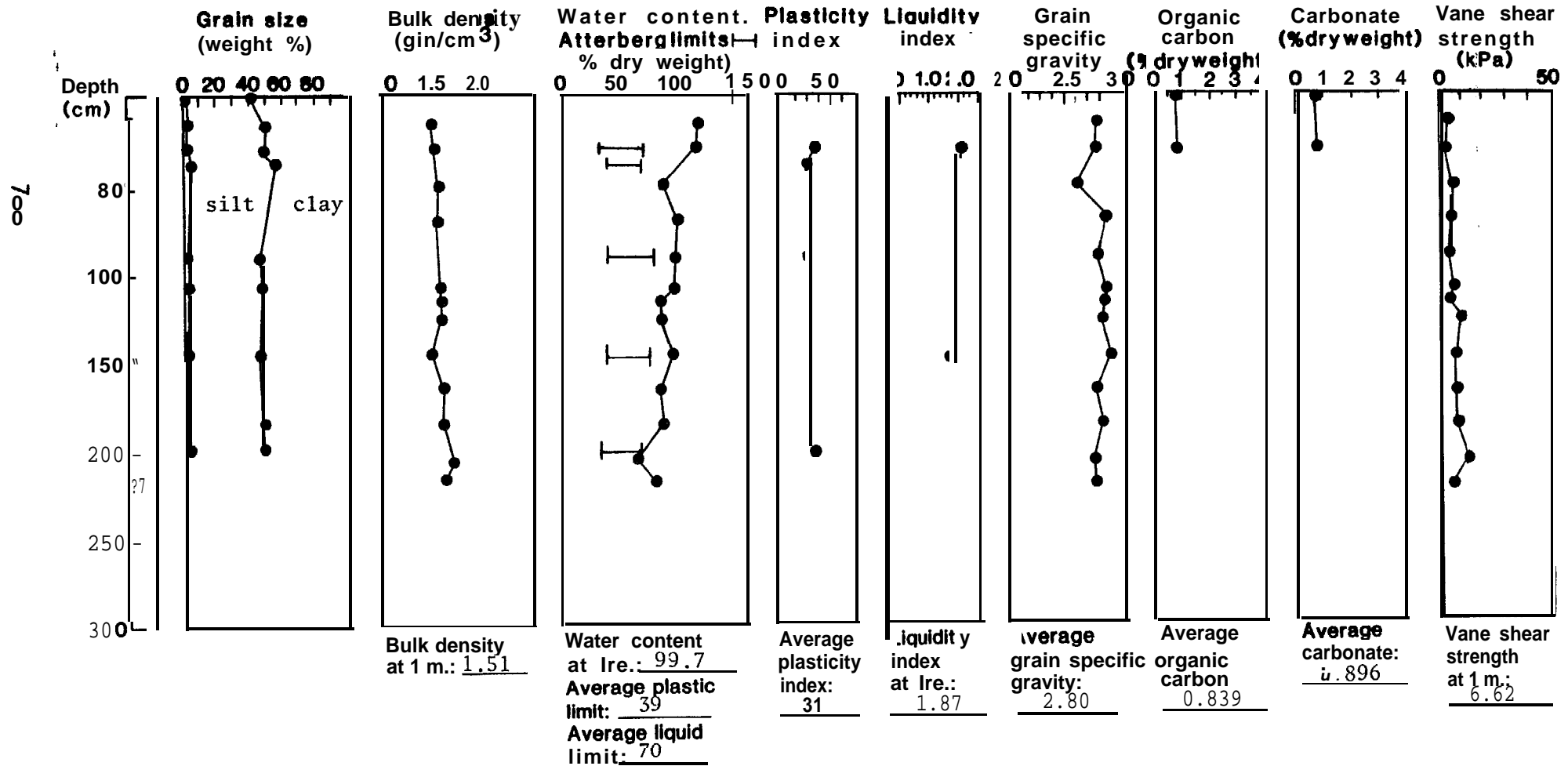
Water depth 225m



Station 510

Location 57°39.22'N 155°17.18'W

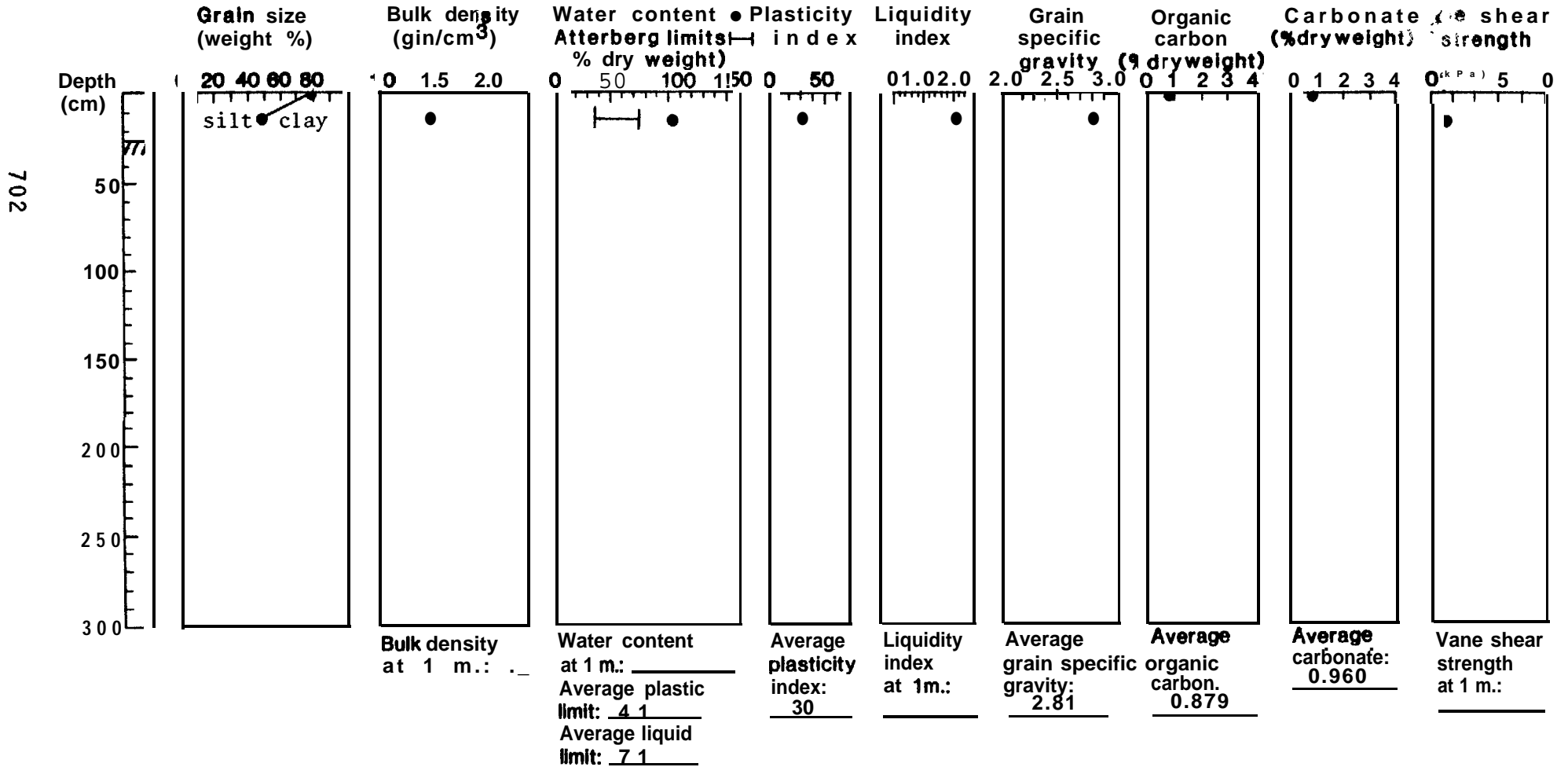
Water depth 305m



Station 512

Location 57°52.5'N 154°14.9'W

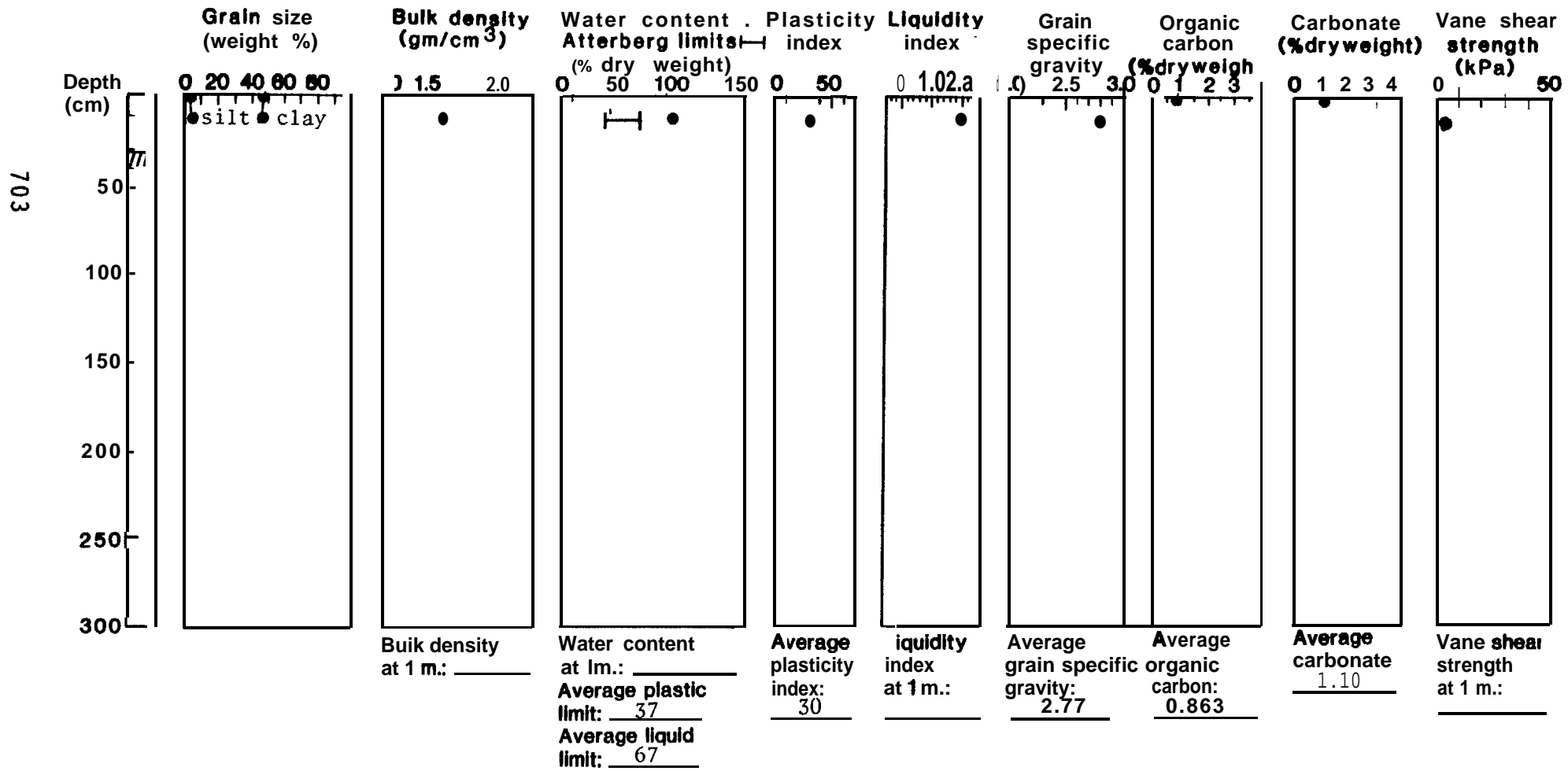
Water depth 195m



Station 513

Location 57°54.8'N 154°19.8'W

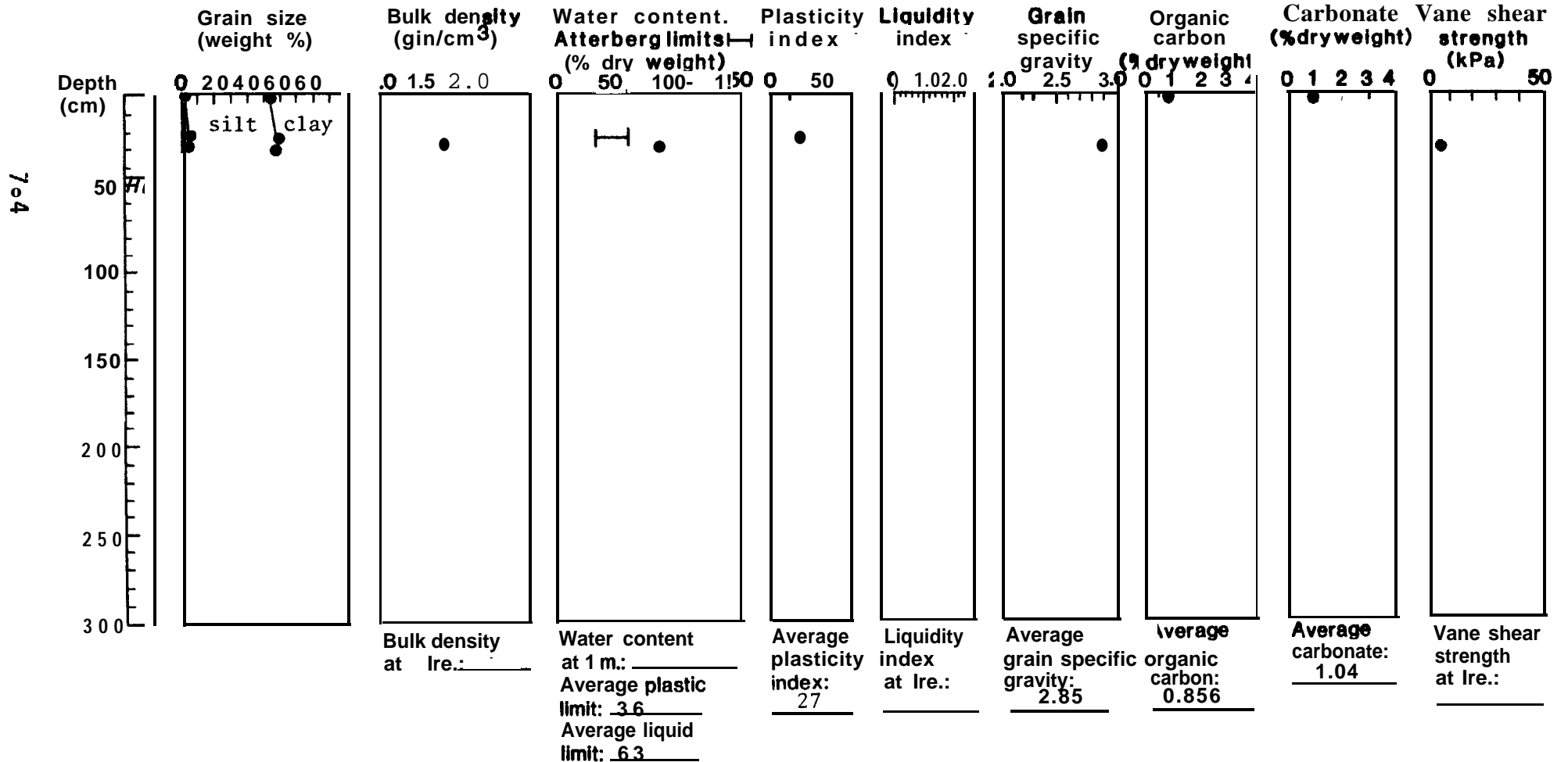
Water depth 205m



Station 514

Location 57°55.3'N 154°25.0'W

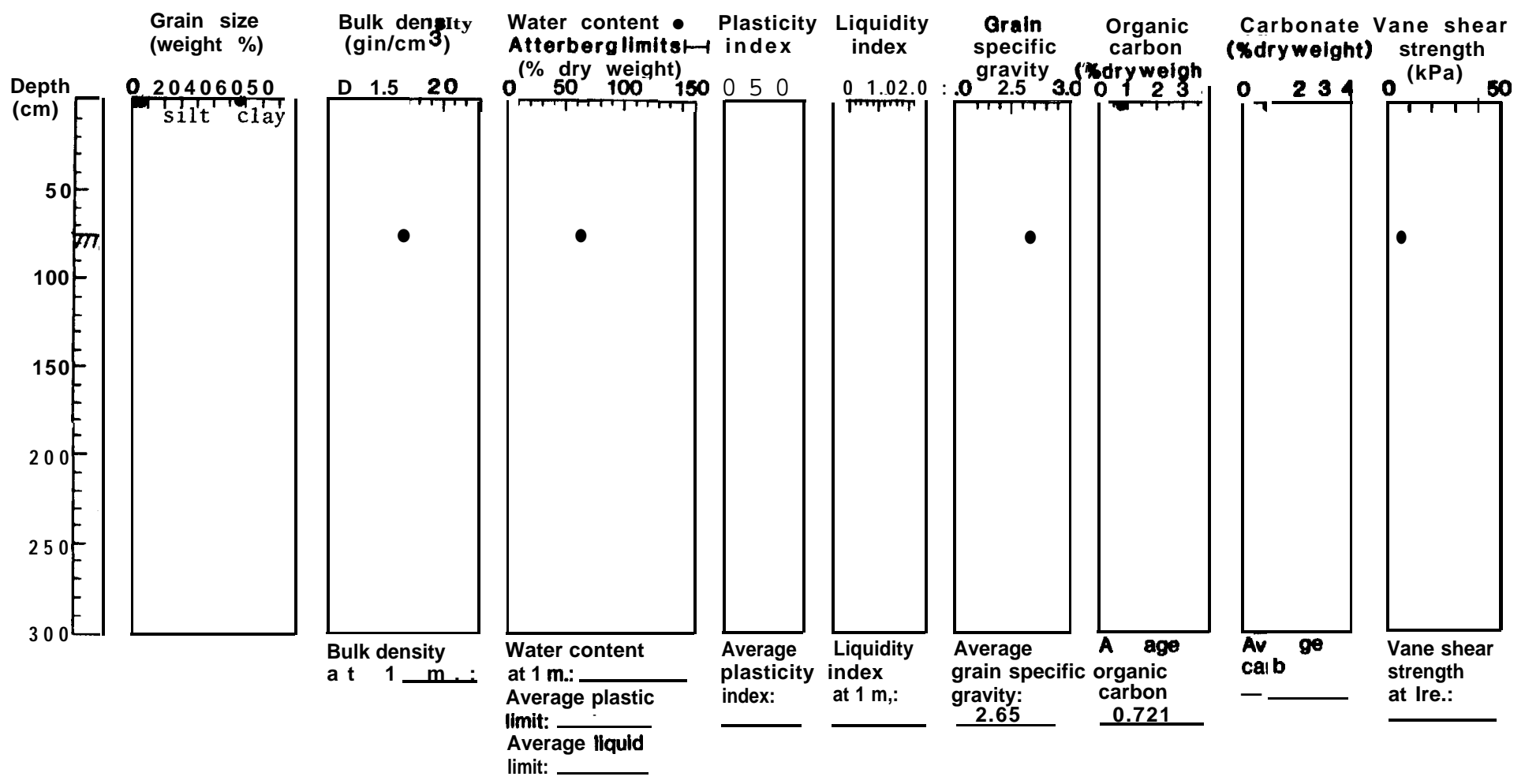
Water depth 222m



Station 515

Location 57°59.0'N 154°27.3'W

Water depth 238m

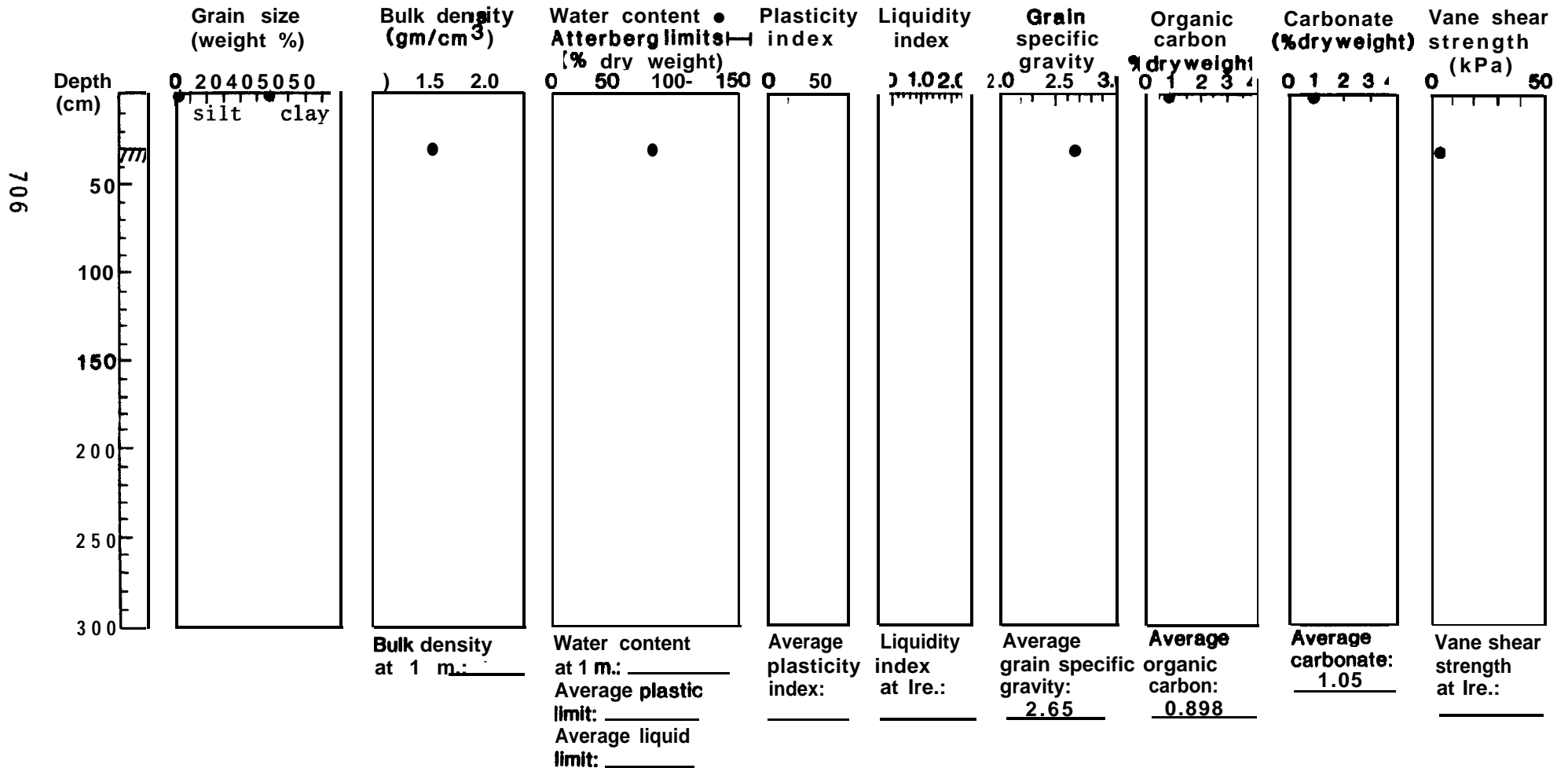


705

Station S16

Location 58°00.3'N 154°10.6'W

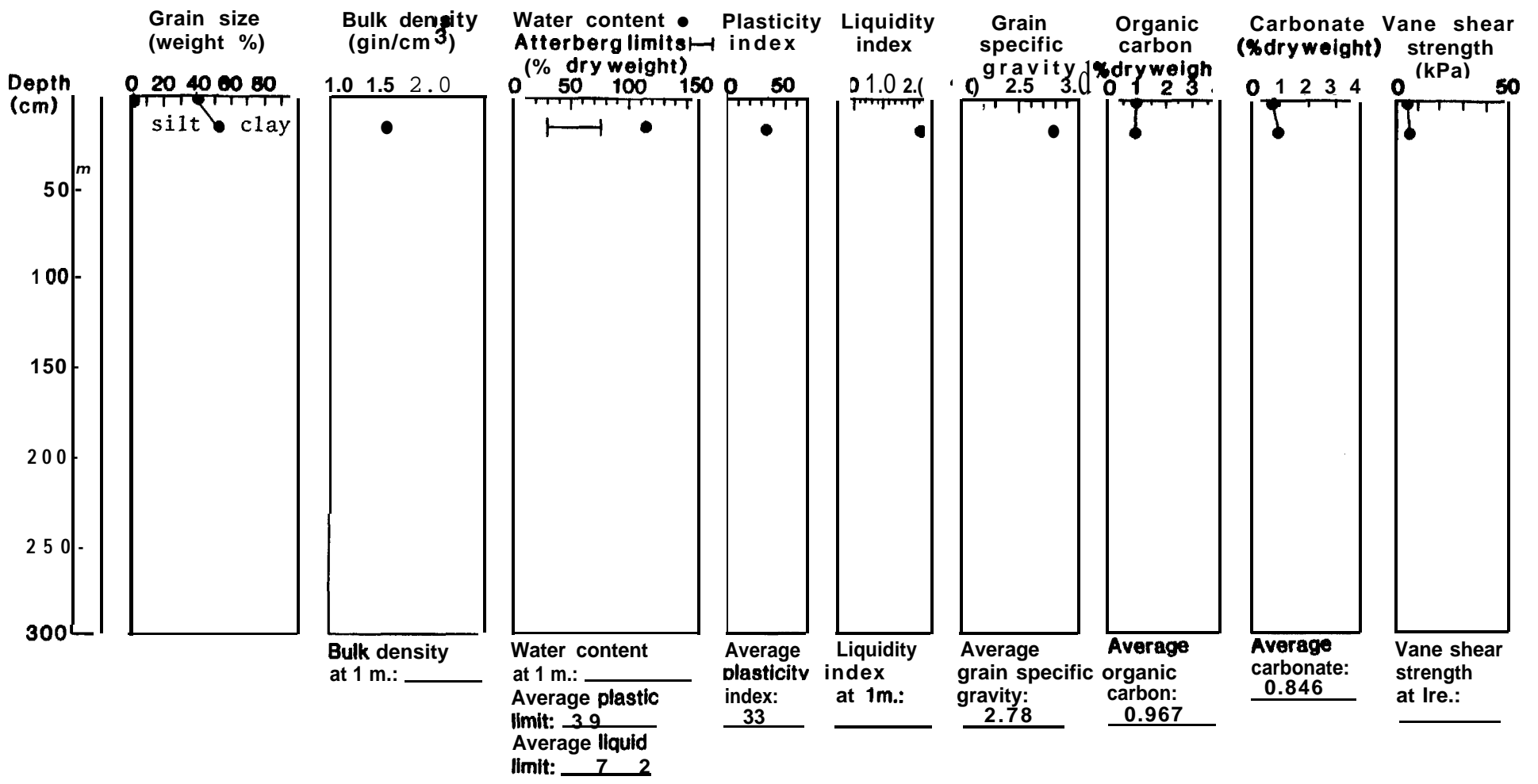
Water depth 205



Station 517

Location 57°55.3'N 154°00.9'W

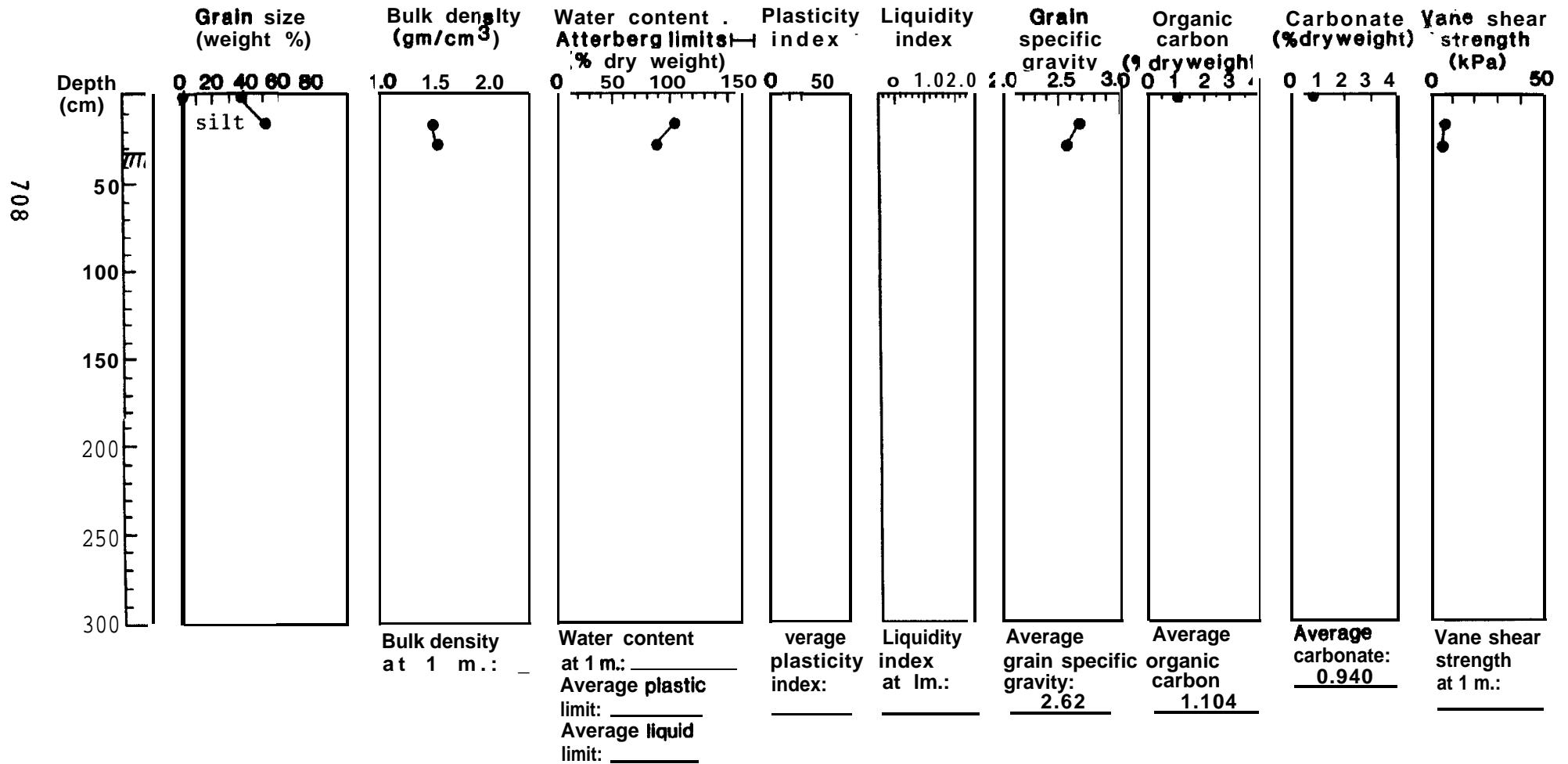
Water depth 180m



Station 518

Location 58°00.3'N 153°51.6'W

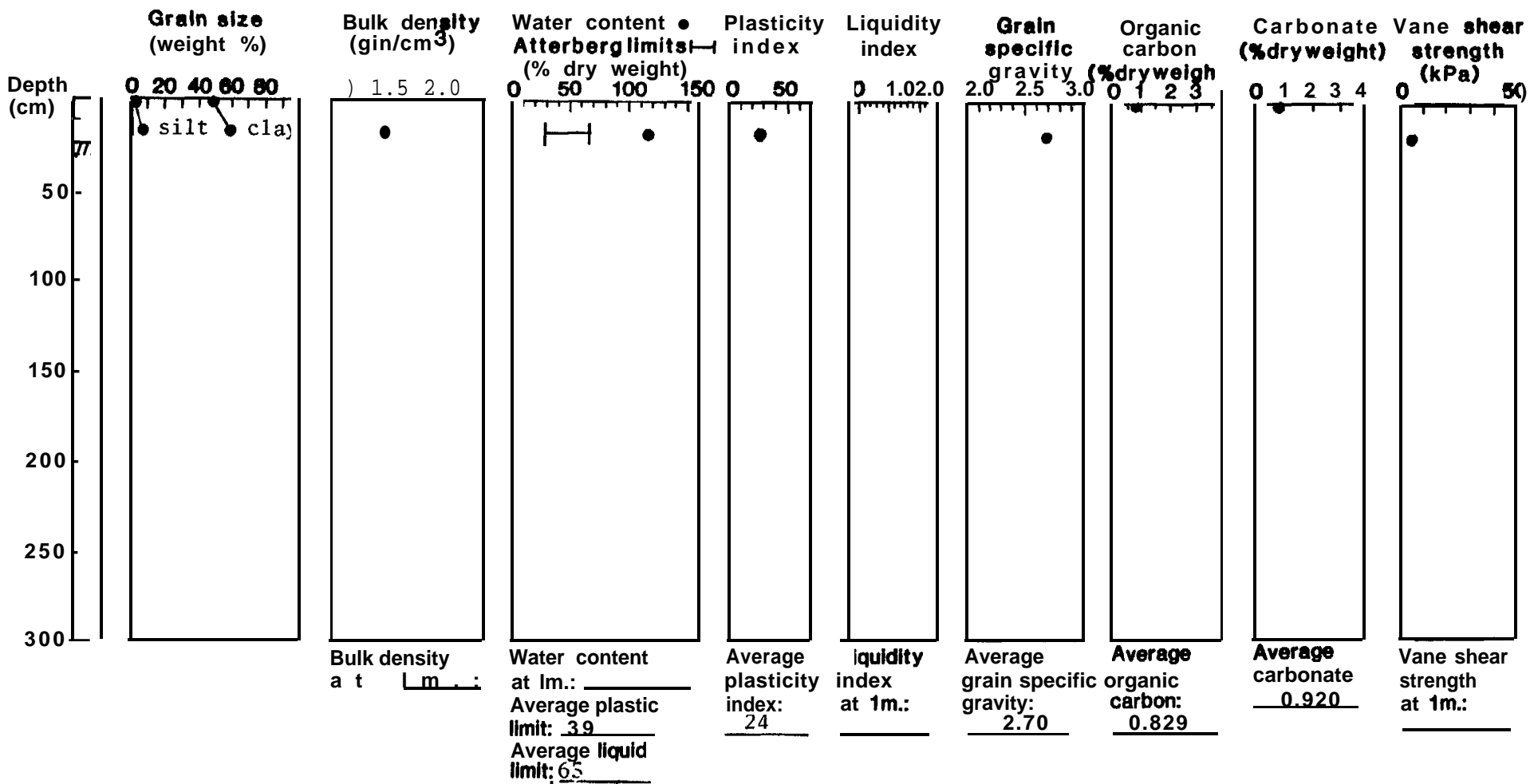
Water depth 180m



Station 519

Location 58°05.5'N 154°01.3'W

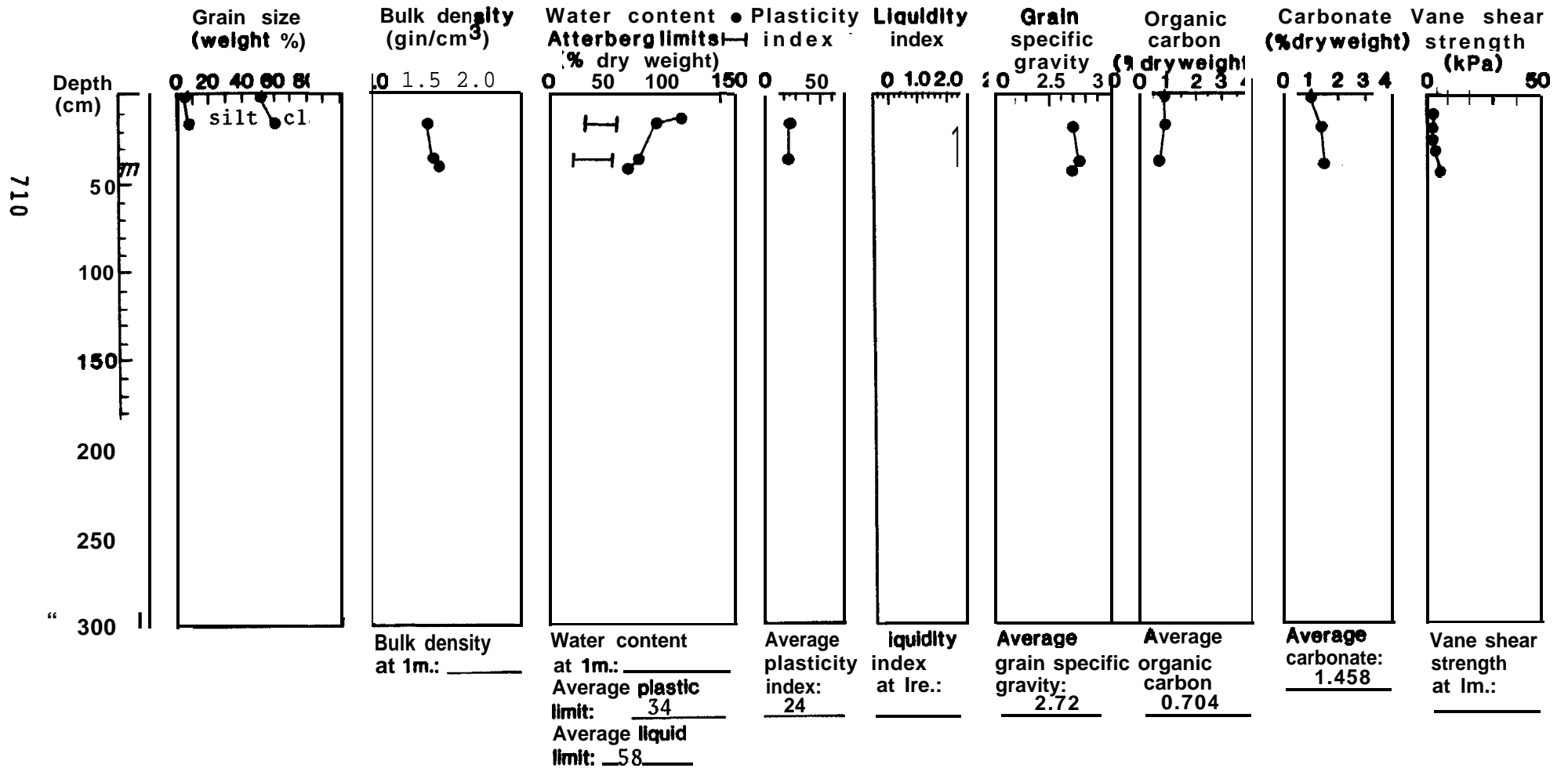
Water depth 200m



Station 520

Location 58°13.2'N 153°56.2'W

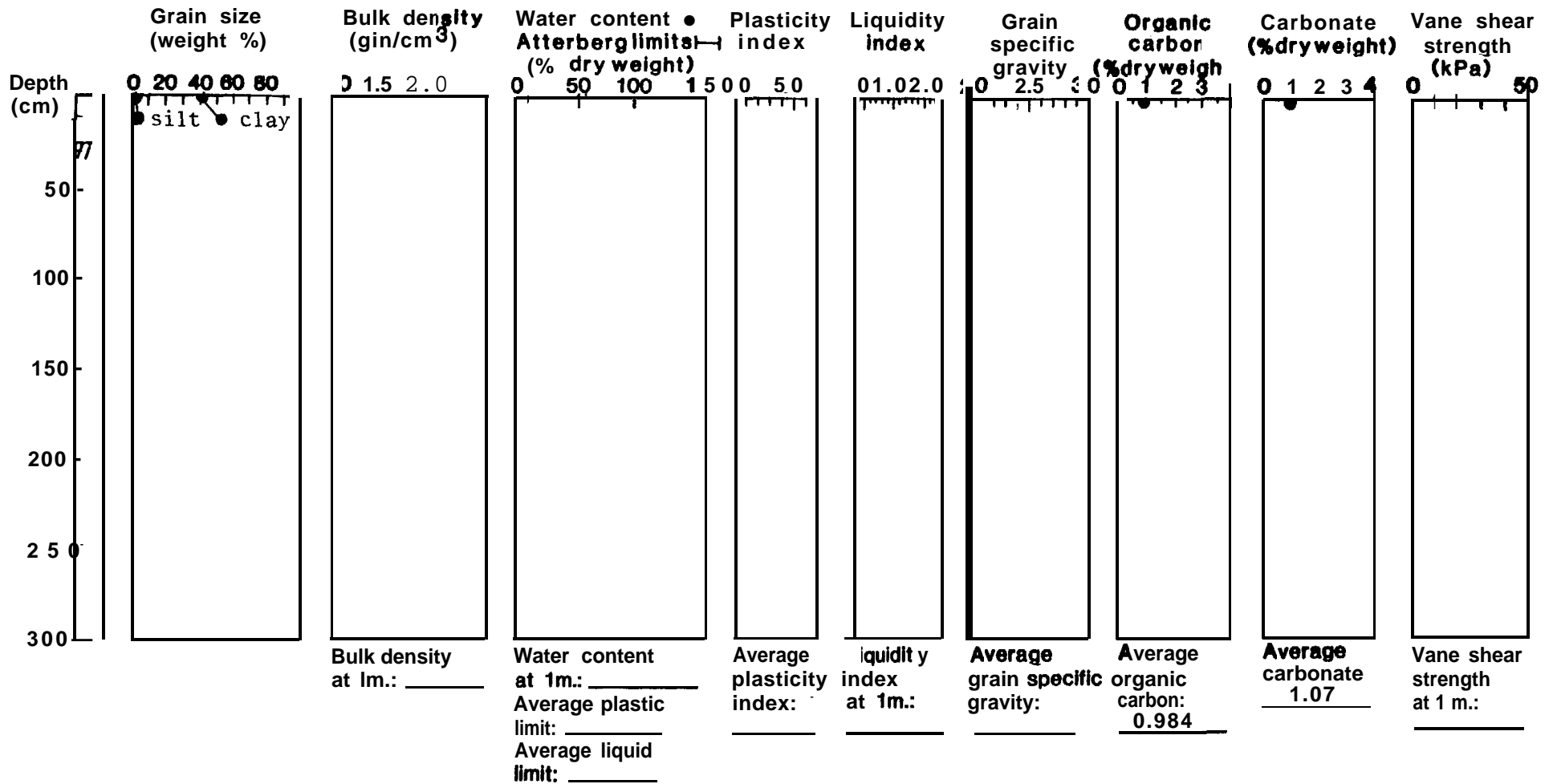
Water depth 213m



Station 521

Location 58°07.93'N 153°45.4'W

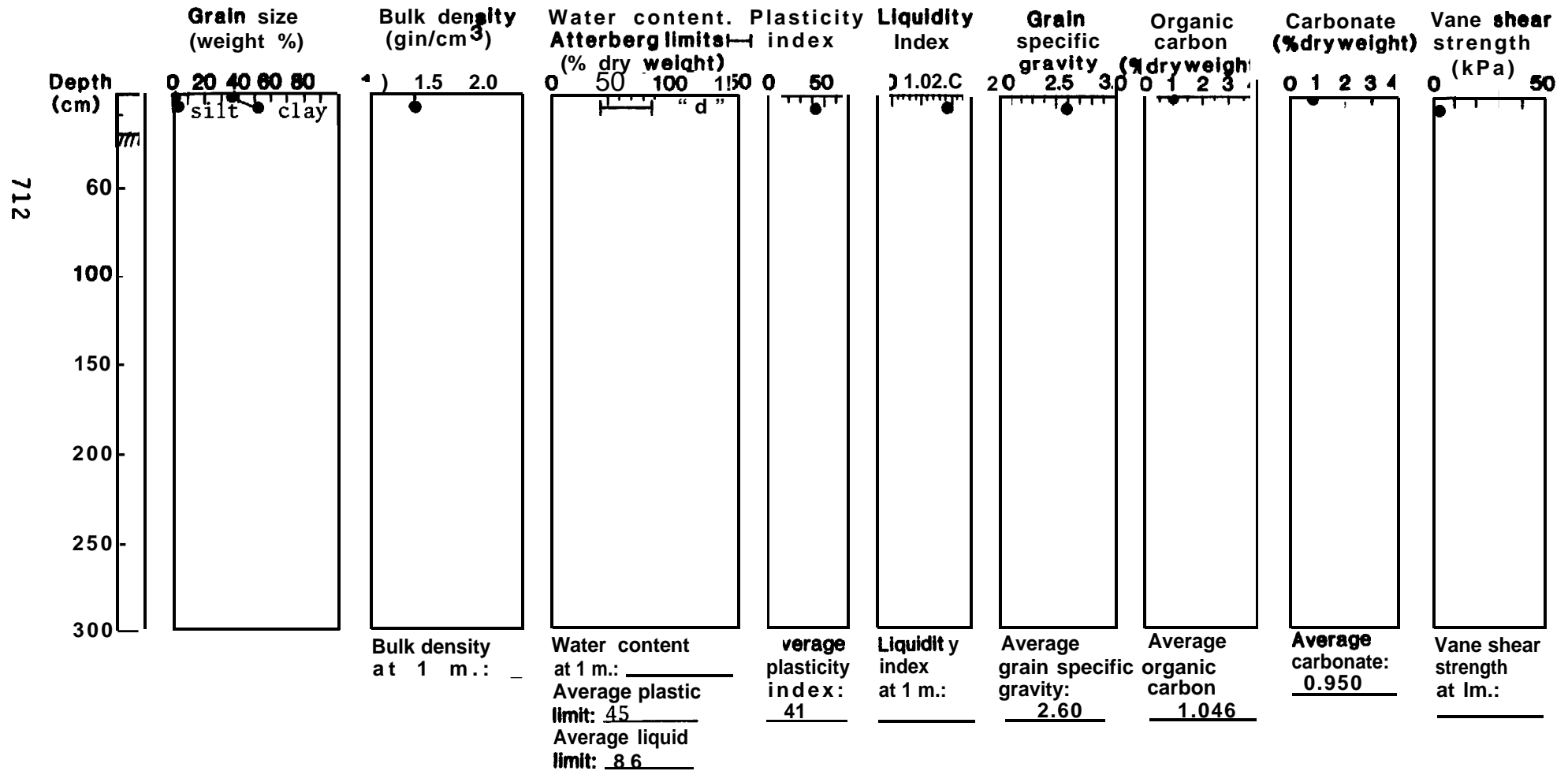
Water depth 185m



Station 522

Location 58°05.5'N 153°41.1'W

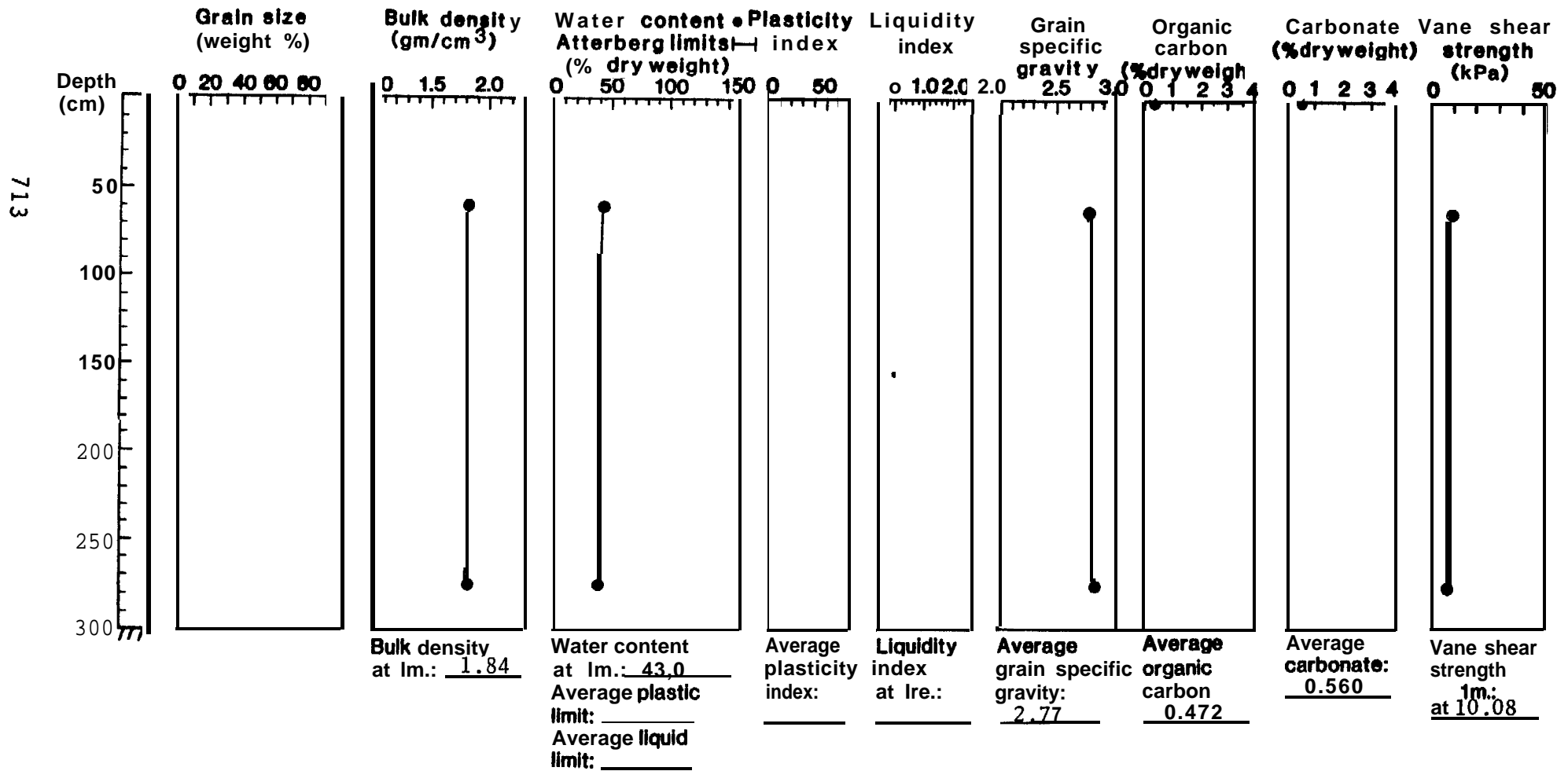
Water depth 185m



Station 523

Location 58°01.7'N 153°34.2'W

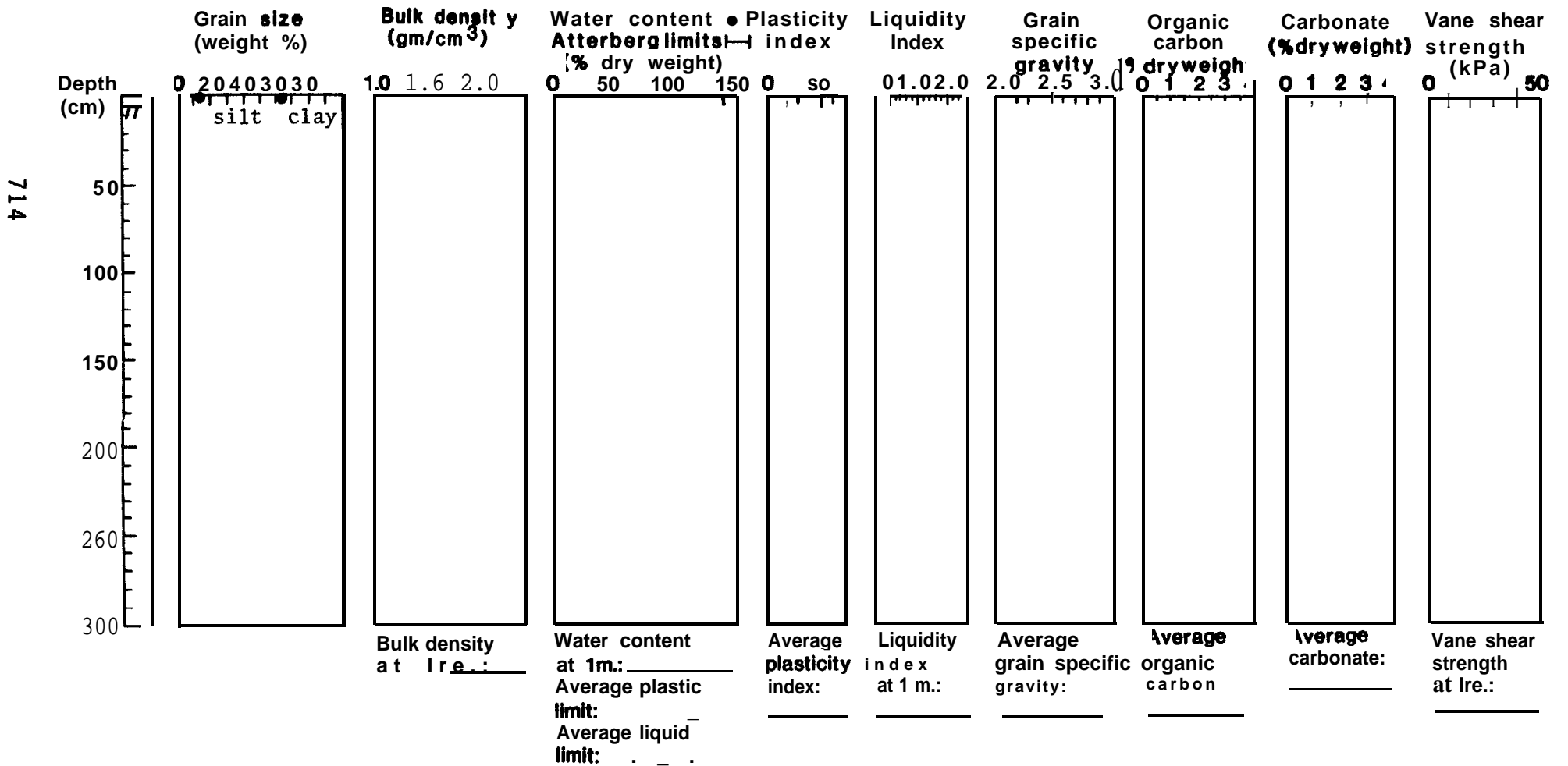
Water depth 130m



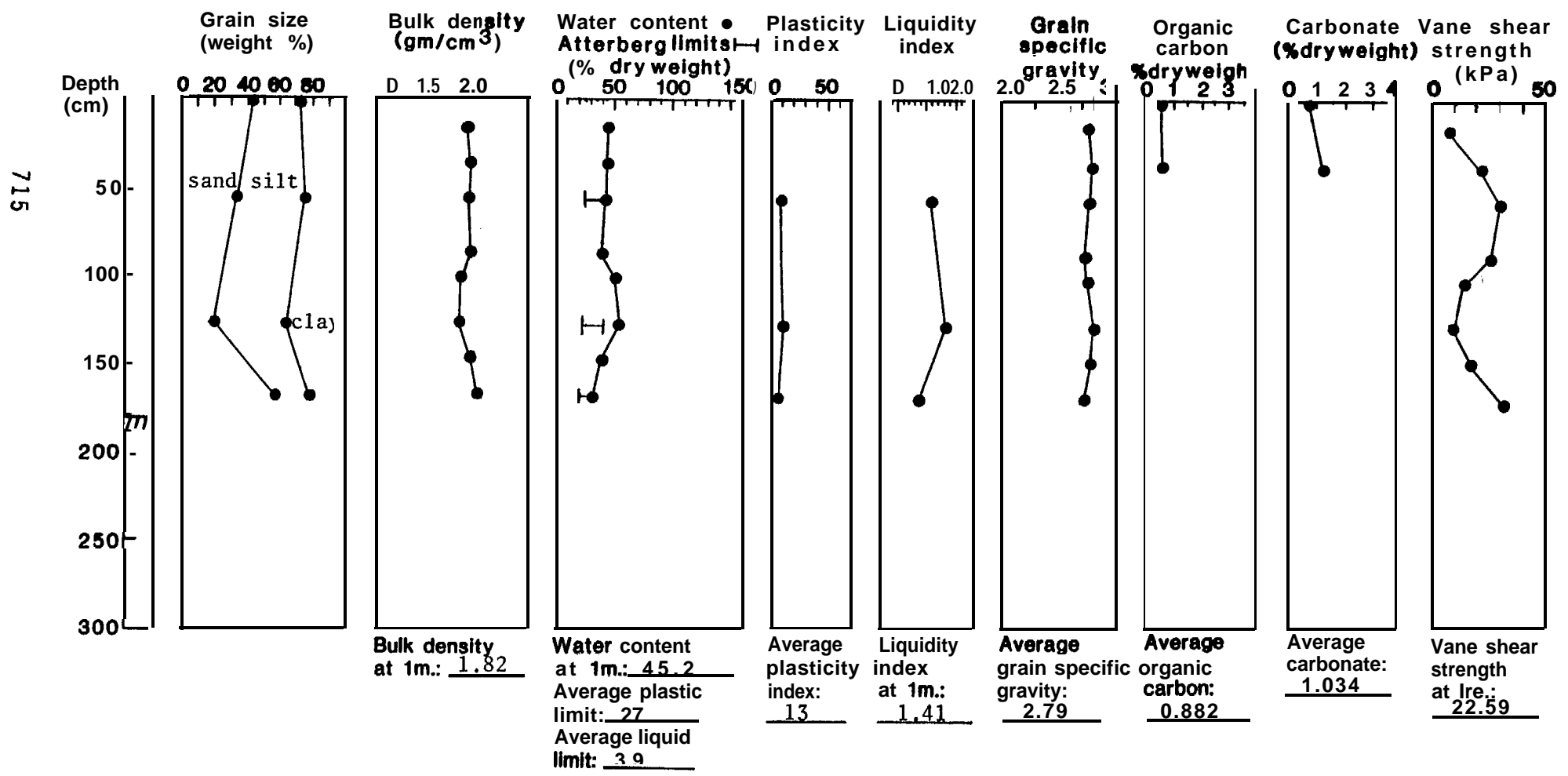
Station 524

Location 58°15.94'N 153°41.87'W

Water depth 175m



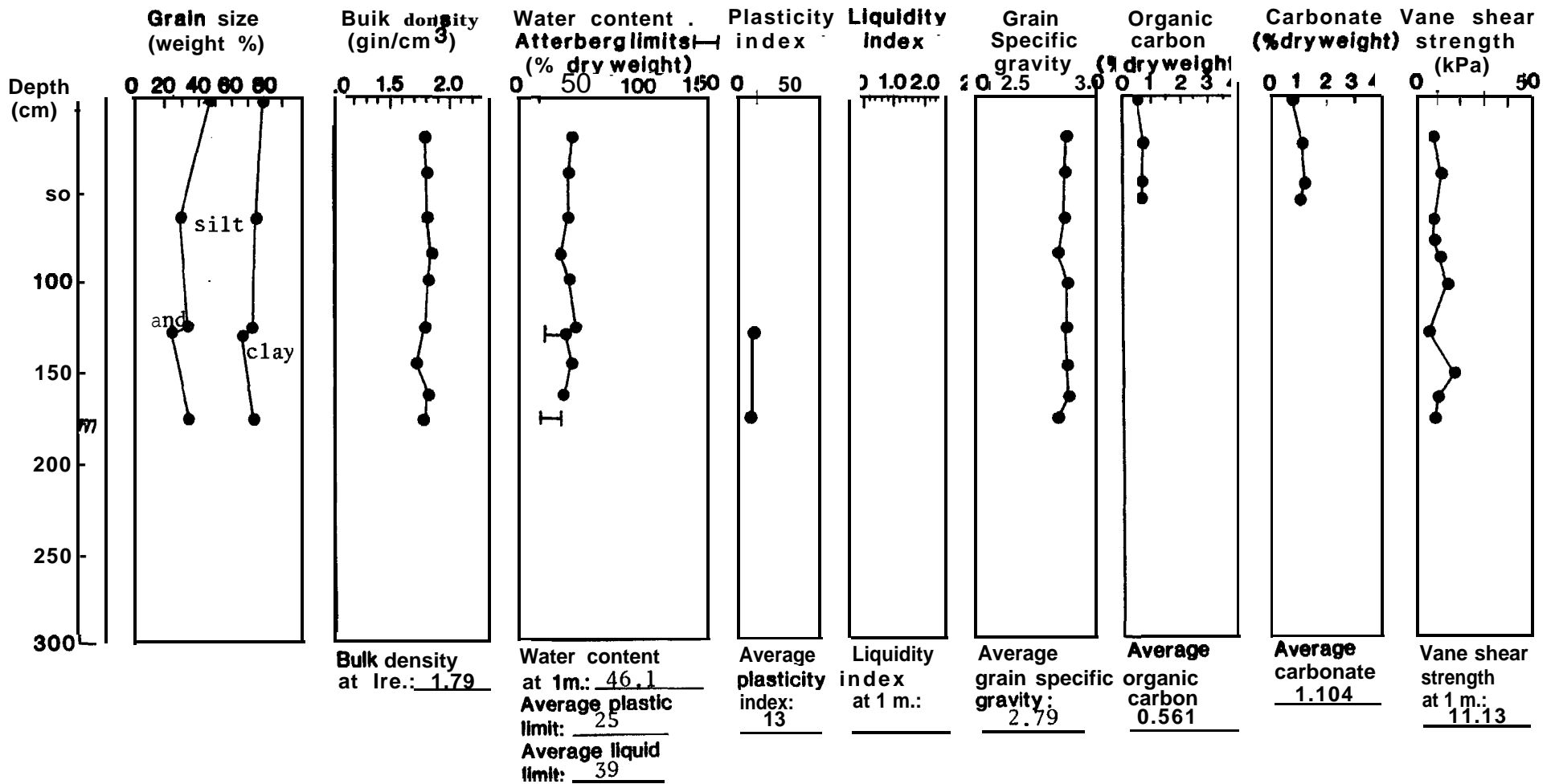
Station 525 Location 58°23.7'N 153°37.2'W Water depth 158m



Station 526

Location 58°29.0'N 153°27.1'W

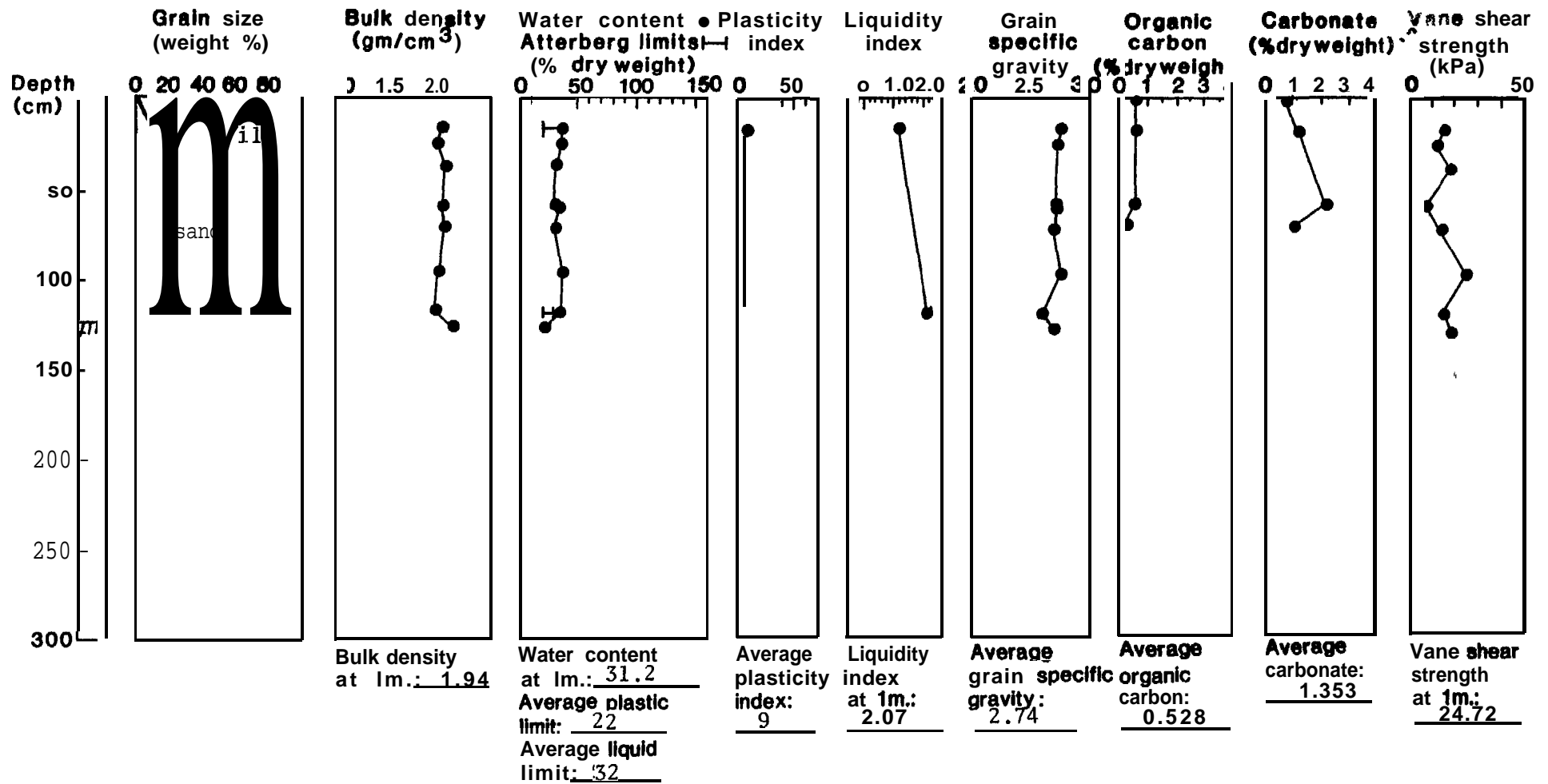
Water depth 138m



Station 527

Location 58°34.2'N 153°17.6'W

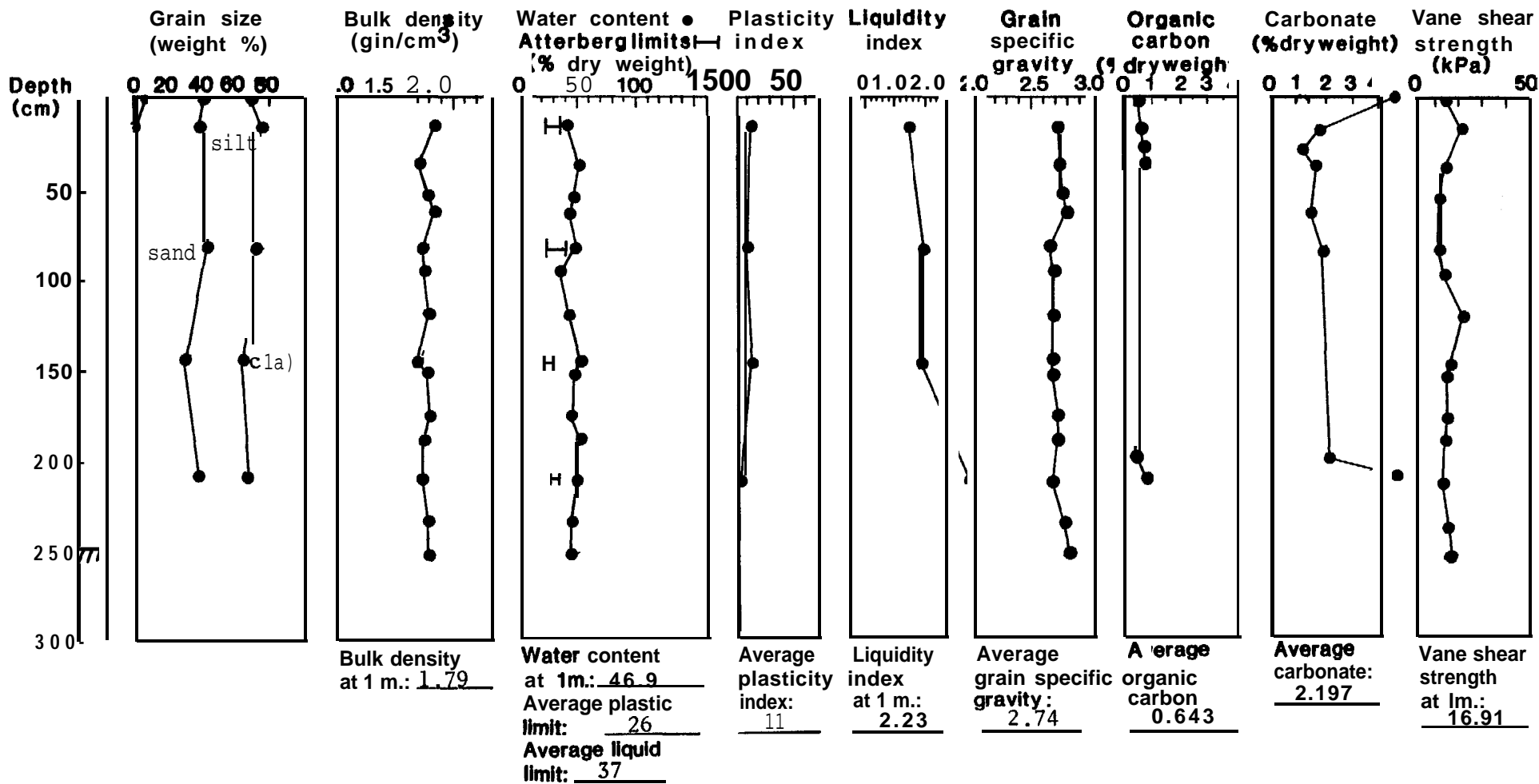
Water depth 153m



Station 528

Location 58°39.4'N 153°0.7'W

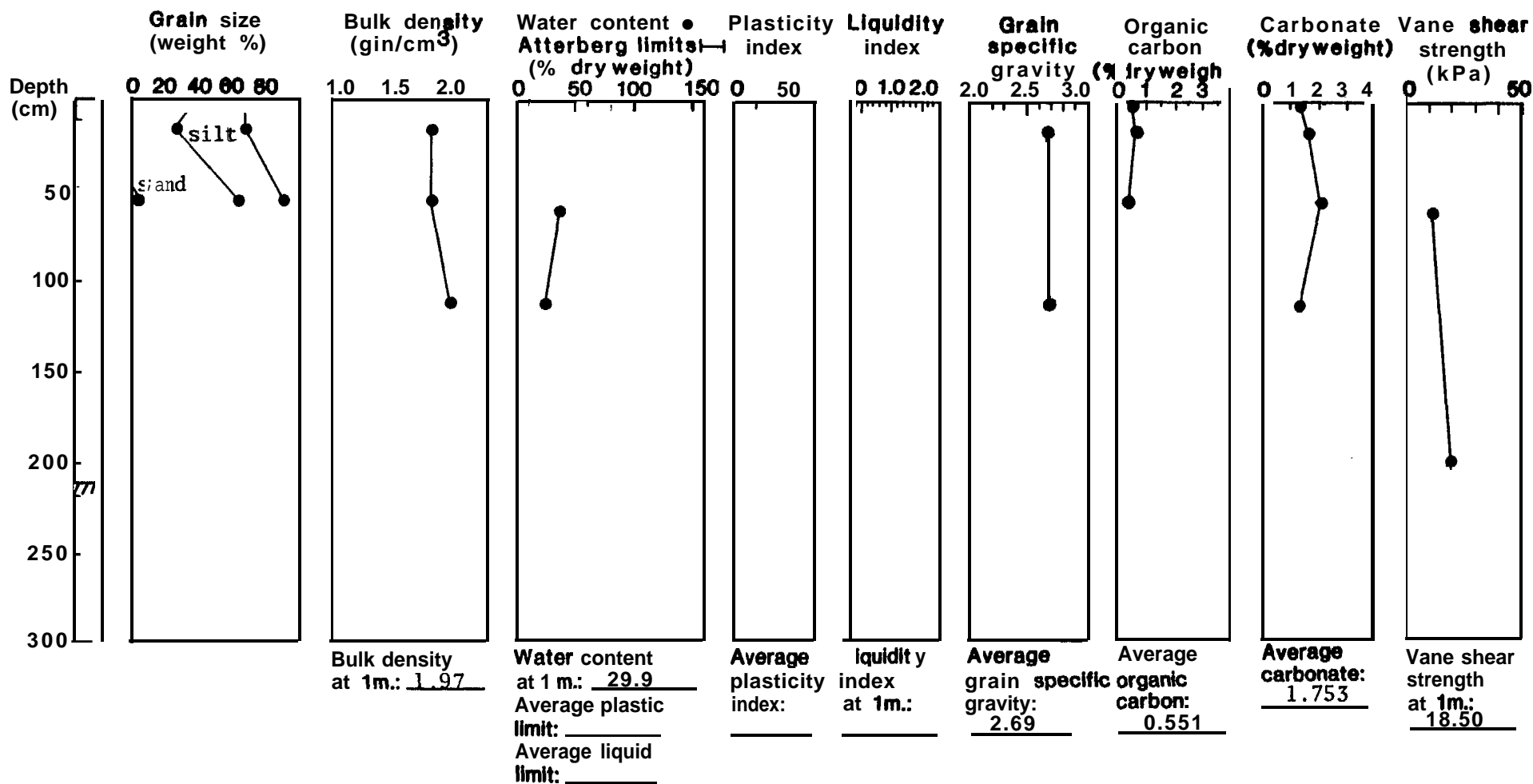
Water depth 159m



Station 529

Location 58°44.4'N 152°57.4'W

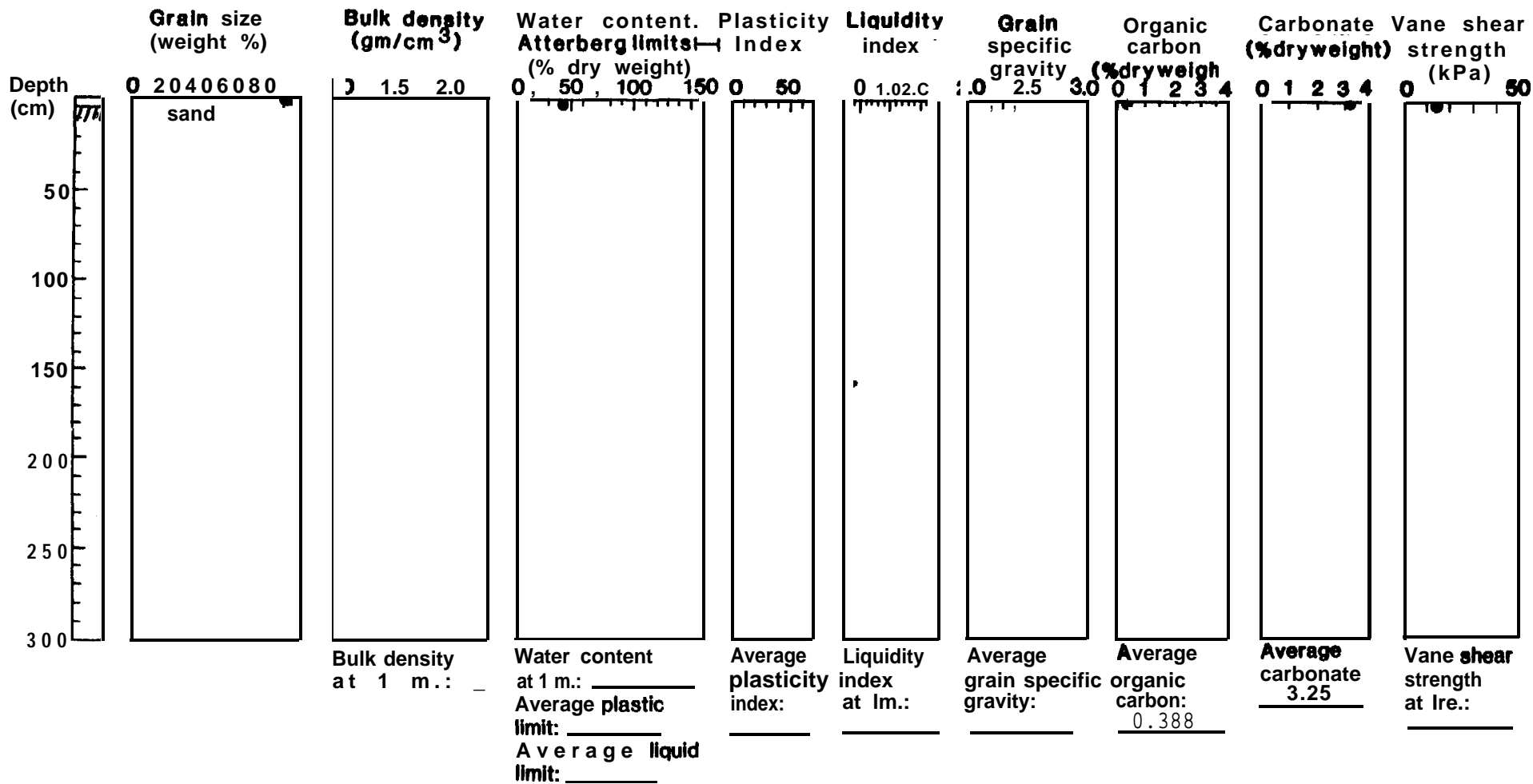
Water depth 136m



Station 531

Location 58 °54.9'N 152 °37.3'W

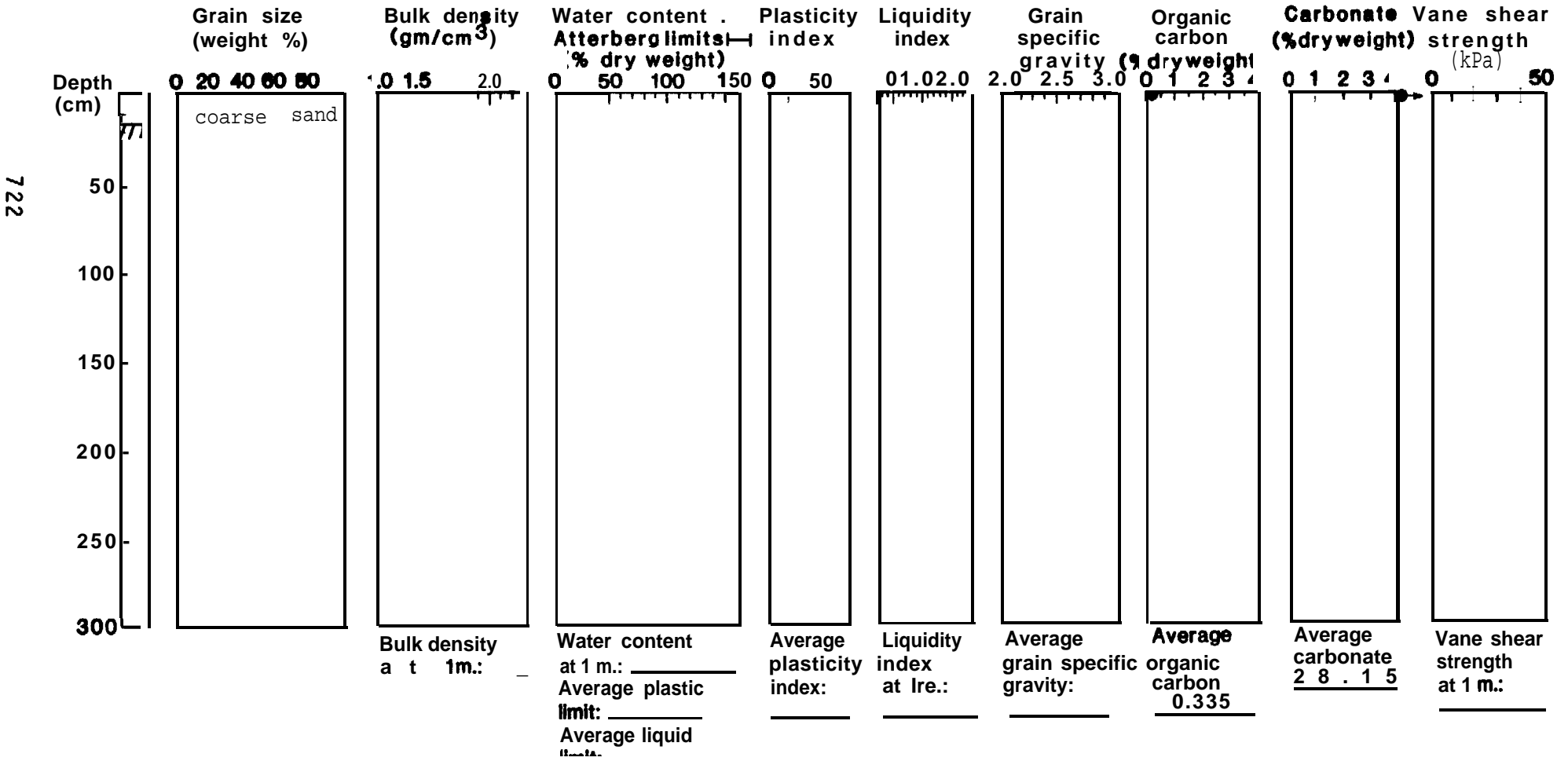
Water depth 161m



Station 532

Location 58°45.85'N 152°27.98'W

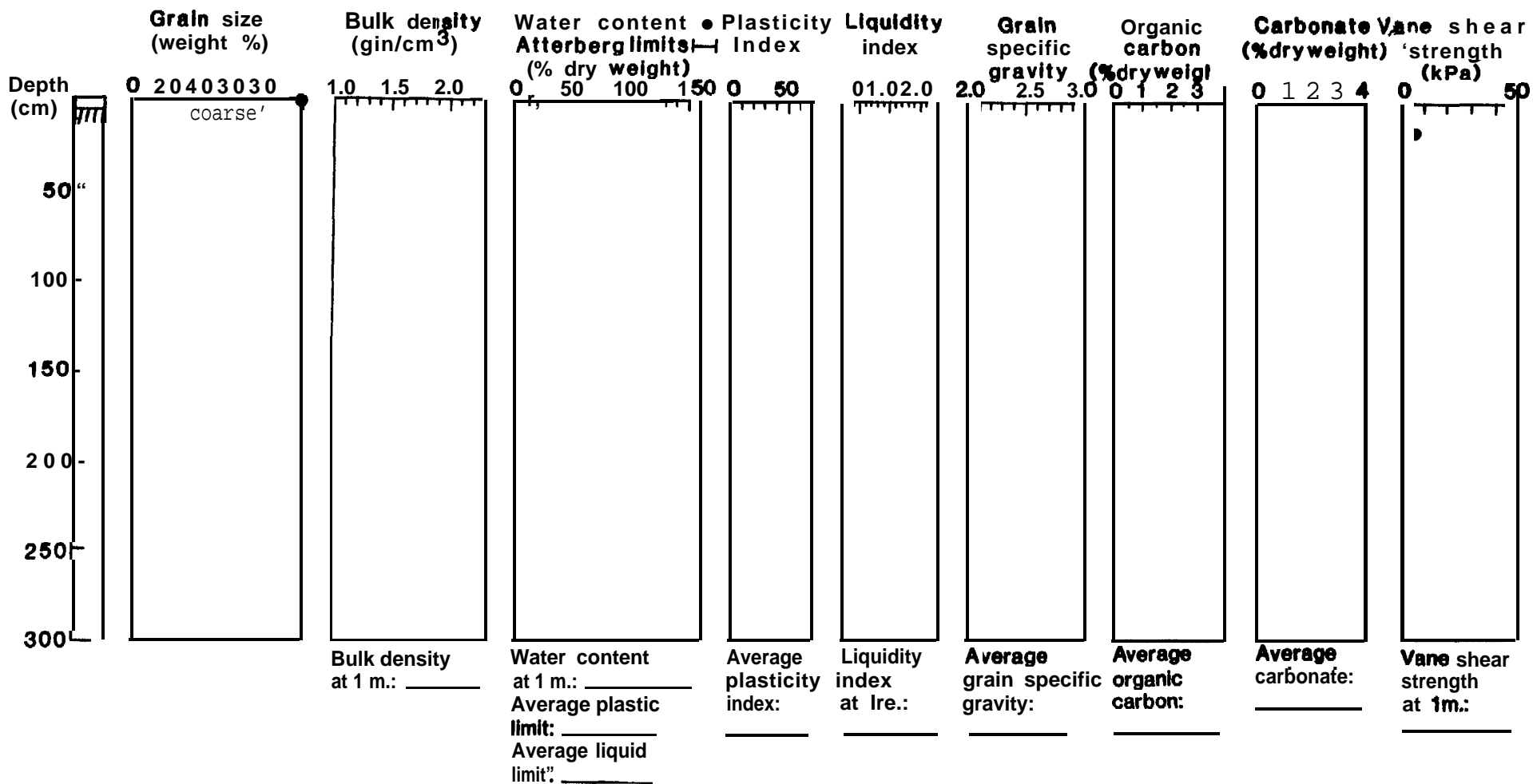
Water depth 195m



Station 533

Location 58°50.4'N 152°23.9'W

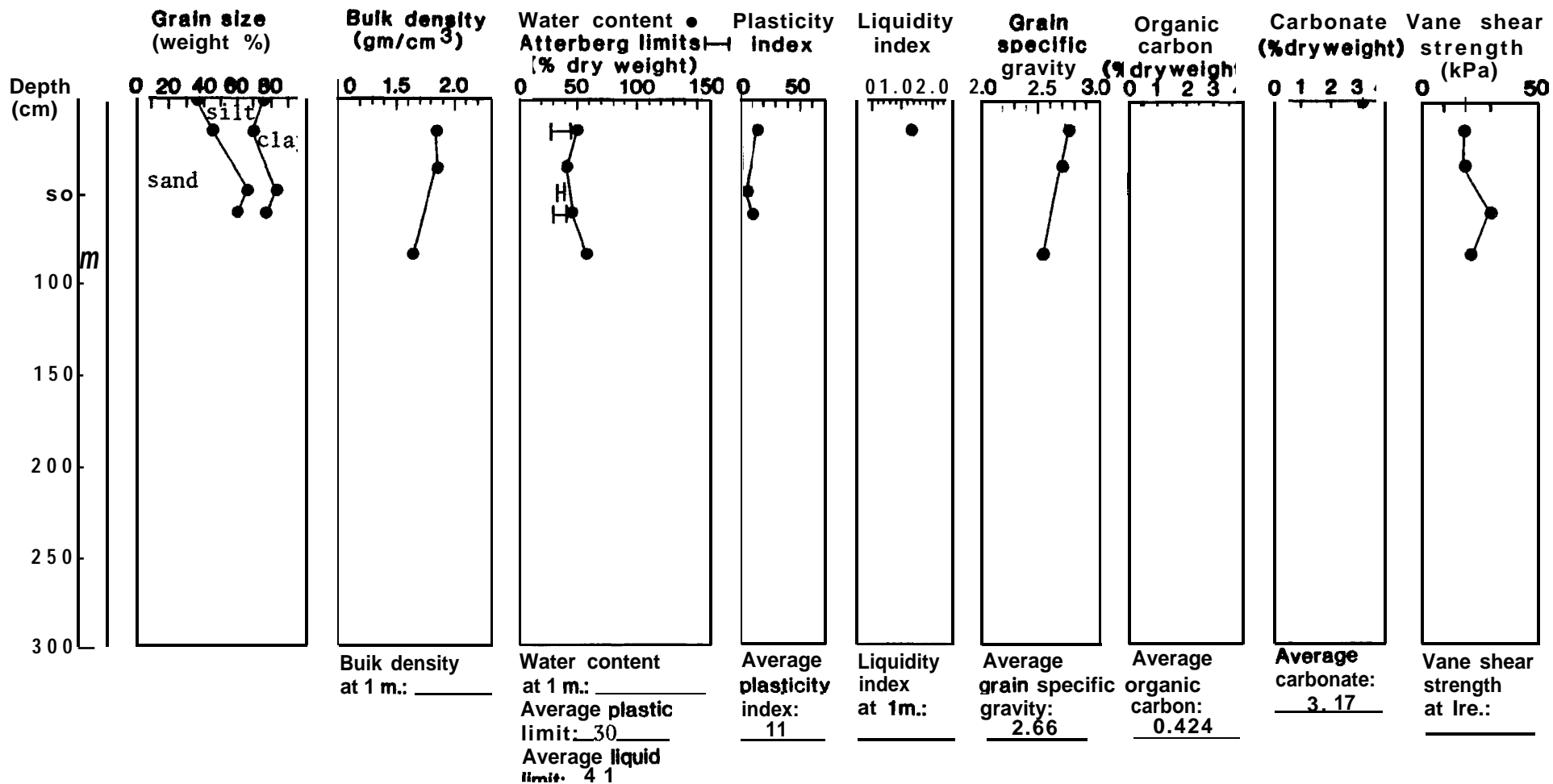
Water depth 120m



Station 534

Location 58°39.6'N 152°47.1'W

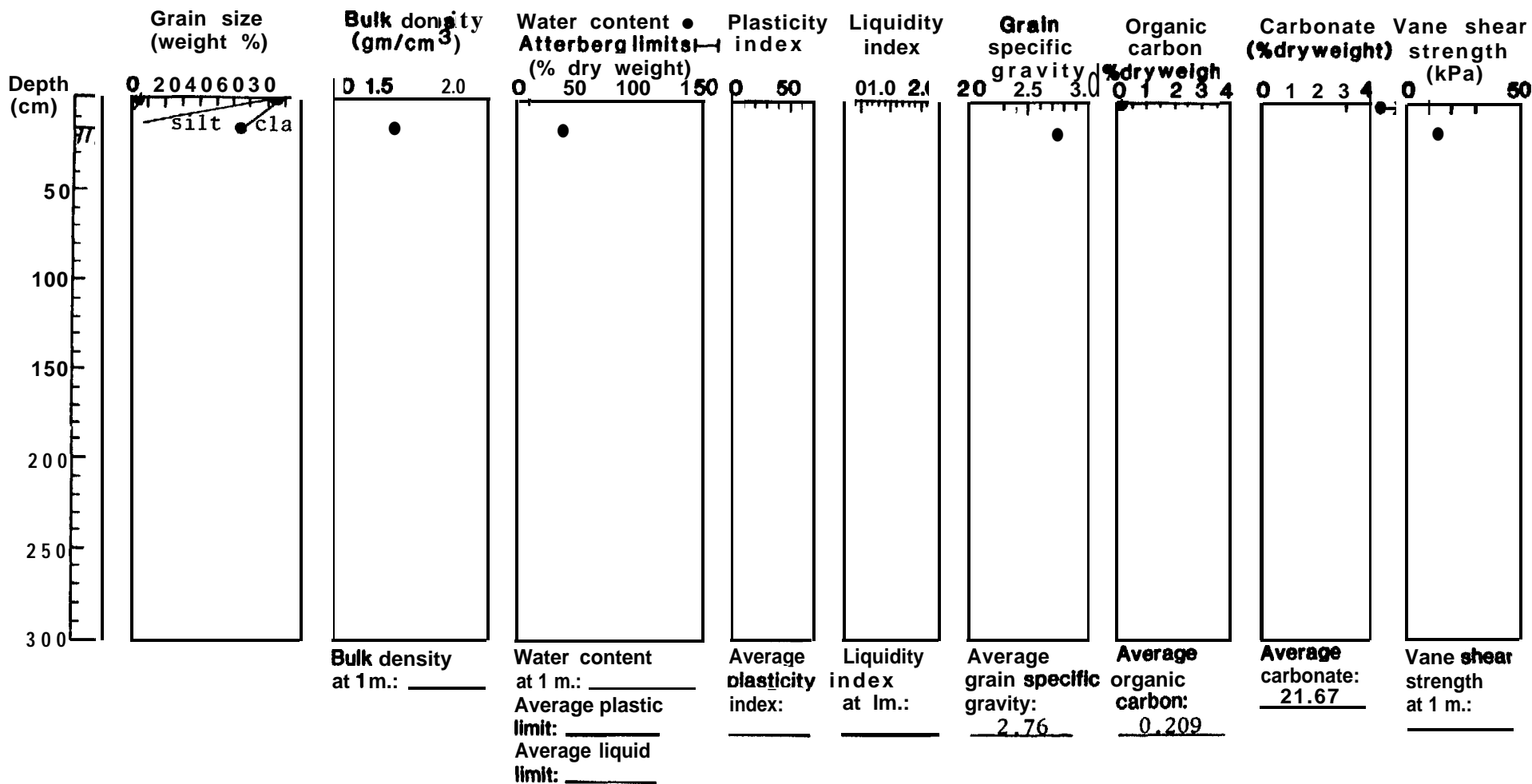
Water depth 185m



Station 535

Location 58°37.0'N 152°42.0'W

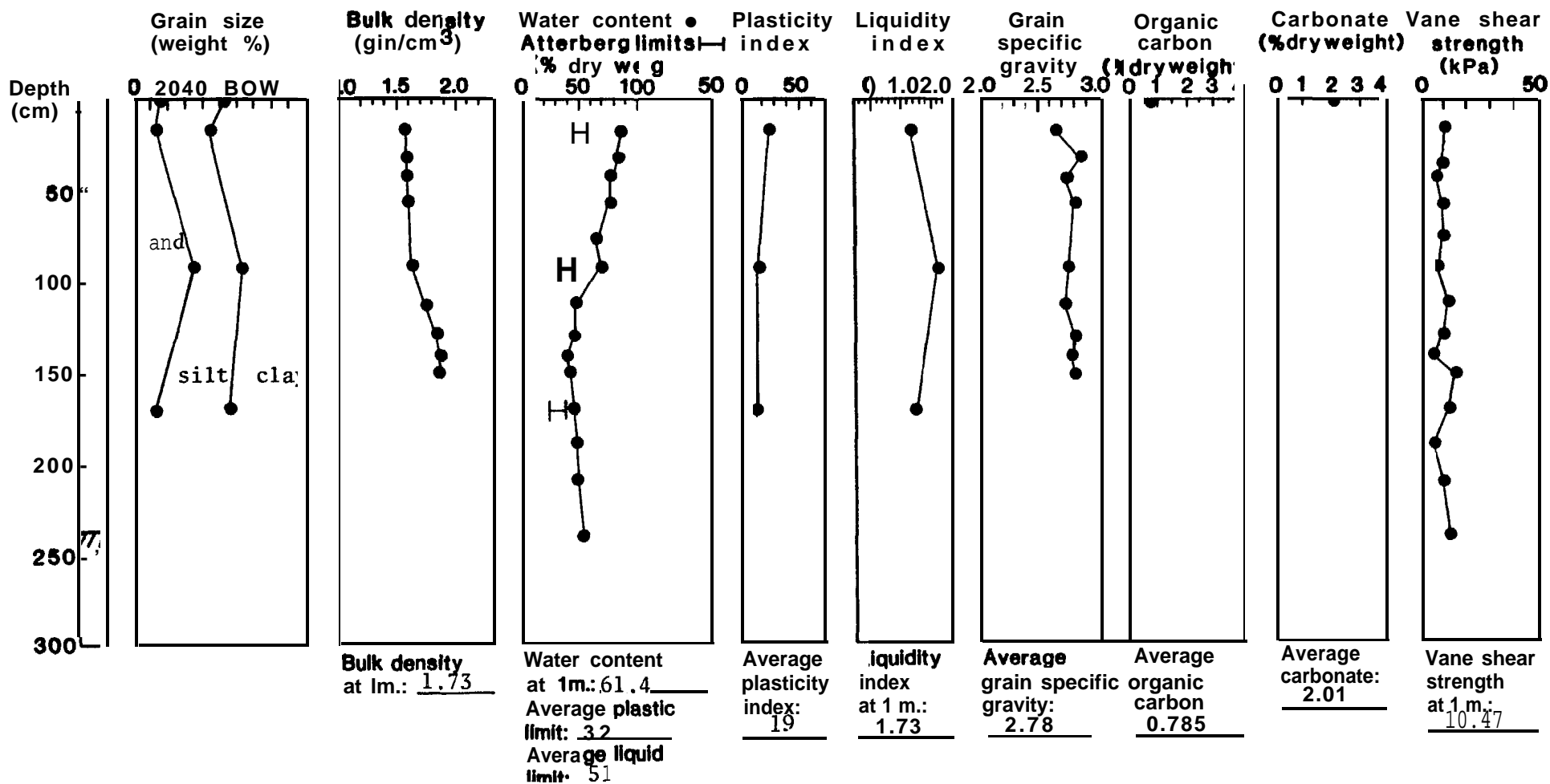
Water depth 98m



Station 536

Location 58°31.4'N 152°52.6'W

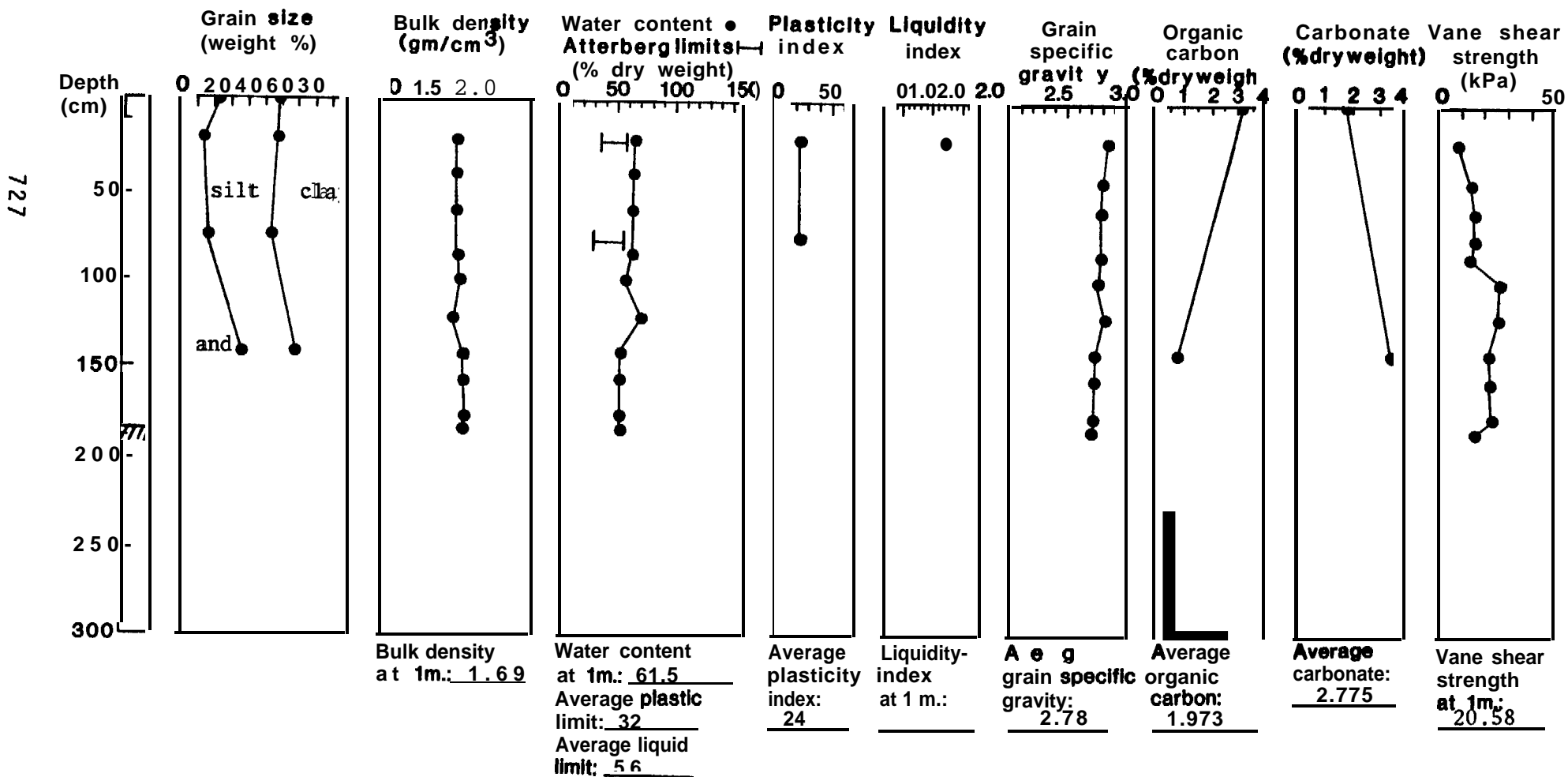
Water depth 190m



Station 537

Location 58°29.0'N 153°07.6'W

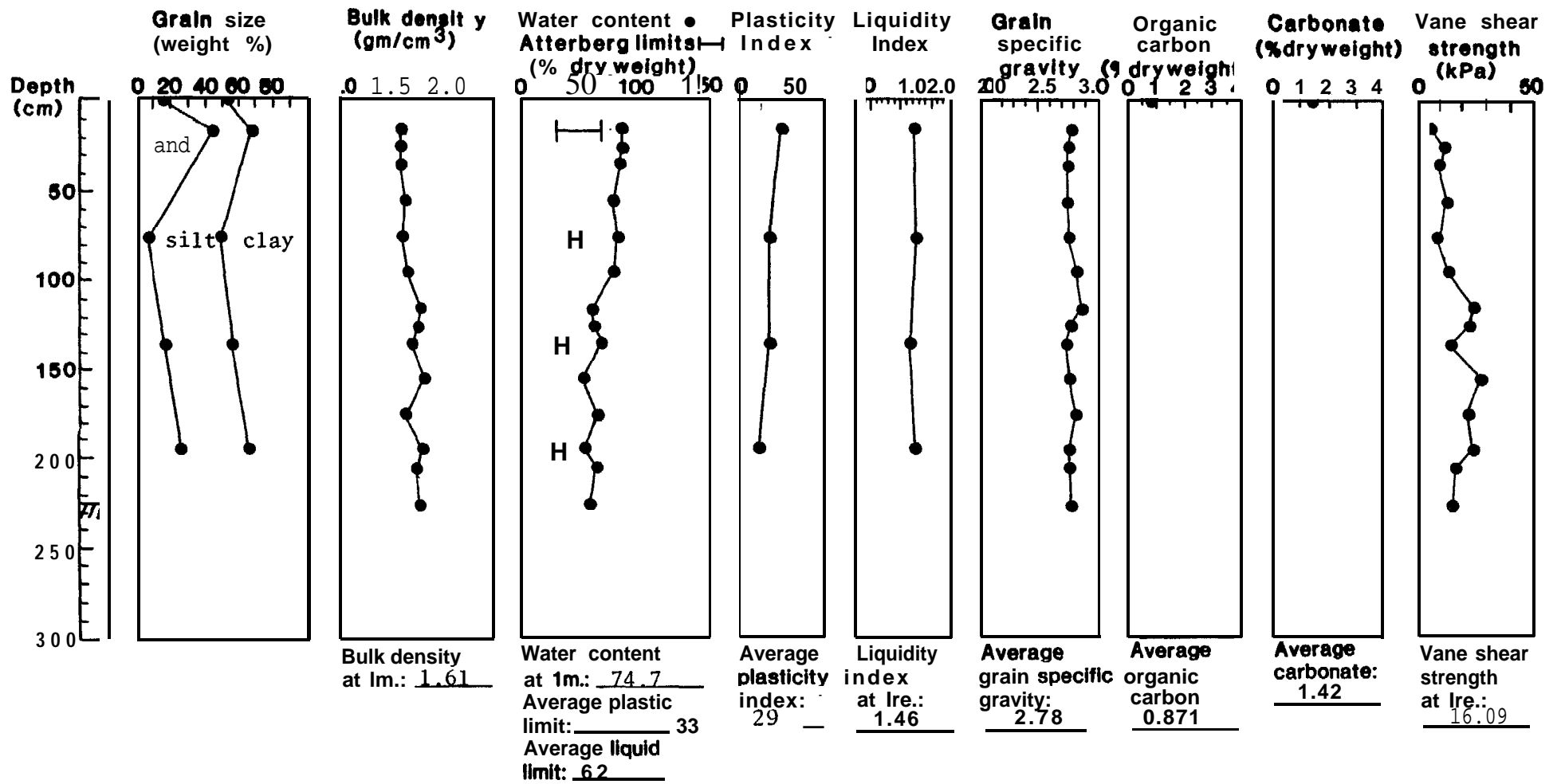
Water depth 160m



Station 538

Location 58°25.2'N 153°00.2'W

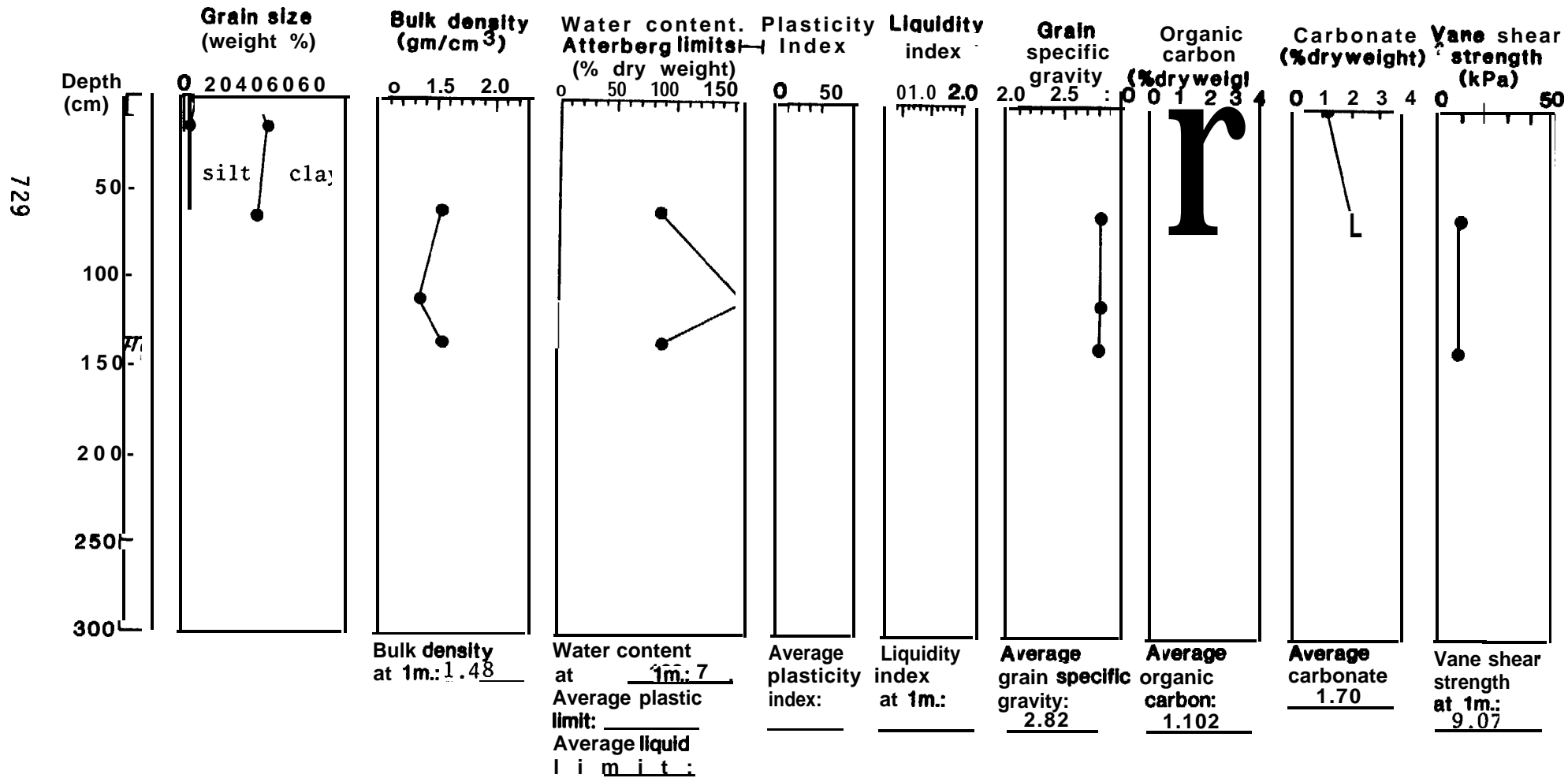
Water depth 190m



Station 539

Location 58°21.3'N 153°12.4'W

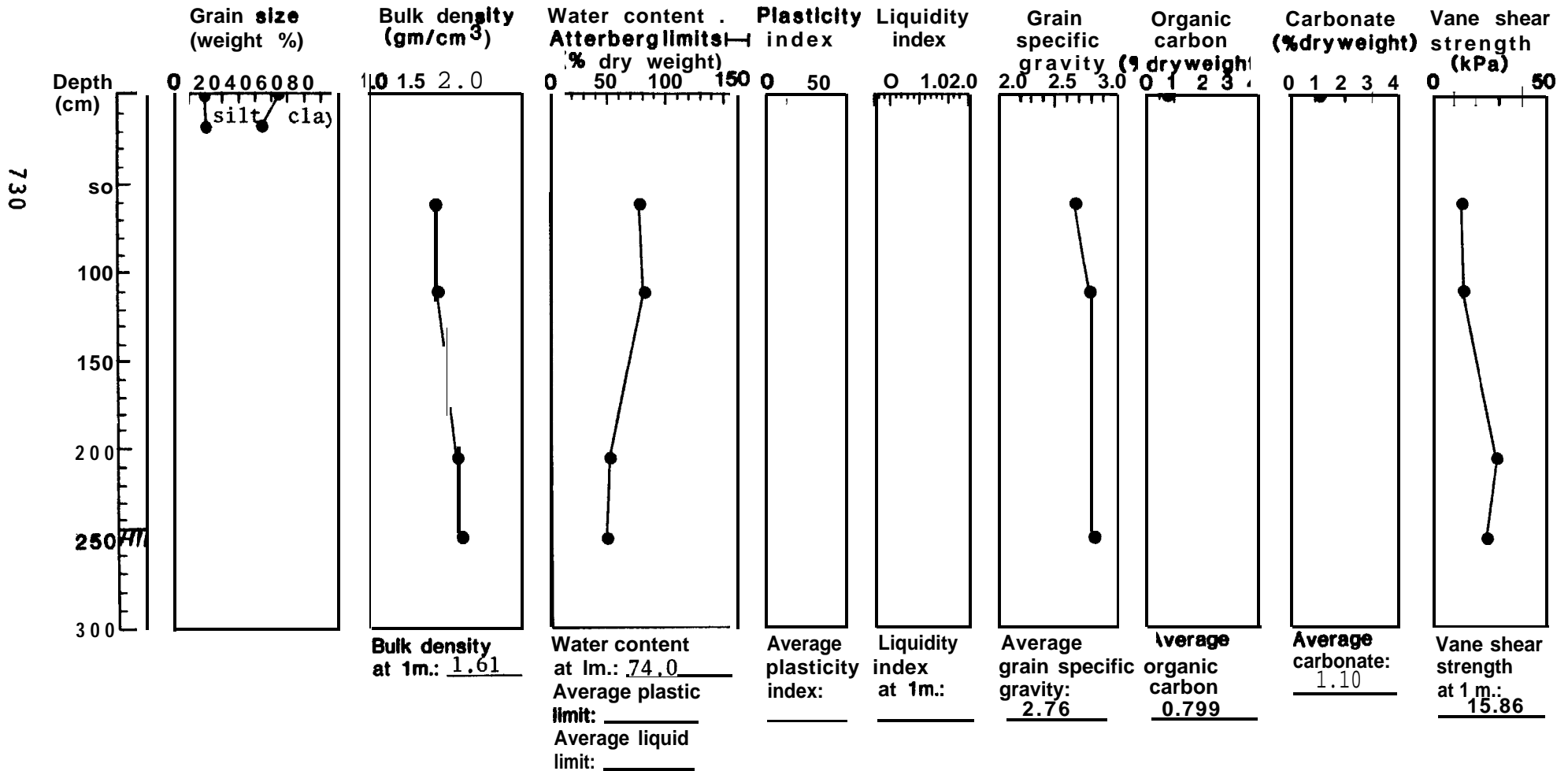
Water depth 175m



Station 540

Location 58°21.5'N 153°07.6'W

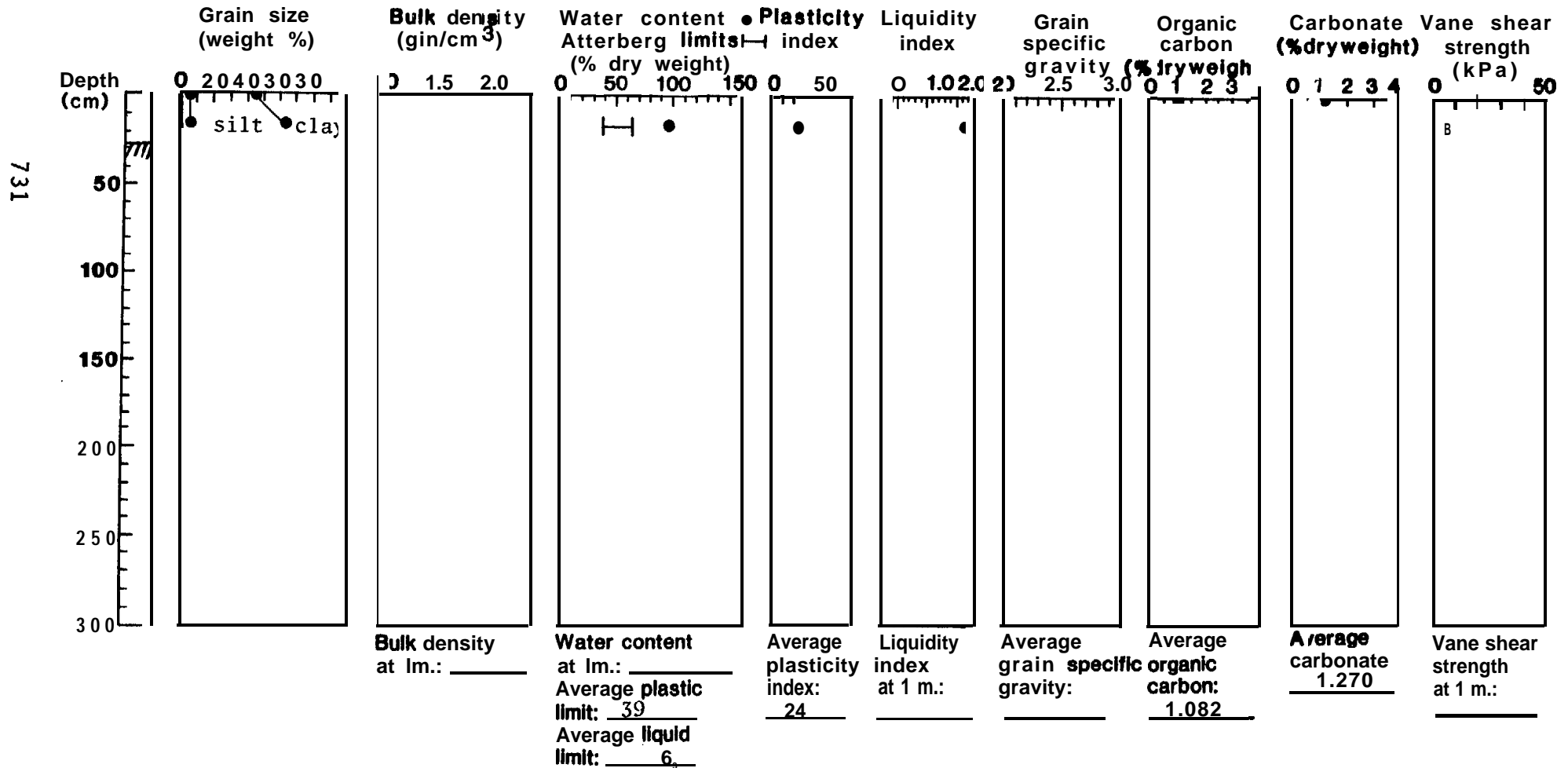
Water depth 210m



Station 541

Location 58°15.8'N 153°22.0'W

Water depth 167m

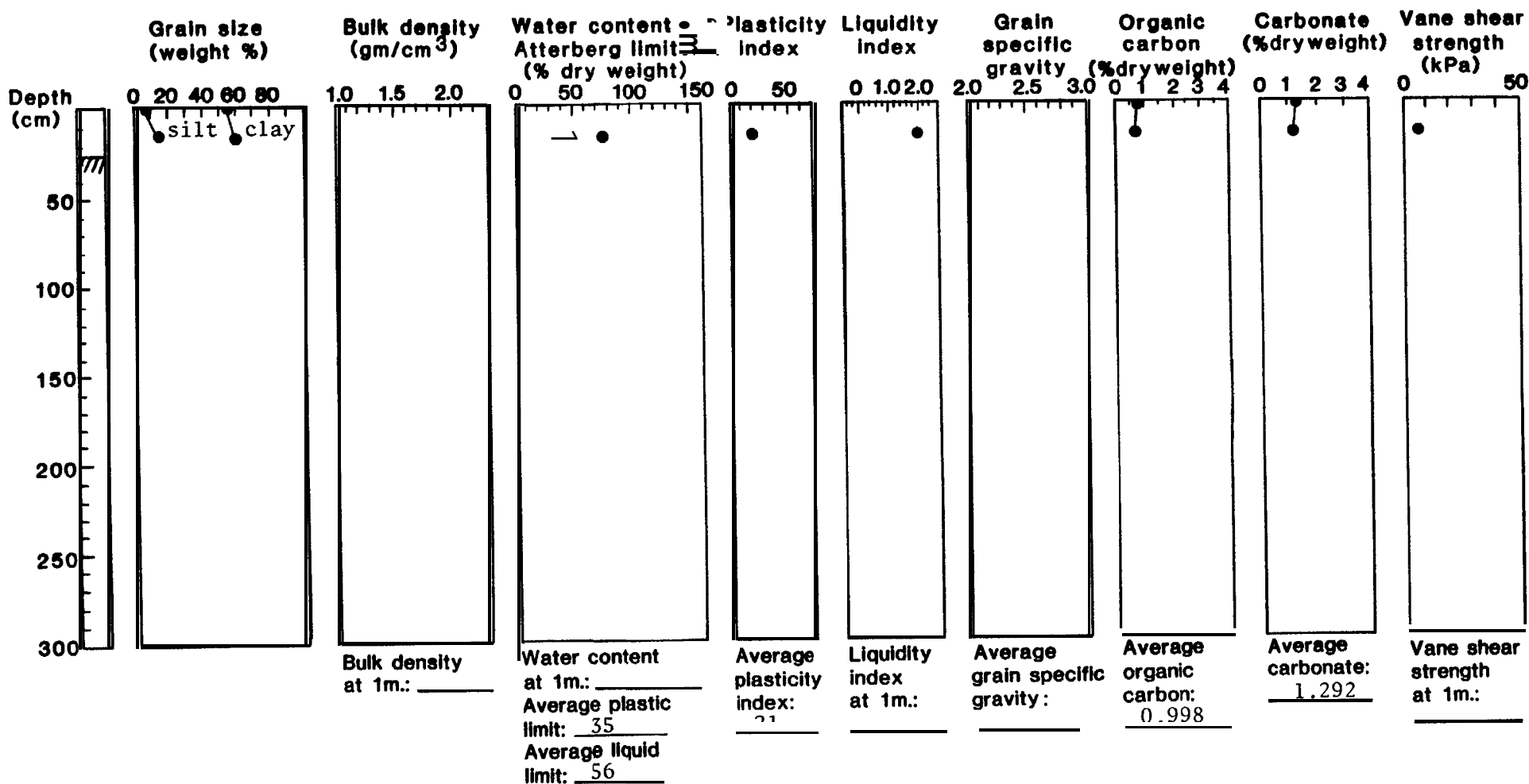


Station 542

Location 8°18.6'N 153°26.9'W

Water depth 155m

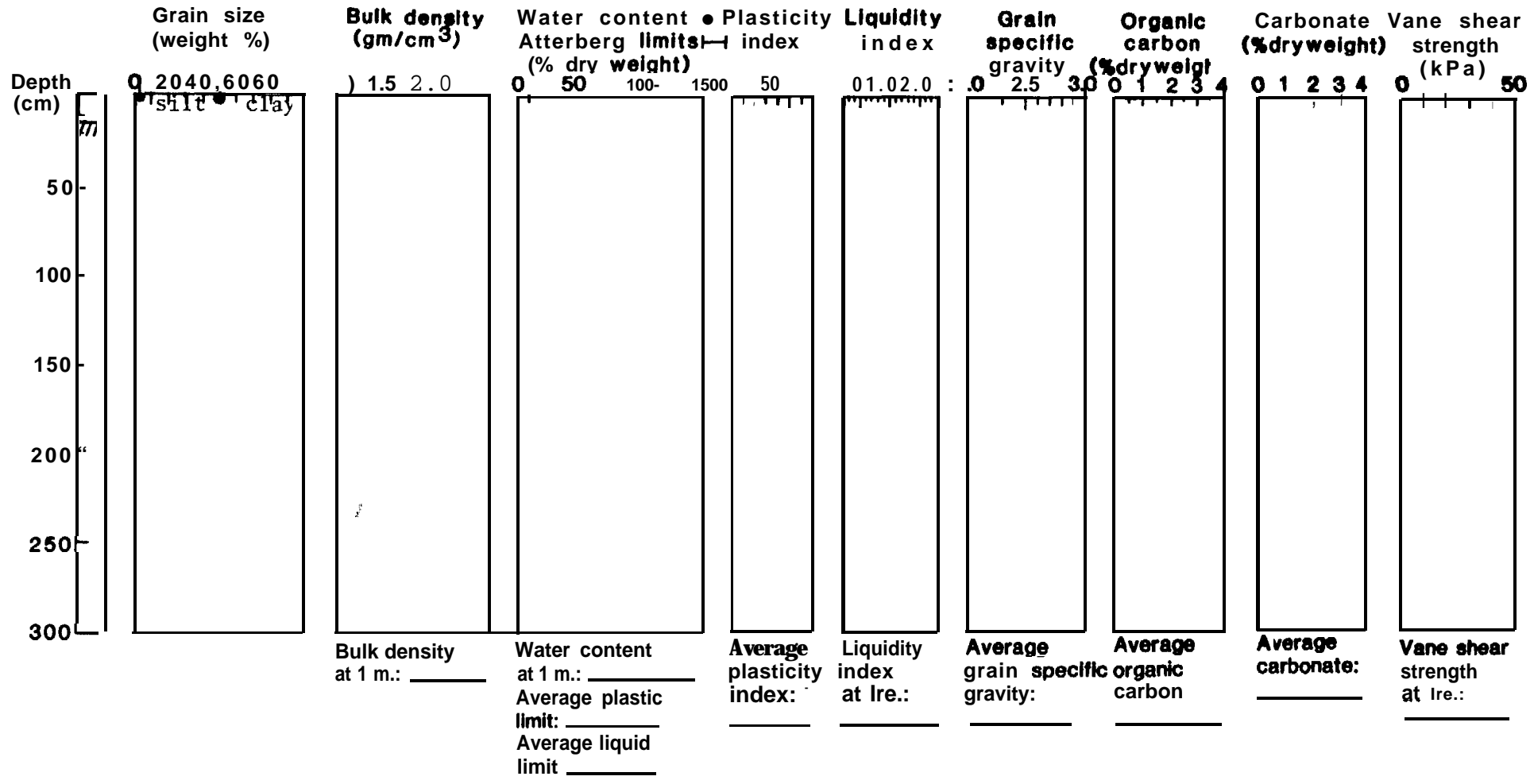
732



Station 543

Location 58 °10.77'N 153 °31.97'W

Water depth 180m

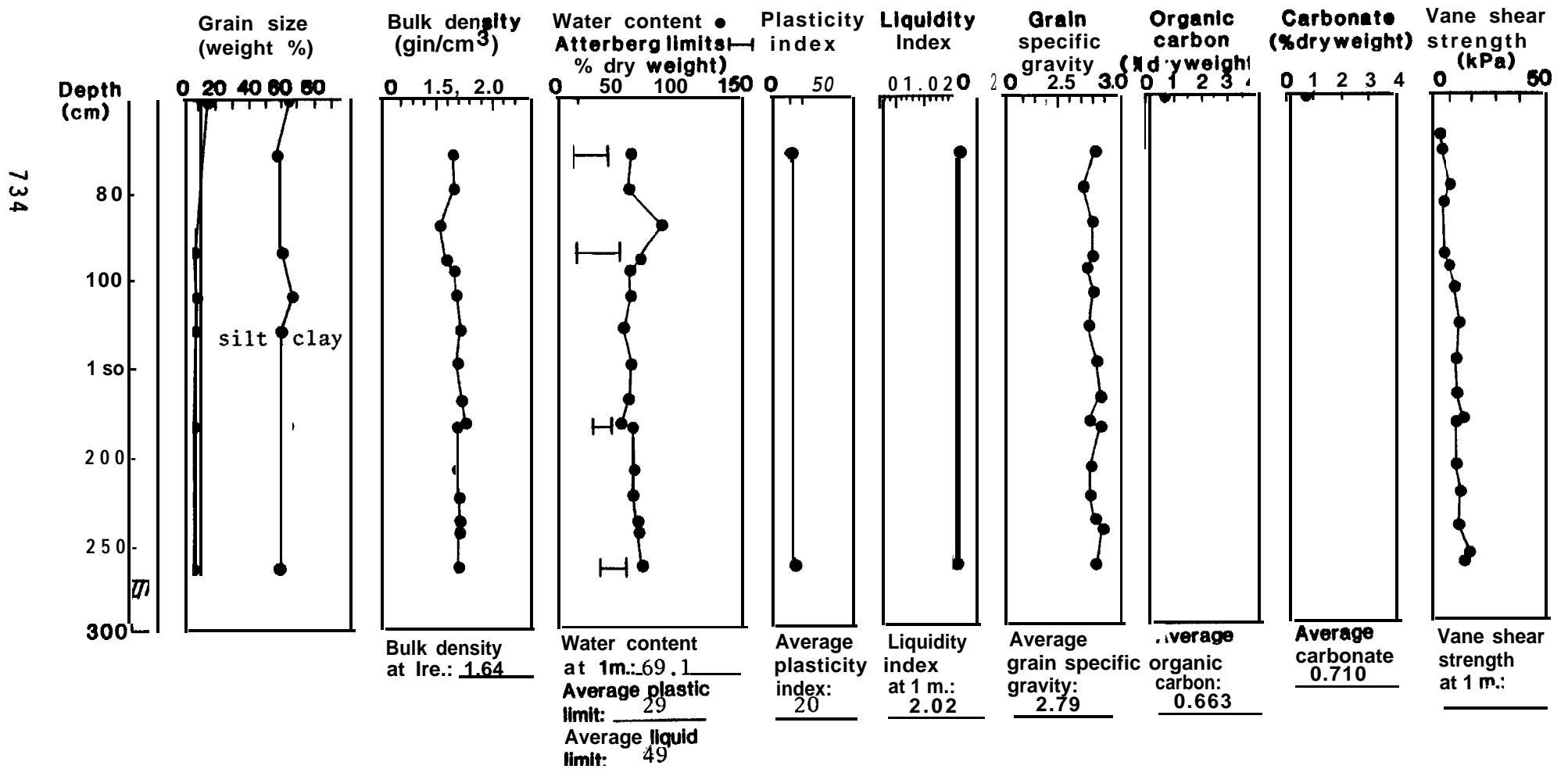


733

Station 545

Location 58 °22.5'N 153°53.5'W

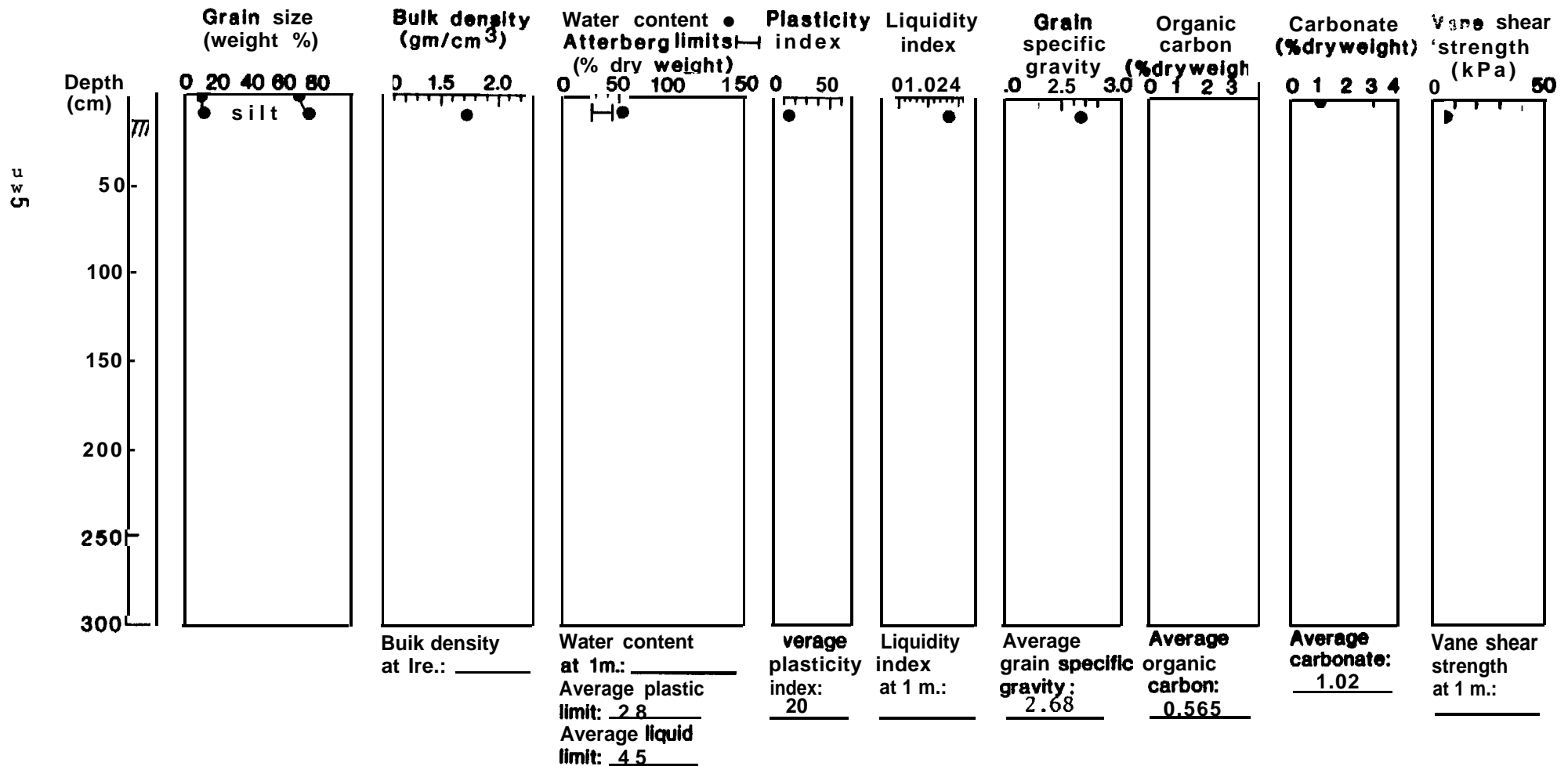
Water depth 175m



Station 546

Location 58°28.8'N 153°37.0'W

Water depth 97m

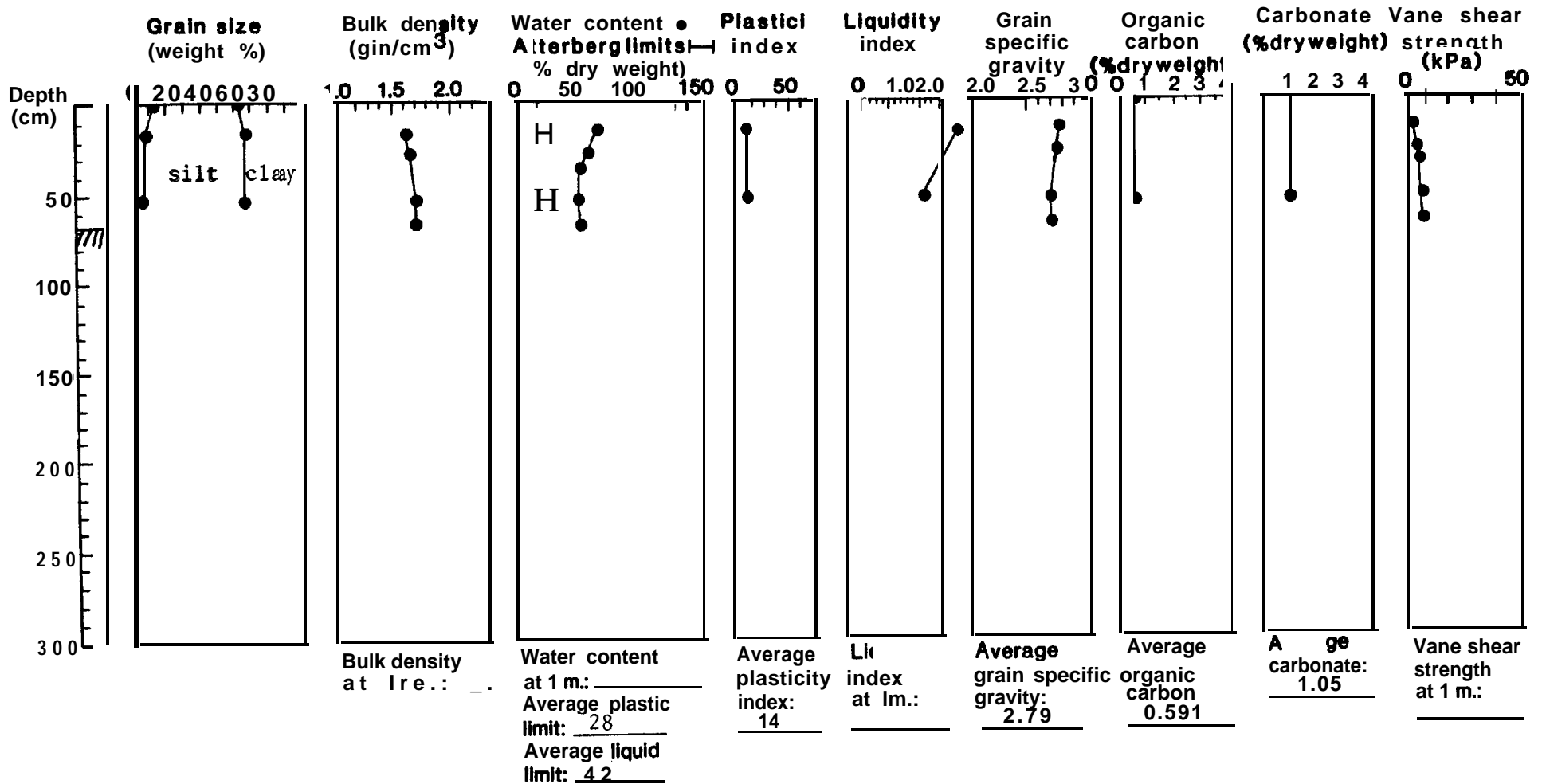


Station 547

Location 58°33.0'N 153°34.4'W

Water depth 89m

736

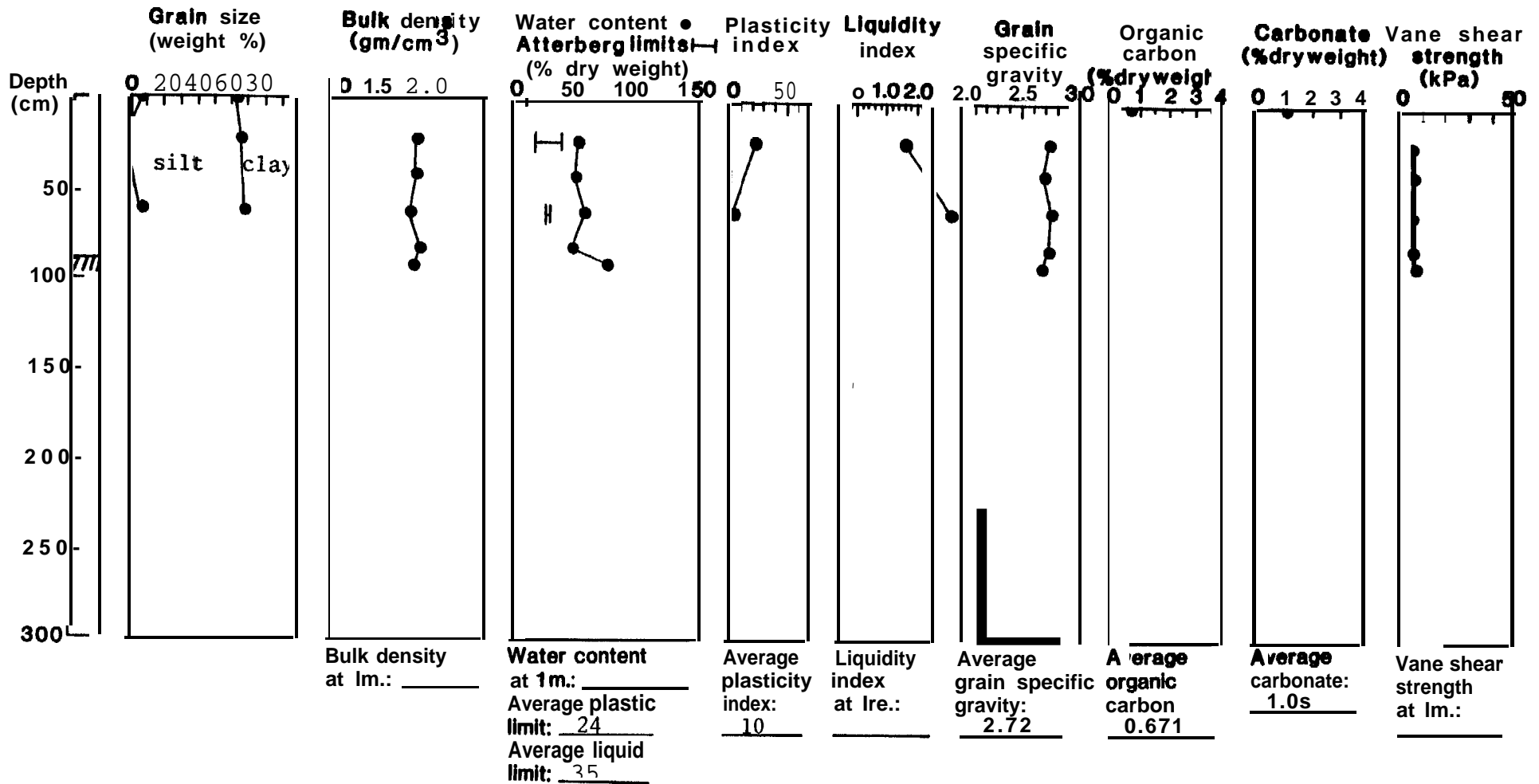


Station 548

Location 58 °37.9'N 153 °25.1 'W

Water depth 64m

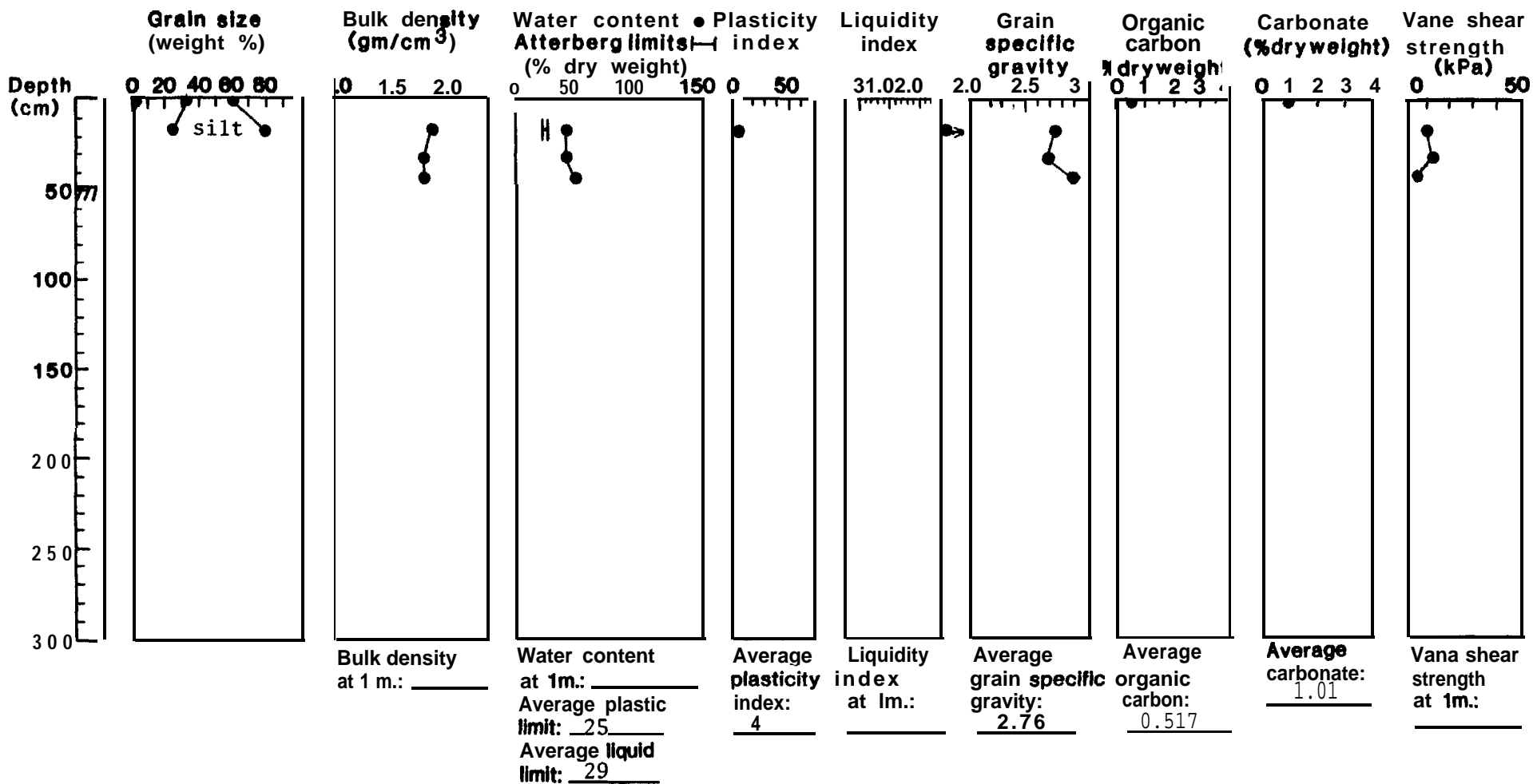
737



Station 549

Location 58°43.3'N 153°15.0'W

Water depth 87m

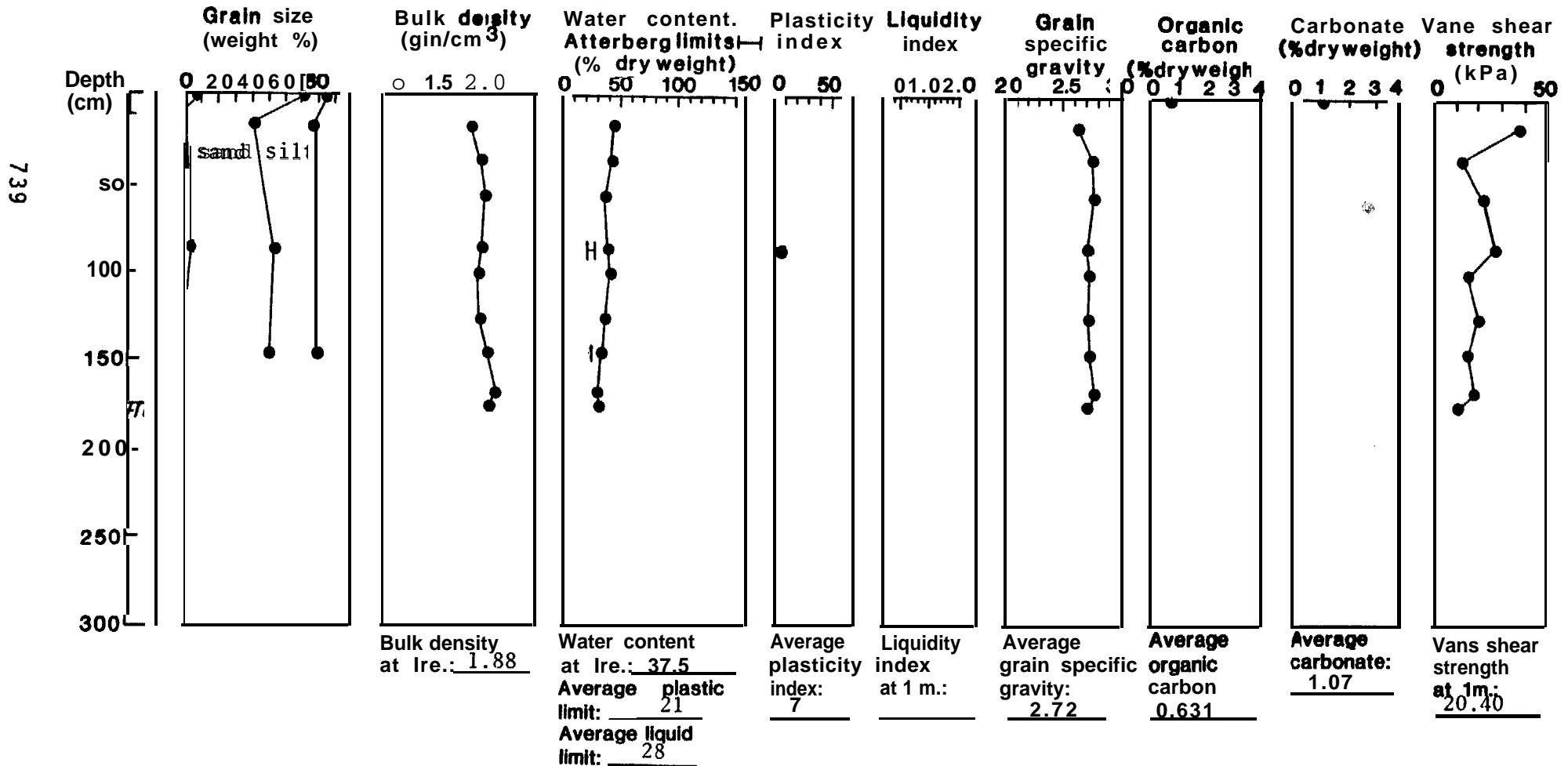


738

Station 550

Location 58°50.8'N 153°10.3'W

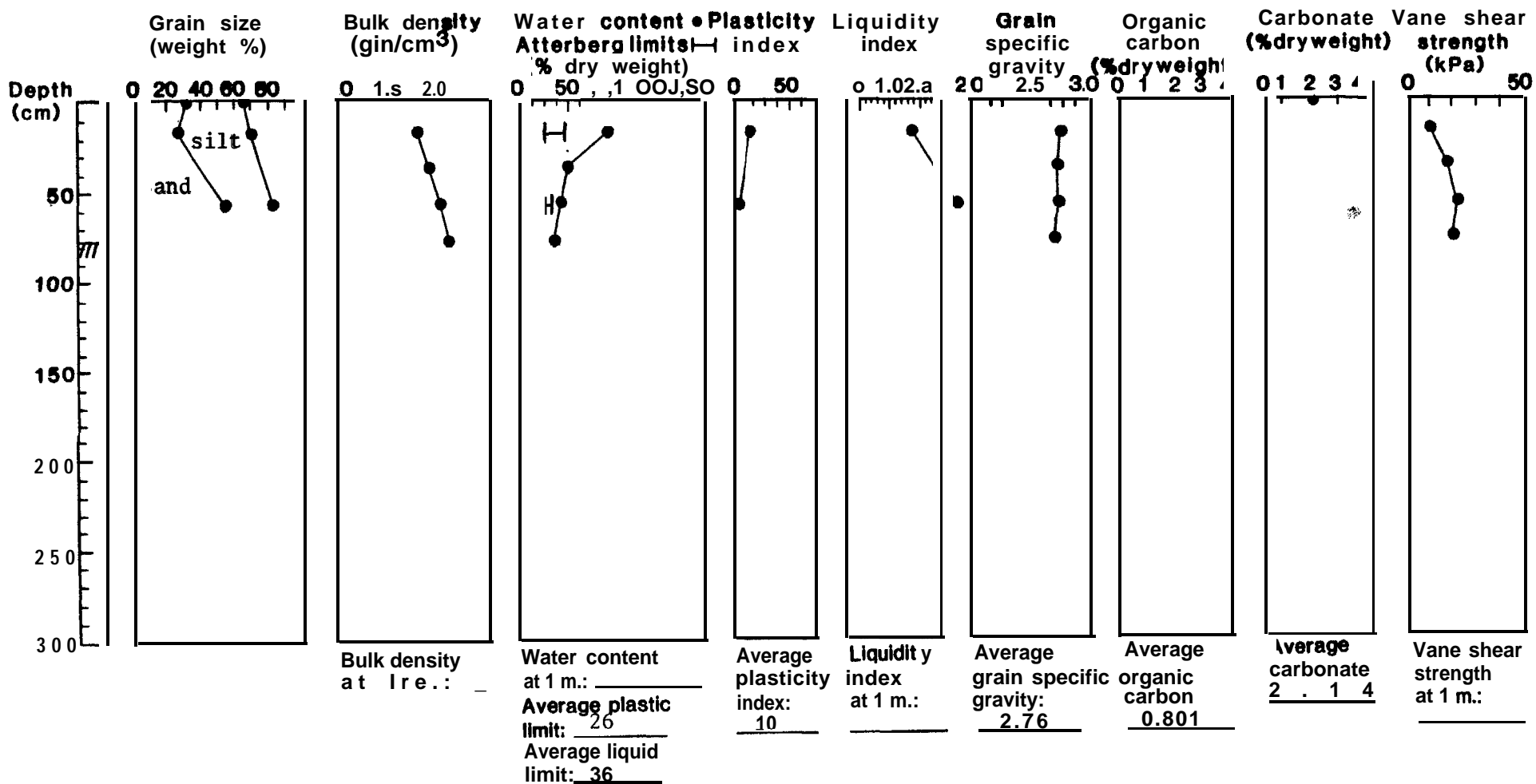
Water depth 165 m



Station 551

Location 58°53.6'N 152°54.4'W

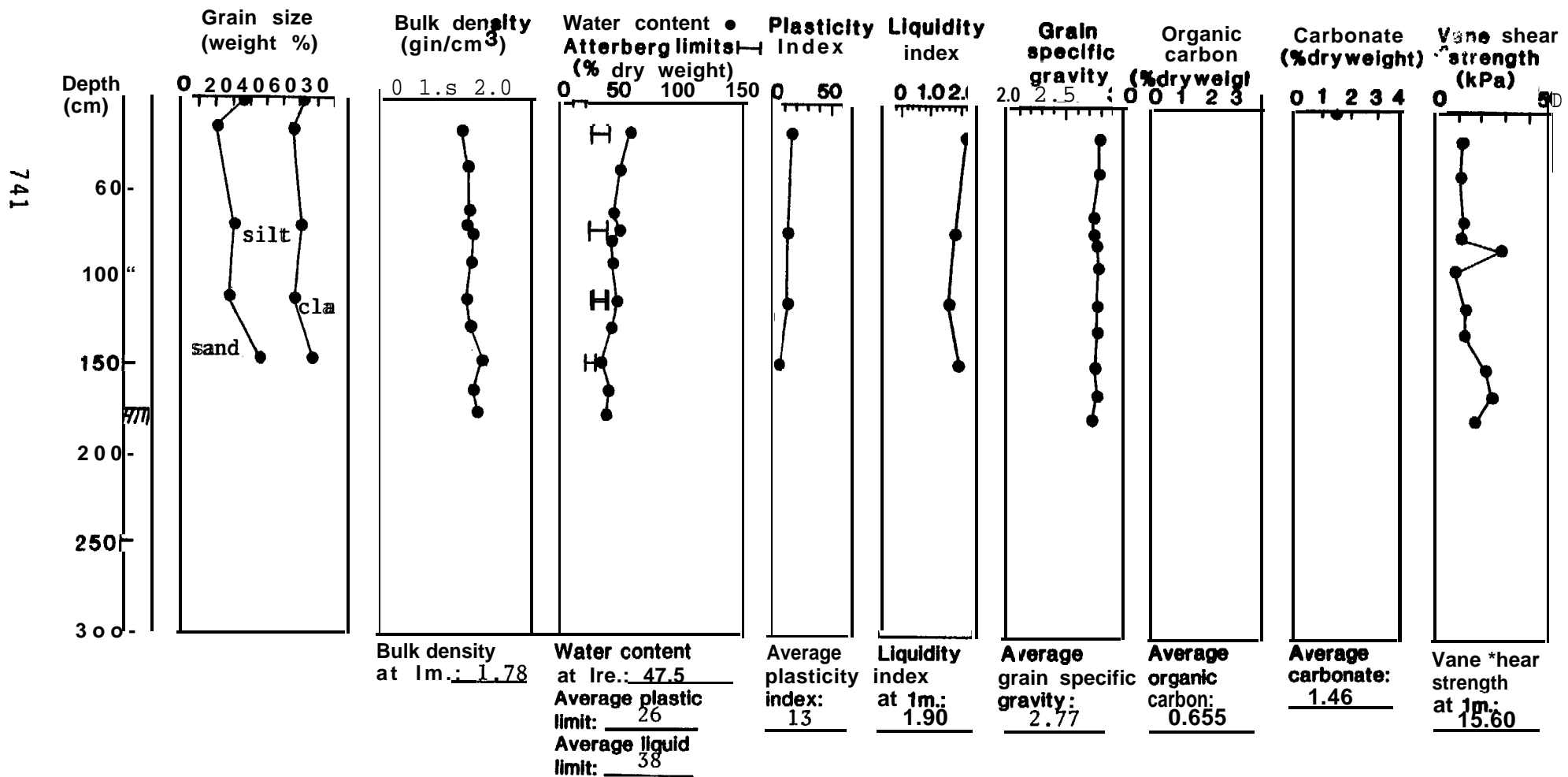
Water depth 155m



Station 552

Location 58°47.2'N 153°02.5'W

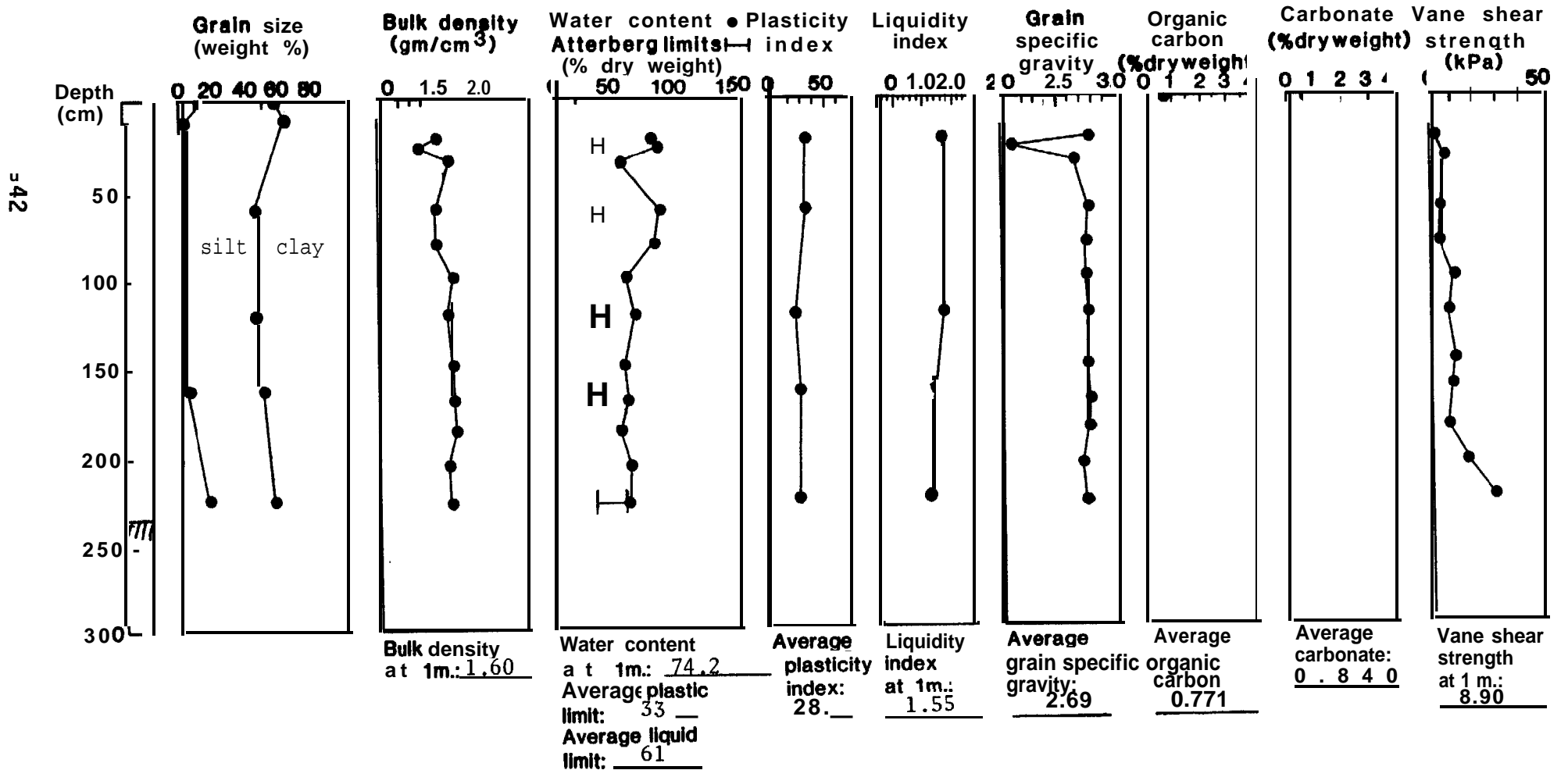
Water depth 135m



Station 640

Location 58 °15.3'N 153 °59.26'W

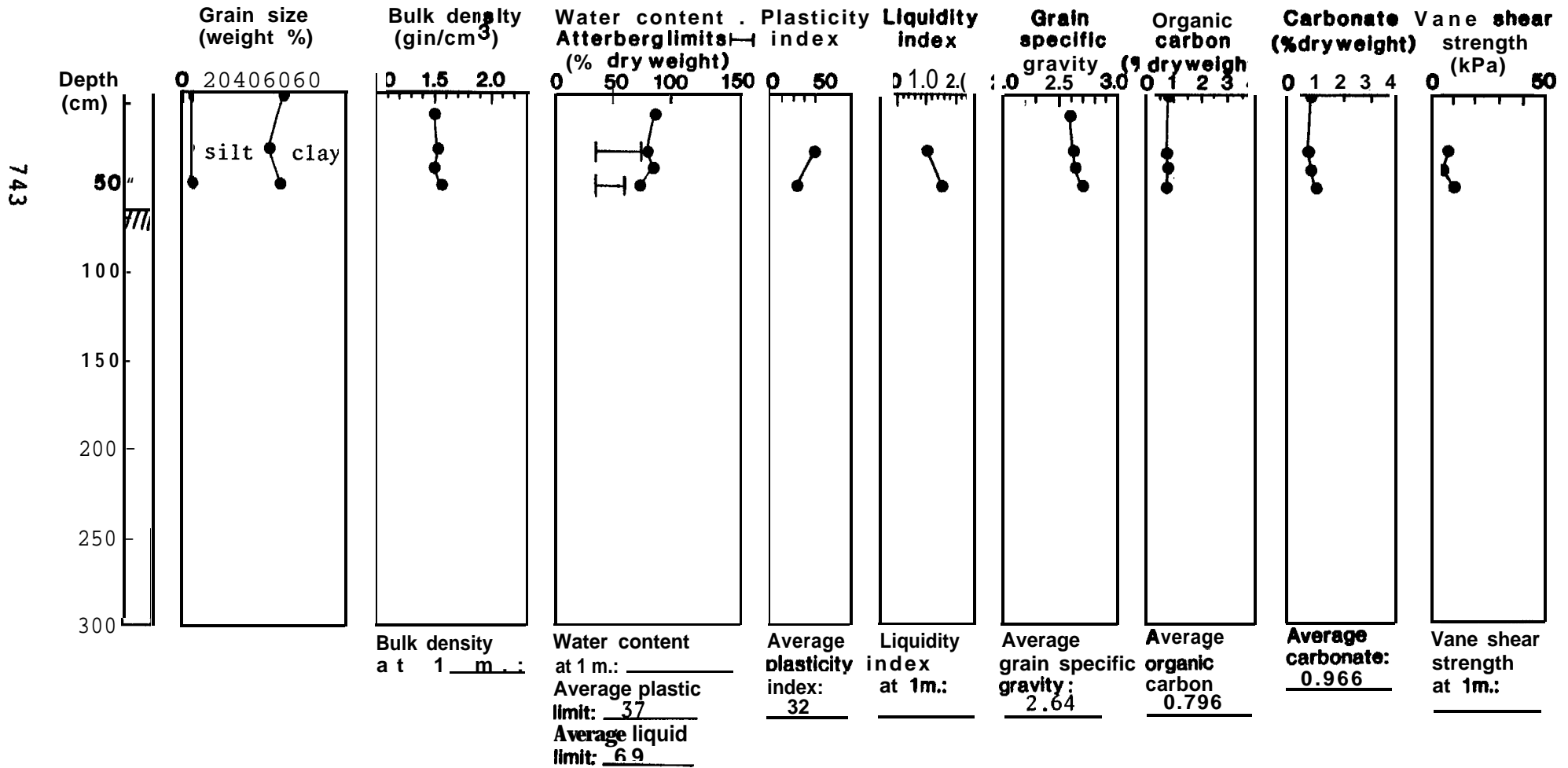
Water depth 274m



Station 643

Location 58°05.7'N 154°09.1'W

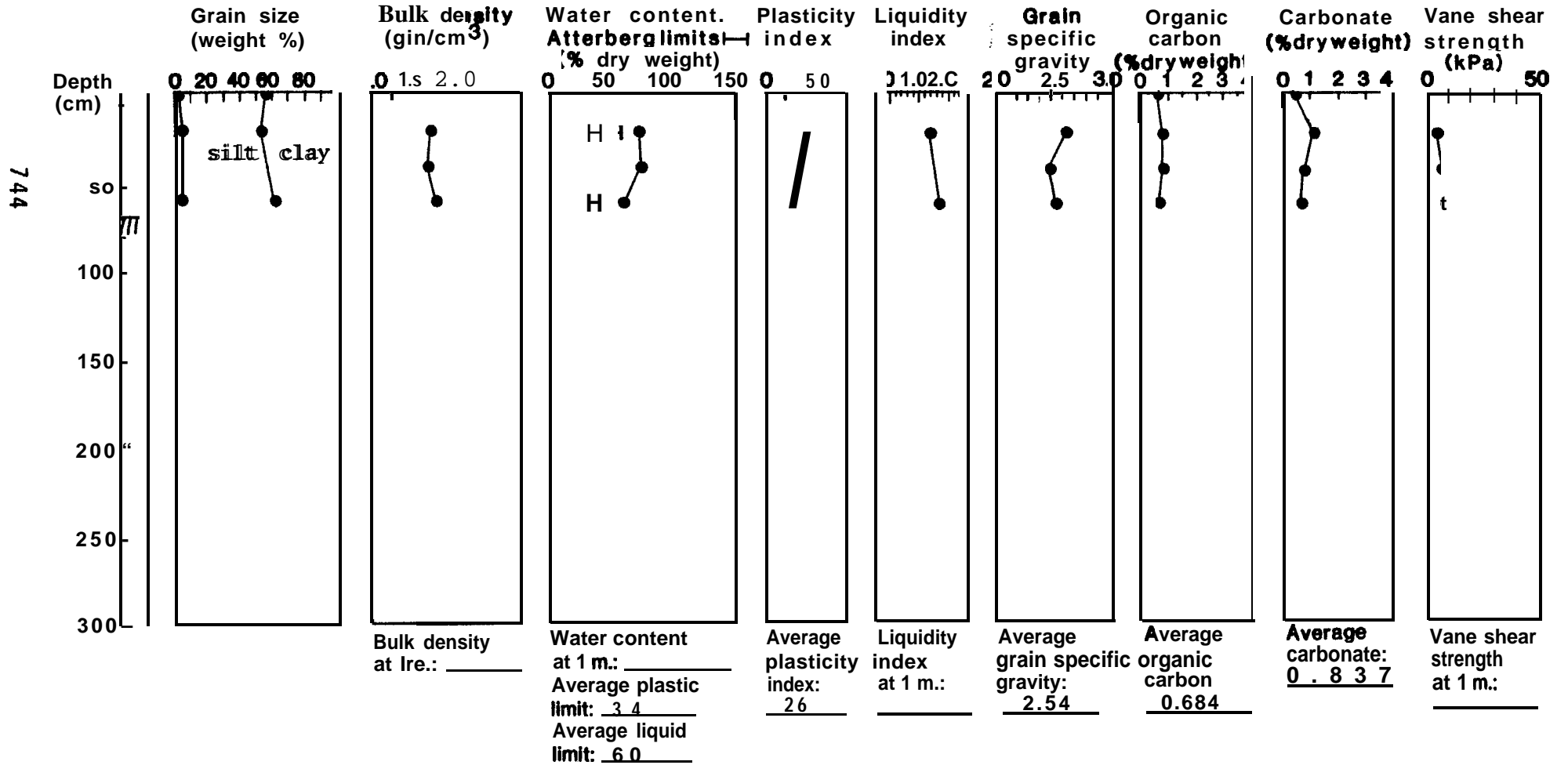
Water depth 288m



Station 644

Location 57°54.6'N 154°33.9'W

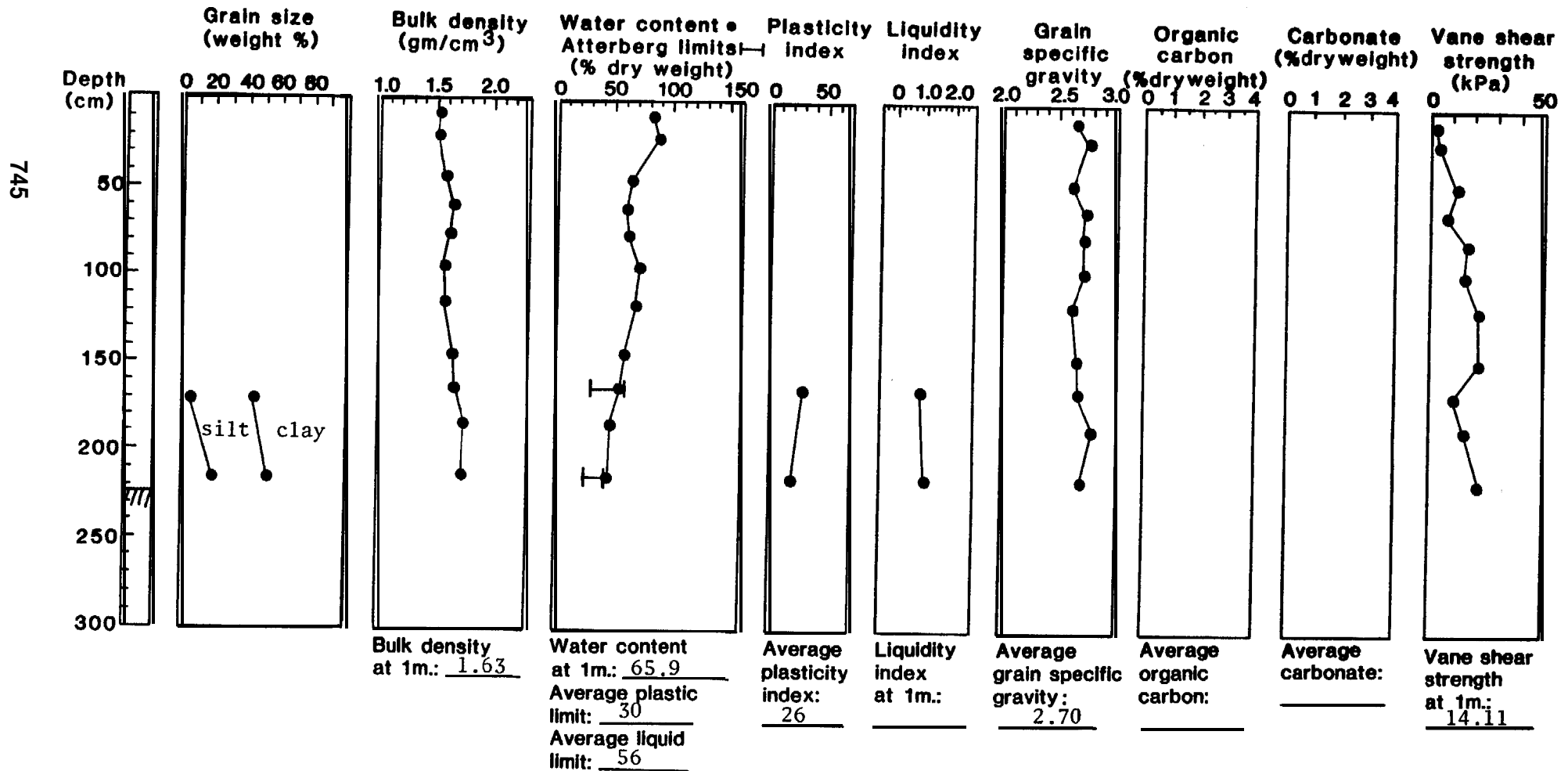
Water depth 278m



Station 645

Location 57°47.0'N 154°58.8'W

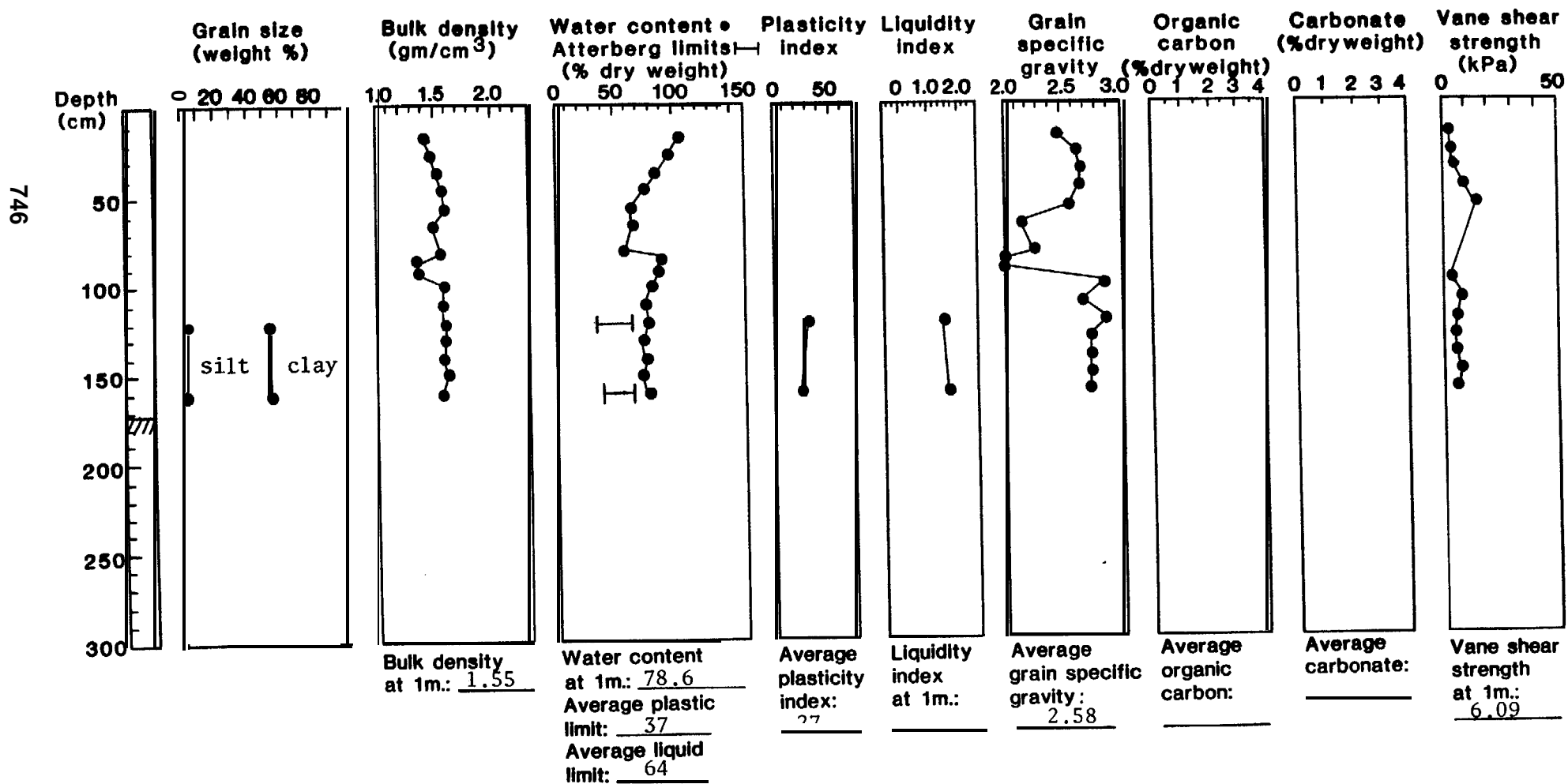
Water depth 315m



Station 646

Location 57°55.3'N 154°17.5'W

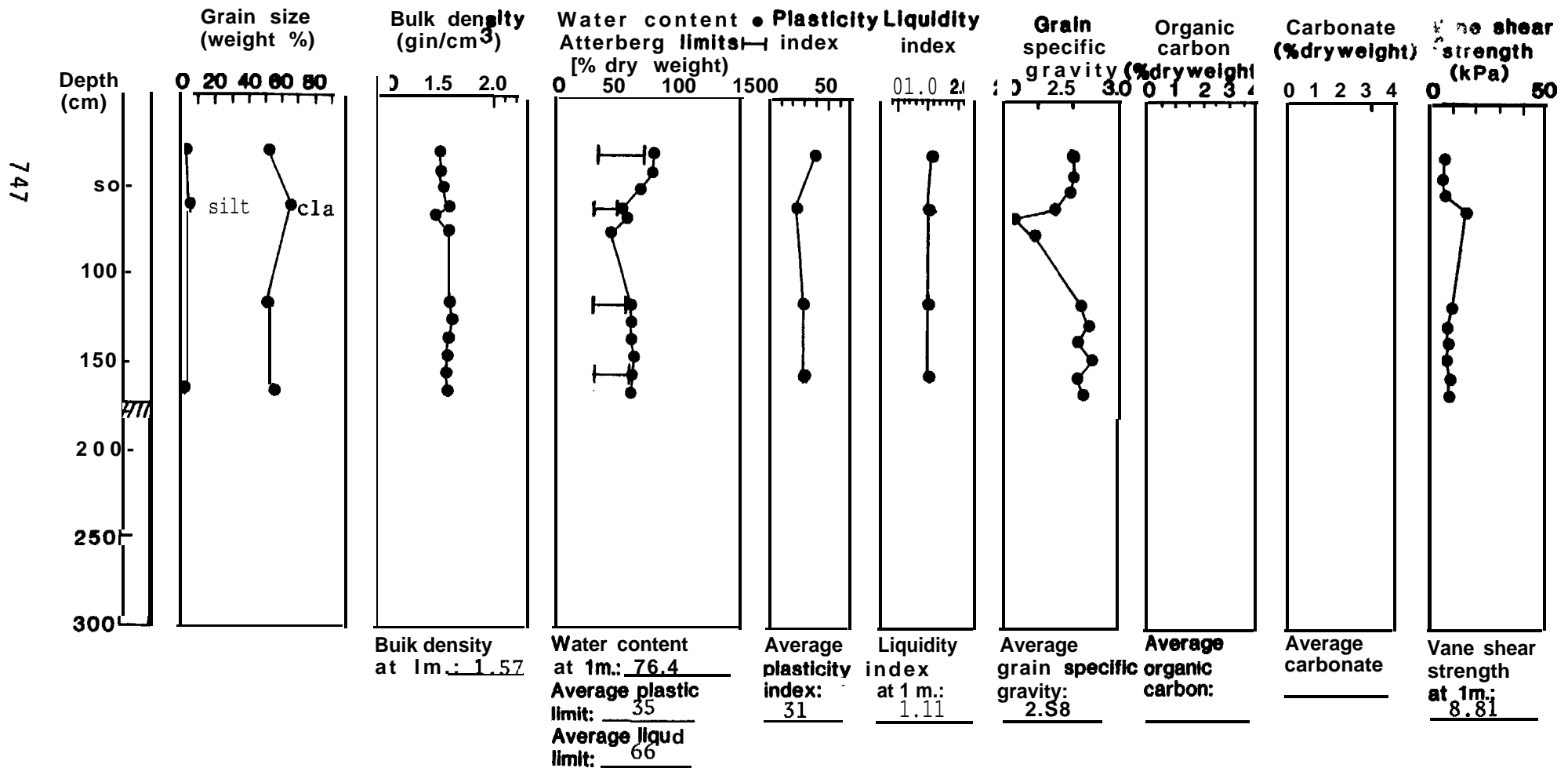
Water depth 216m



Station 647

Location 57°59.8'N 154°10.7'W

Water depth 220m

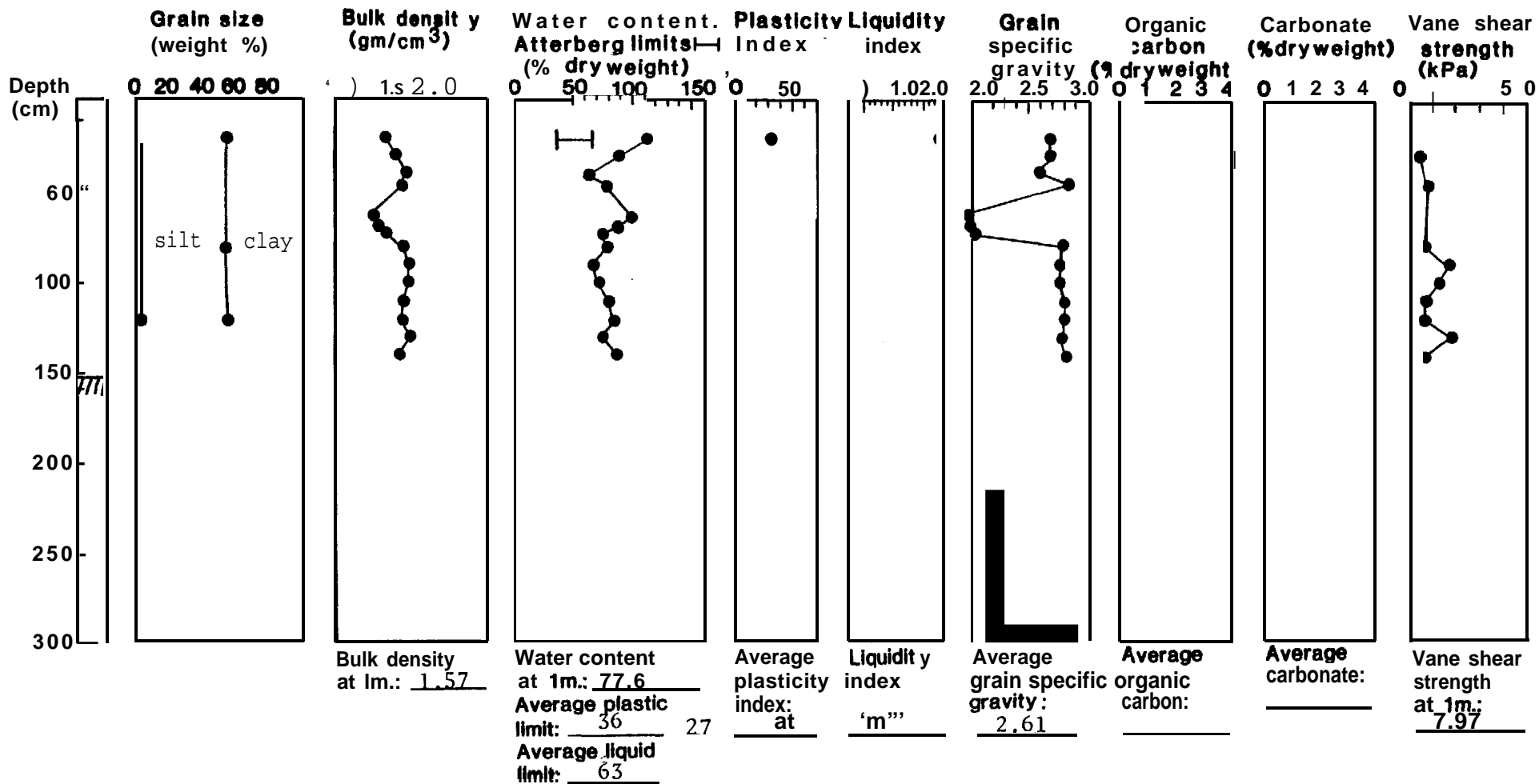


Station 649

Location 58°04.7'N 154°01.9'W

Water depth 209m

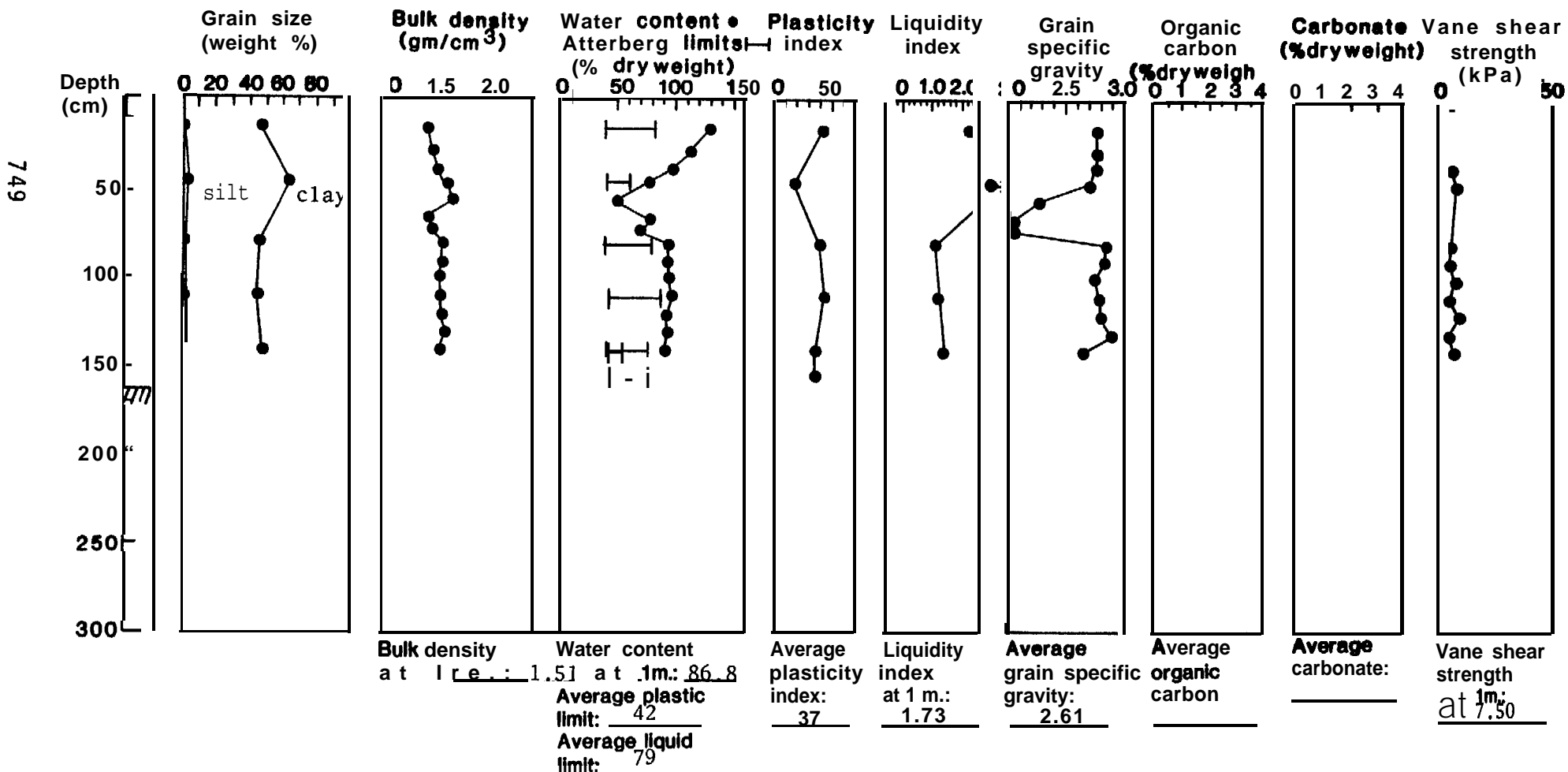
748



Station 650

Location 57°5s.0 'N 154°01.1'W

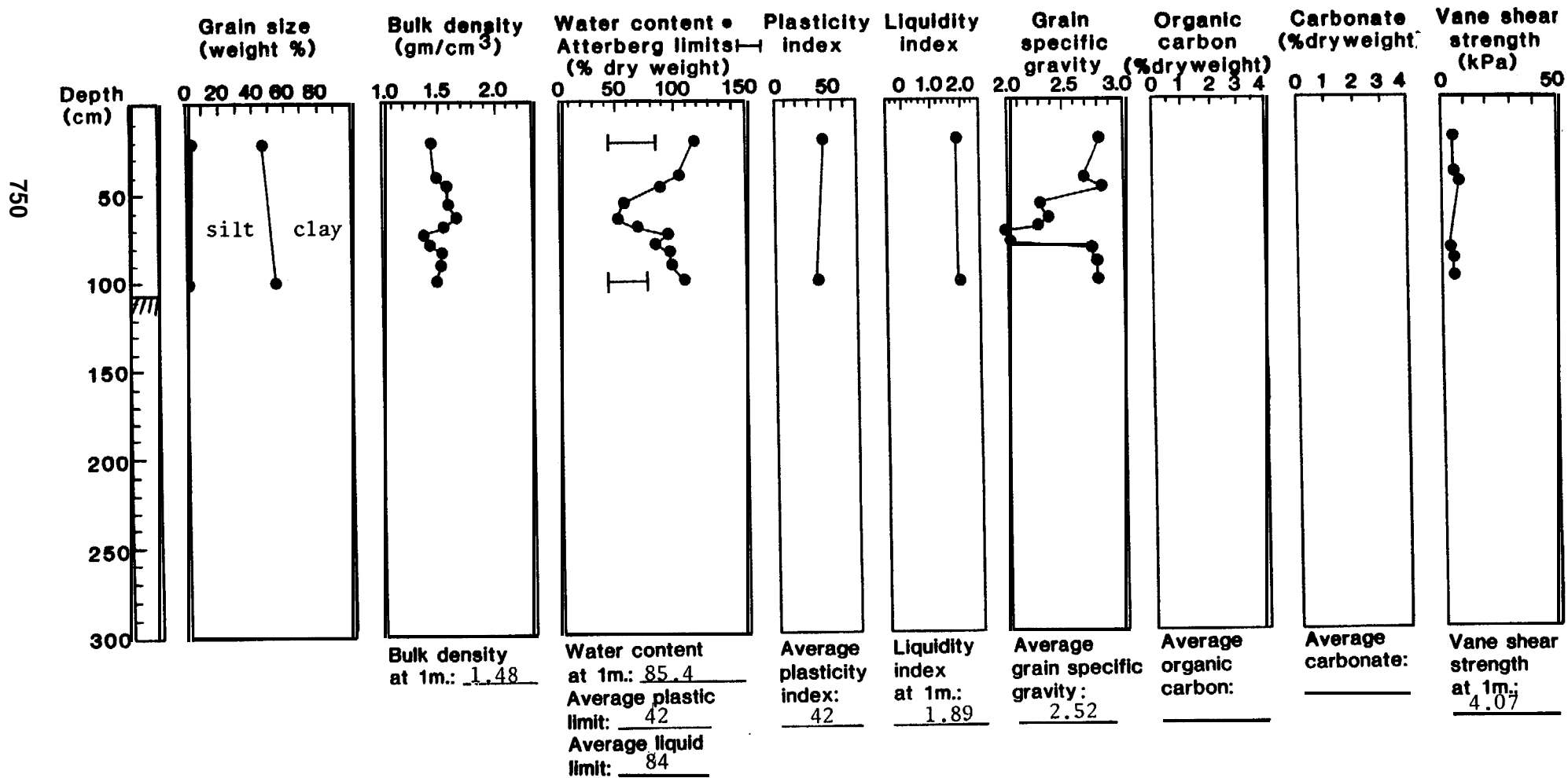
Water depth 199m



Station 651

Location 58°00.1'N 153°52.6'W

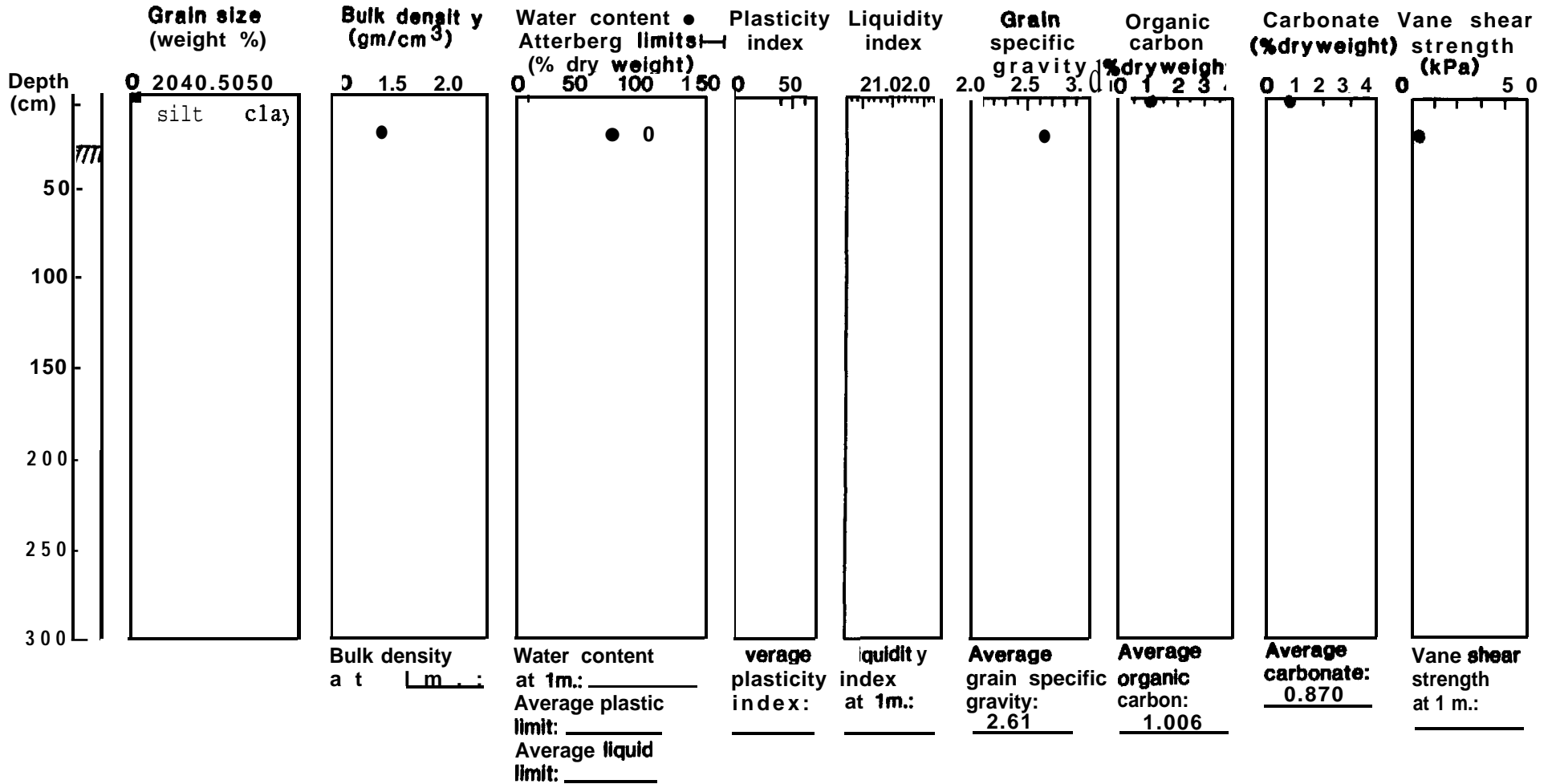
Water depth 194m



Station 654

Location 57°07.4'N 154°09.0'W

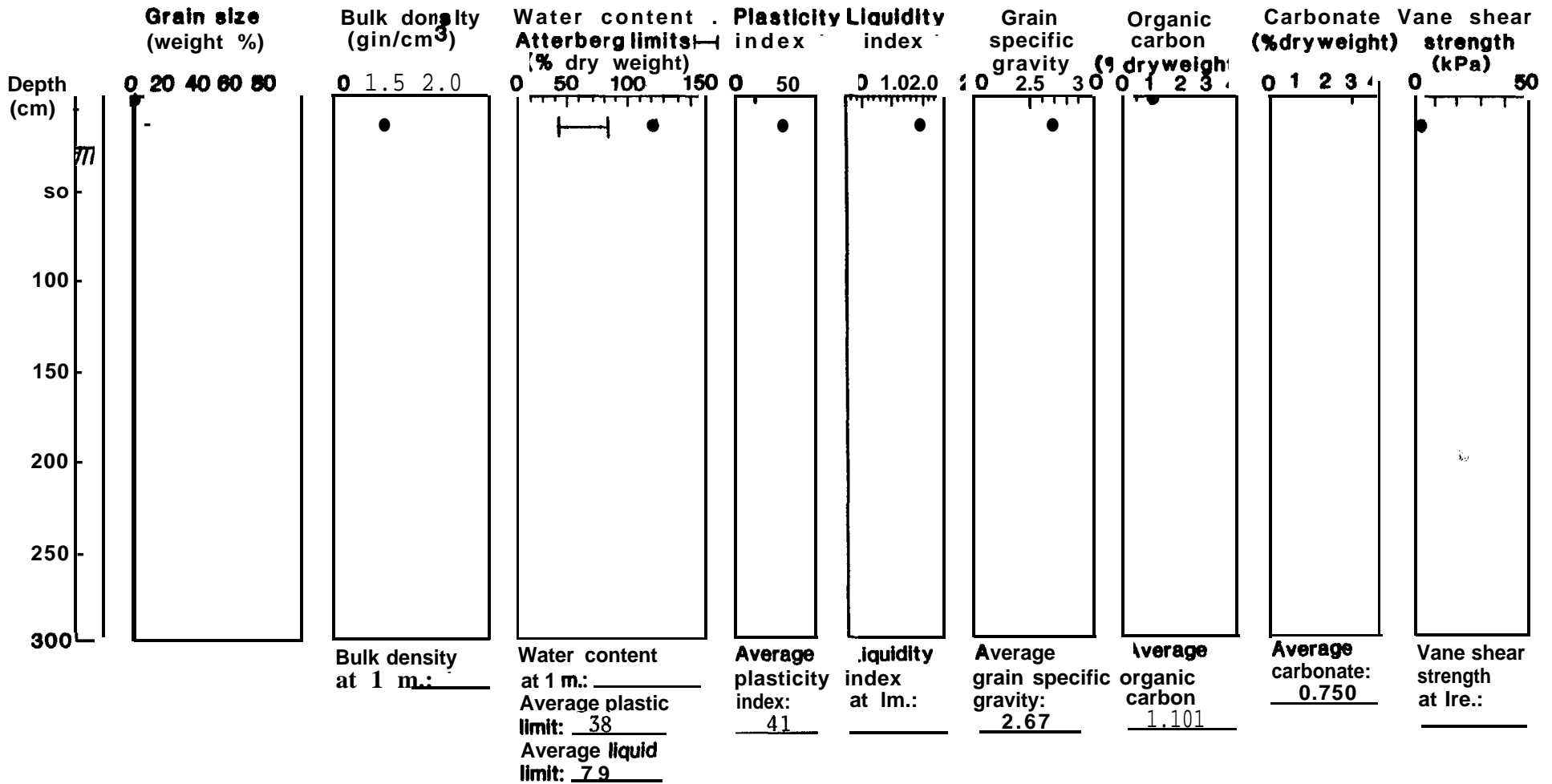
Water depth 232m



Station 655

Location 57°51.8'N 154°09.0'W

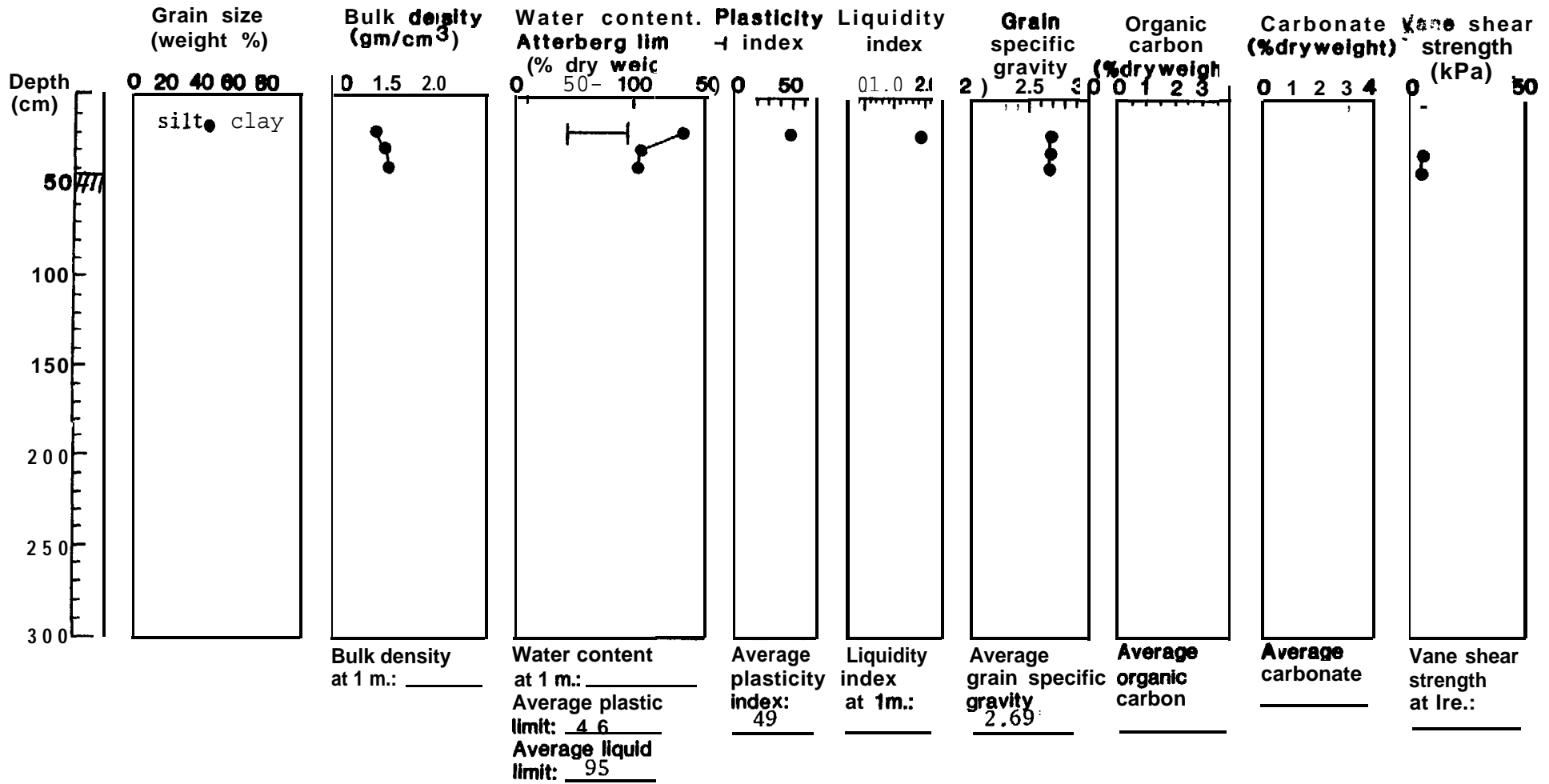
Water depth 204



station 656

Location 58°05.7'N 153°43.8'W

Water depth 194m

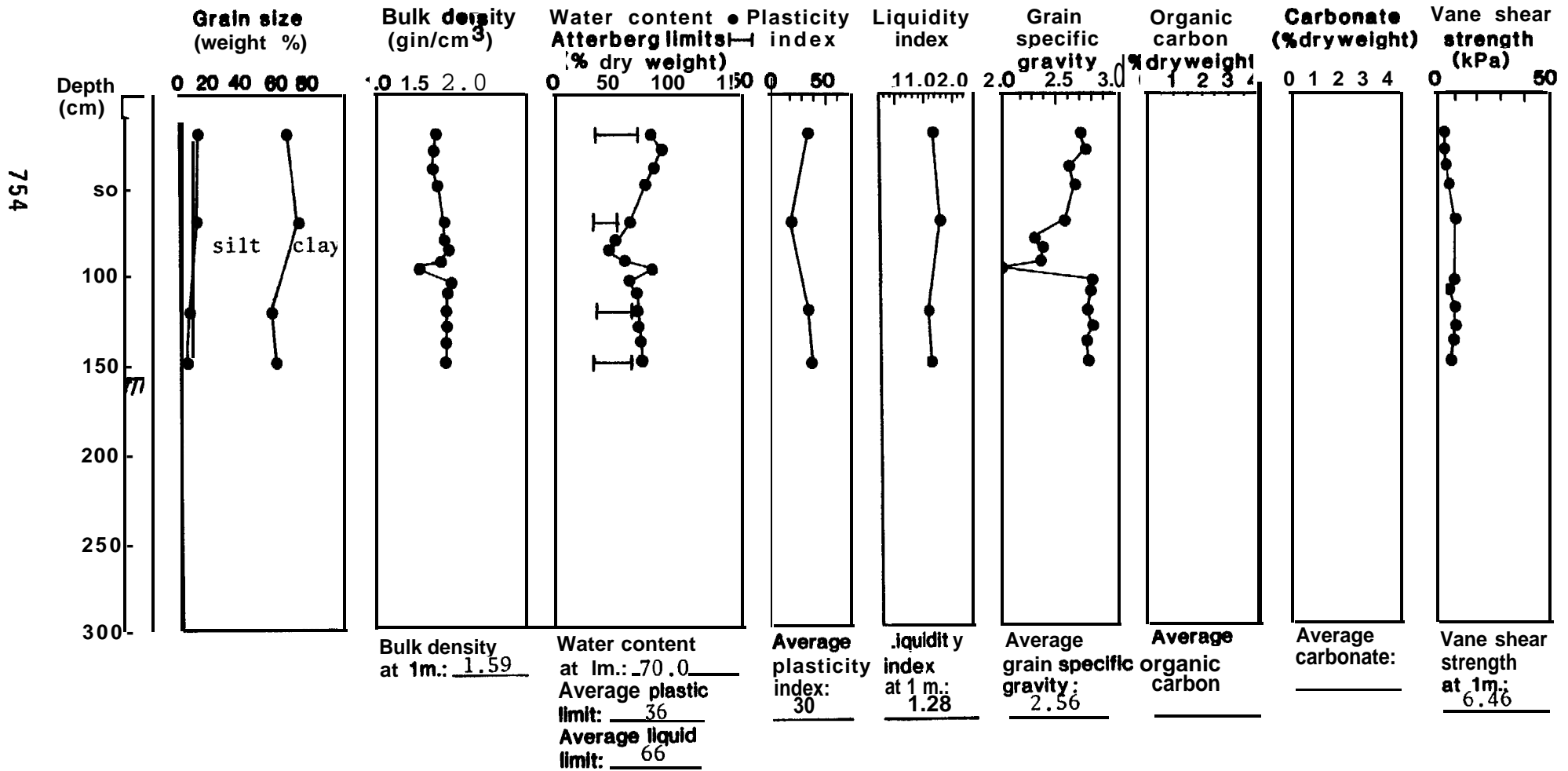


753

Station 657

Location 58°12.9'N 153°57.4'W

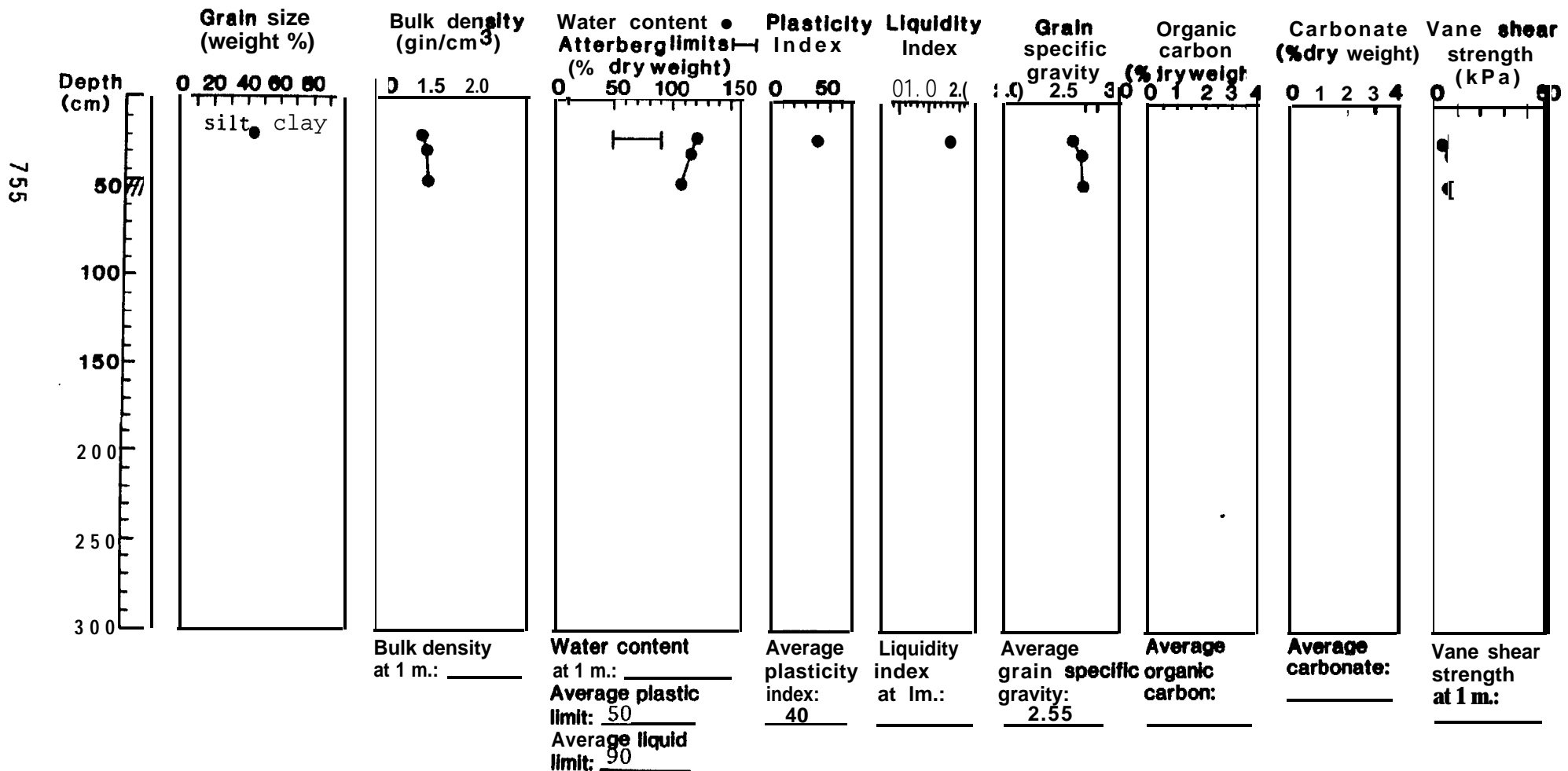
Water depth 232m



station 658

Location 58°10.6'N 153°32.6'W

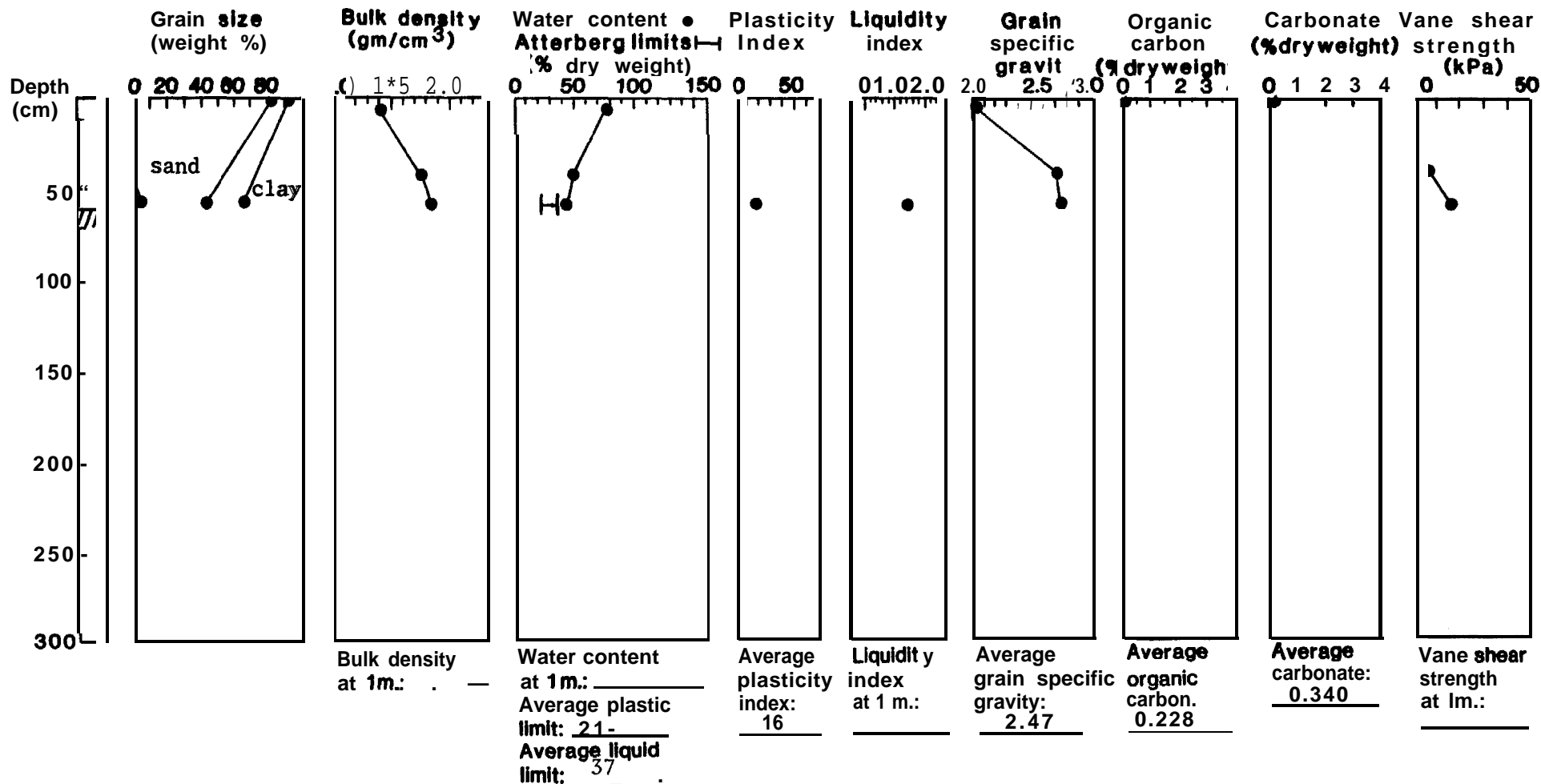
Water depth 190m



Station 1559

Location 58°01.8'N 153°28.5'W

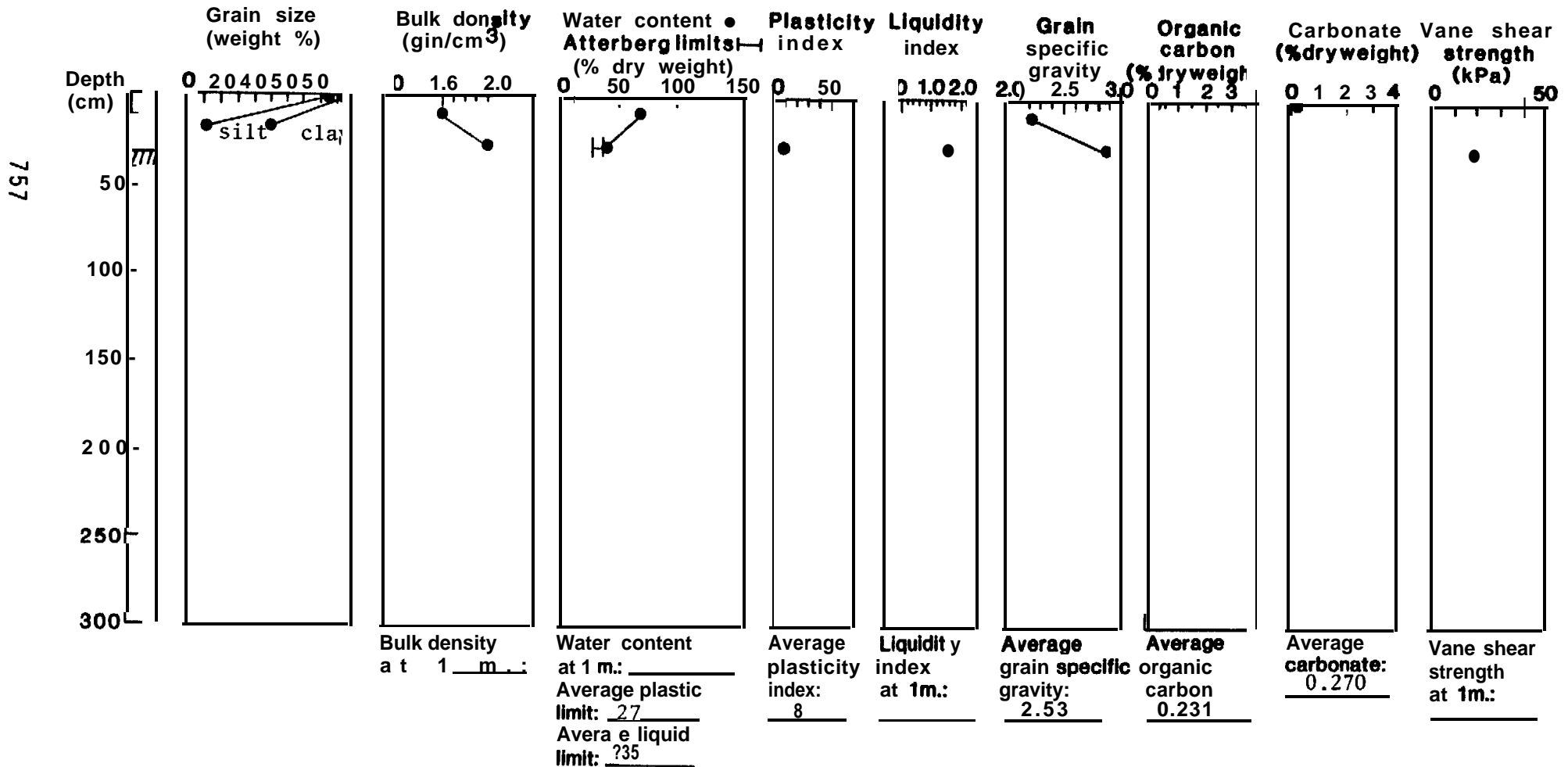
Water depth 112m



Station 660

Location 58°03.9'N 153°32.9'W

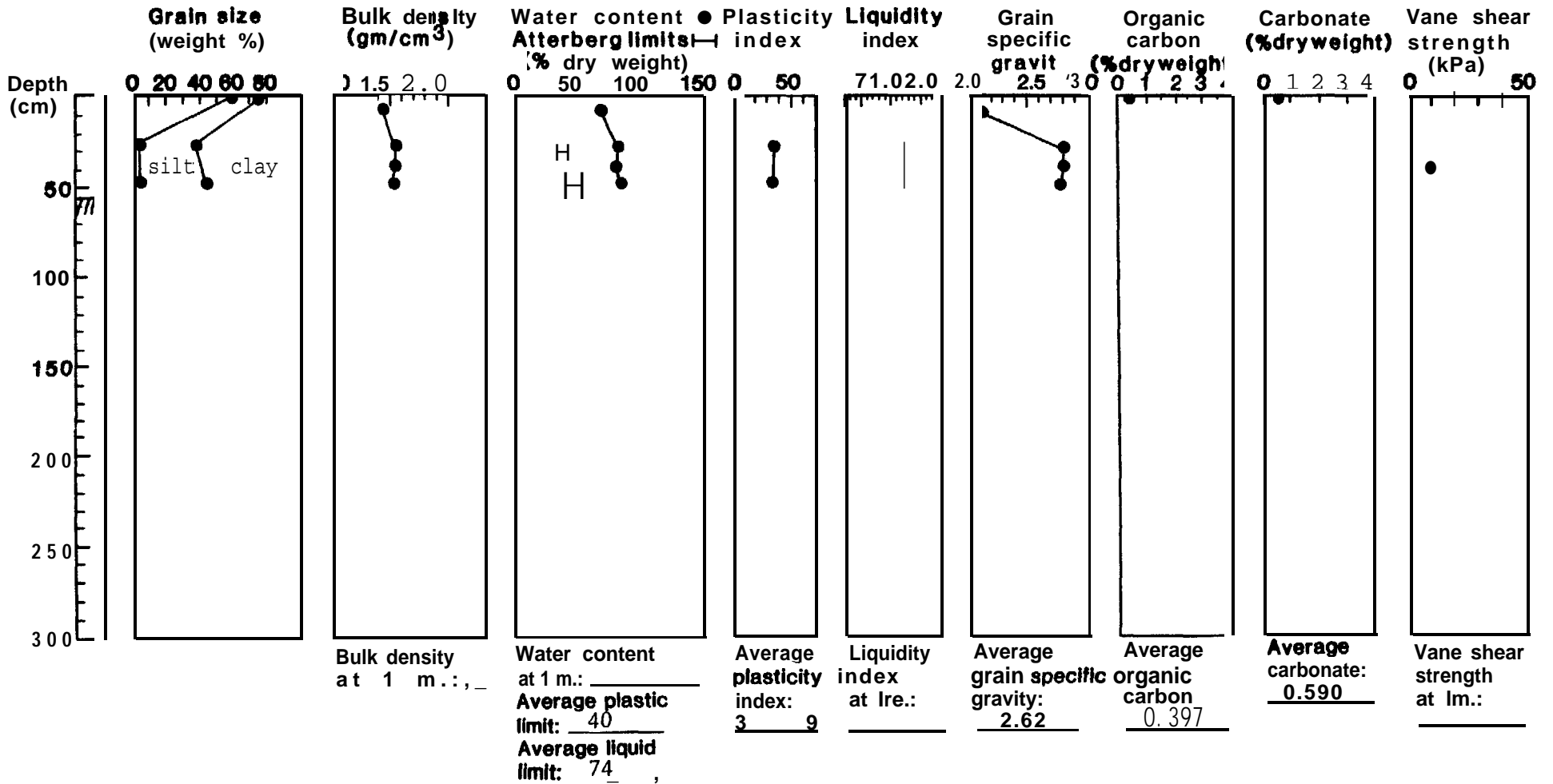
Water depth 146m



Station 661

Location 58°06.50'N 153°34.20'W

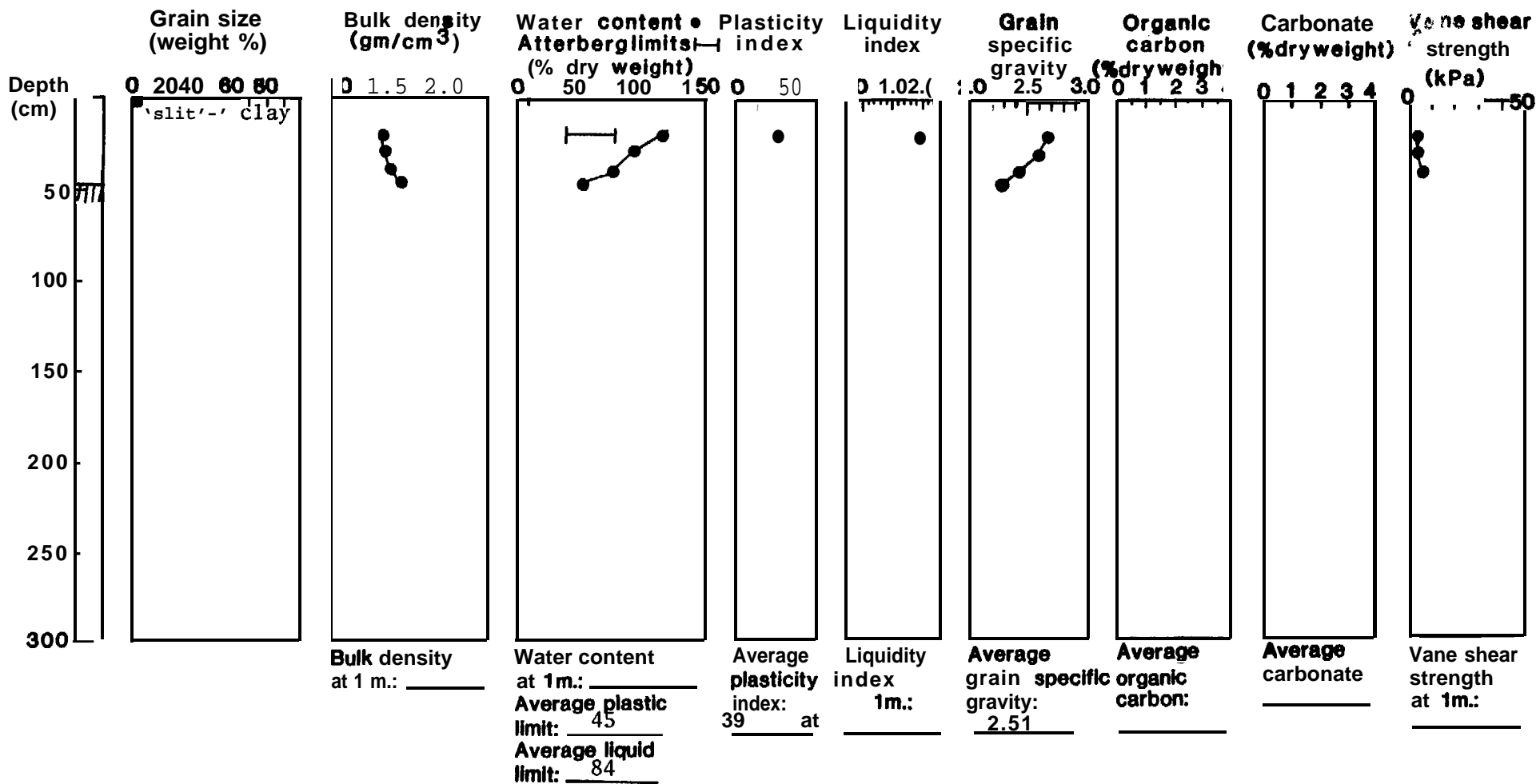
Water depth 238m



Station 662

Location 58°15.80'N 153°23.00'W

Water depth 176m



759

Station 664

Location 58°55.00N 153°36.90W

Water depth 174m

